The Sizes, Shapes, Albedos, and Colors of Cometary Nuclei

Philippe L. Lamy

Laboratoire d'Astronomie Spatiale du C.N.R.S.

Imre Toth

Konkoly Observatory

Yanga R. Fernández

Institute for Astronomy, University of Hawaii

Harold A. Weaver

The Johns Hopkins University Applied Physics Laboratory

Received _____; accepted _____

COMETS II : Chapter 15 – **Version 08 October 2003**

ABSTRACT

We critically review the data on the sizes, shapes, albedos, and colors of cometary nuclei. Reliable sizes have been determined for 65 ecliptic comets (ECs) and 13 nearly–isotropic comets (NICs). The effective radii fall in the range 0.2–15 km for the ECs and 1.6–37 km for the NICs. We note that several nuclei recently measured by the *Hubble Space Telescope* are sub–km in radius, and that only 5 of the 65 well-measured EC nuclei have effective radii larger than 5 km. We estimate that the cumulative size distribution (CSD) of the ECs obeys a single power law with an exponent $q_S = 1.9 \pm 0.3$ down to a radius of $\sim$1.6 km. Below this value there is an apparent deficiency of nuclei, possibly owing to observational bias and/or mass loss. When augmented by 21 Near-Earth Objects (NEOs) that are thought to be extinct ECs, the CSD flattens to $q_S = 1.6 \pm 0.2$. The cumulative size distribution of NICs remains ill-defined because of the limited statistical basis compared to ECs. The axial ratios a/b of the measured nuclei of ECs have a median value of $\sim$1.5 and rarely exceed a value of 2, although it must be noted that the observed a/b values are often lower limits because of uncertainties in the aspect angle. The range of rotational periods extends from 5 to 70 hr. The lower limit is significantly larger than that of main belt asteroids and NEOs ($\sim$2.2 hr, excluding the monolithic fast rotators), and this has implications for the bulk density of cometary nuclei. By combining rotation and shape data when available, we find a lower limit of 0.6 g cm^{-3} for the nucleus bulk density to ensure stability against centrifugal disruption. Cometary nuclei are very dark objects with globally–averaged albedos falling within a very restricted range: 0.02 to 0.06, and possibly even narrower. $(B - V)$, $(V - R)$ and $(R - I)$ color indices indicate that, on average, the color of cometary nuclei is redder than the color of the Sun. There is, however, a large diversity of colors, ranging from slightly blue

to very red. While two comets have well–characterized phase functions with a slope of 0.04 mag deg^{-1}, there is evidence for steeper (2P/Encke, 48P/Johnson) and shallower (28P/Neujmin 1) functions, so that the observed range is 0.025 to 0.06 mag deg^{-1}. The study of the physical properties of cometary nuclei is still in its infancy, with many unresolved issues, but significant progress is expected in the near–future from current and new facilities, both ground-based and space-borne.

1. INTRODUCTION

1.1. Motivation for Studying Cometary Nuclei

There are many reasons why the investigation of cometary nuclei can advance our understanding of the solar system, and this topic is discussed in detail by *Weidenschilling* (2004) and by *Lunine et al.* (2004). Briefly, cometary nuclei are the most primitive observable objects remaining from the era of planetary formation. As such, they provide information on the thermophysical conditions of the protoplanetary disk and on the formation mechanism for the icy planetesimals from which the cores of the outer planets were built. Furthermore, the physical evolution of cometary nuclei over the past 4.6 Gyr must be explained within the context of any unified theory of the solar system, and comparative studies of cometary nuclei and dynamically–related bodies (e.g., transneptunian objects and Centaurs; see *Jewitt* 2004) should provide insights into the physical and collisional histories of these objects.

Through impacts over the age of the solar system, cometary nuclei have significantly affected the formation and evolution of planetary atmospheres and have provided an important source of volatiles, including water and organic material, to the terrestrial

planets. Interest has been building recently in the contribution of cometary nuclei to the Earth impact hazard, which has previously focussed mainly on asteroids. Another important motivation for studying cometary nuclei is that their bulk properties may dictate what steps should be taken for hazard mitigation in the event of a predicted collision.

1.2. Origin and evolution of cometary nuclei

Various scenarios have been proposed to explain how cometary nuclei formed from the microscopic grains within the dusty disk of the solar nebula (*Weidenschilling* 2004). Different formation mechanisms may have been operational at different places within the nebula, and this may have led to diversity in the physical properties of cometary nuclei depending on where they formed. Even if there was a common formation mechanism for all cometary nuclei, diversity could persist because of differences in the physical and chemical conditions at different heliocentric distances (e.g., collisional environment, chemical composition, radiation environment, etc.).

Dynamical arguments support the hypothesis that cometary nuclei originate from at least two different regions of the solar system: the vast majority of the ecliptic comets are thought to be collisional fragments of Kuiper belt objects (the so-called *transneptunian* objects; see *Duncan et al.* 2004, and *Barucci et al.* 2004), while most of the long-period and Halley-type comets probably formed in the vicinity of the giant planets and were subsequently ejected to the Oort cloud where they were stored for most of their lifetimes (*Dones et al.* 2004).

We follow the classification scheme proposed by *Levison* (1996) and distinguish between ecliptic comets (ECs) and nearly-isotropic comets (NICs). This scheme is not profoundly different from the historical tradition, but it has the merit of being based

on strict dynamical parameters, namely the Tisserand parameters of comets that are (nearly) constants of motion with respect to Jupiter. ECs have $2 \leq T_J \leq 3$ and are equivalent to the Jupiter-family comets, including 2P/Encke although it is now practically decoupled from Jupiter. ECs in general have orbital periods less than 20 years, hence the quasi-correspondence with the population of short-period comets. NICs have $T_J < 2$ and group together the Halley-type comets (which have a lower limit on their periods, in general, of 20 years) and the long-period comets (old and new). Based on their dynamical histories, the population of NICs is further divided into two subpopulations: (i) dynamically new NICs, which are on their first pass through the inner solar system and typically have semi-major axes, a, greater than $\sim 10^4$ AU, and (ii) returning NICs, which have previously passed through the inner solar system and typically have $a \leq 10^4$ AU. The returning NICs are further divided into two subclasses: external returning comets (ERCs) with periods greater than 200 years, and Halley-type comets (HTCs) with orbital periods less than 200 years. We note that short-period comets 8P/Tuttle (P_{orb} =13.51 years, $T_J = 1.623$), 96P/Machholz 1 (P_{orb} =5.26 years, $T_J = 1.953$) and 126P/IRAS (P_{orb} =13.29 years, $T_J = 1.987$) are now classified as NICs.

Because of their different origin, the question arises as to whether the two populations (ECs and NICs) have intrinsically different physical properties, or whether they reflect a continuous spectrum of planetesimals in the early solar system, making them more similar than different. The nuclei of ECs suffer significant heating episodes during their frequent passages through the inner solar system, where sublimation processes erode the surface layers, devolatilize the interior, and possibly alter the shape and structure of the nucleus. *Weissman* (1980) showed that ~10% of the NICs split on their first perihelion passage and *Levison et al.* (2002) suggested that 99% of them are disrupted sometime during their dynamical evolution. This may suggest different physical properties for the ECs and the NICs, although convincing, direct evidence of such differences has not yet been found.

In summary, there are a variety of processes associated with the formation and evolution of comets that could affect the physical properties of cometary nuclei. There should be no expectation that comets form a homogeneous group with respect to their physical properties, and it will be interesting to investigate possible correlations of those properties with the comet's place of origin and its subsequent history.

1.3. Historical perspective

To understand how far we have progressed in the study of cometary nuclei, we summarize briefly some of the important results of the 20^{th} Century. As is commonly done, we define the border between "pre-history" and "recent history" to have been crossed with the publication of the classic paper on cometary nuclei by *Whipple* (1950).

1.3.1. Pre-history.

Before 1950, the paradigm governing the cometary "nucleus" did not involve a central, monolithic body. Rather, the "nucleus" was envisaged as an unbound agglomeration of meteoritic solids. In this *sandbank* model, described by *Lyttleton* (1953, 1963), all the particles comprising a comet were on independent, but very similar orbits, and there was no gravitational binding. This model was consistent with the observations of many cometary phenomena, i.e., the morphological complexity of the inner comae of comets, as well as (qualitatively) the odd behaviors that comae sometimes display. The term "nucleus" itself was used with imprecision, as noted by e.g., *Bobrovnikoff* (1931) and *Vorontsov-Velyaminov* (1946). Most often, the "nucleus" merely referred to the peak in the surface brightness distribution, which is frequently called the "central condensation."

The basic misconception of this era was a drastic overestimation of the typical size of

cometary nuclei, which most researchers thought were tens of kilometers in size. Reports of observers resolving disks of the "nuclei" probably provided the motivation for this misconception. In hindsight, we now recognize that observers were merely seeing the steeply–sloped surface brightness distribution of the inner coma. However, a few researchers thought cometary nuclei were monoliths, as small as 1 km in diameter or even less, on the basis of the starlike appearance of comet 7P/Pons-Winnecke when observed close to Earth in 1927 (*Slipher* 1927; *Baldet* quoted by *Vorontsov-Velyaminov* 1946). Further impediments to a proper understanding of cometary nuclei were the poorly-constrained albedo and phase–darkening behavior. The idea of a nucleus, or dust grains for that matter, with a very low albedo did not become acceptable until after the spacecraft flybys of 1P/Halley in 1986.

1.3.2. Recent History.

The "dirty snowball" model proposed by *Whipple* (1950) envisaged the nucleus as "a conglomerate of ices ... combined in a conglomerate with meteoric materials." Two significant improvements over the sandbank idea were the model's ability to adequately explain both the cometary nongravitational motion and the gas production rate.

With this paradigm established, the future interpretation of data established the relatively (compared to pre-1950) small sizes of nuclei. Photographic data taken by *Roemer* (1965, 1966, 1968) set constraints on the sizes of many nuclei, although at this time the albedo was still thought to be much higher than the currently accepted mean. Furthermore, there was still the problem of unresolved comae around distant comets. Generally, Roemer's photographic observations were not taken at sufficiently large heliocentric distances for the comets to be inactive, and they were significantly contaminated by unresolved coma. *Delsemme and Rud* (1973) tackled the problem of albedo by comparing the nuclear

brightness far from the Sun and the gas production rate close to the Sun, and derived albedos that seemed to confirm the high values of conventional wisdom. However, we now know that nuclear sizes based on cometary activity are lower limits, making the derived albedos upper limits, owing to the fact that typically only a small fraction of the nucleus surface is active.

Several significant steps forward were taken in the 1980s. Simultaneous thermal-infrared and optical measurements were made (discussed in §3.3) establishing that nuclear albedos were low. In 1983 Comet IRAS–Araki–Alcock made an extremely close approach to Earth, and the synthesis of data using modern observational techniques resulted in a fairly complete description of that nucleus (size, albedo, shape, rotation; *Sekanina* 1988). Finally, the flotilla of spacecraft flying by comet 1P/Halley confirmed beyond any doubt that a single, solid body lies at the center of a comet.

The past decade has witnessed a major observational effort to study cometary nuclei using medium to large ground-based telescopes and space telescopes outfitted with charged coupled device (CCD) detectors, and this has resulted in a wealth of new data. Indeed, most of our understanding of cometary nuclei as a population has been derived from observations made during the past decade.

1.4. Observing Cometary Nuclei

The overarching observational goal for studies of cometary nuclei is to understand their ensemble properties, which is accomplished in several ways. The most common observations involve visible–wavelength photometry, from which the color and the product of the cross-section and albedo can be measured. More detailed observations at these wavelengths, such as time series of data at multiple epochs, provide clues on the shape

and rotation state of the nucleus. Observations at wavelengths longer than $\sim$5 μm, in the thermal–infrared, provide data on both the size and albedo and constrain the thermal properties of the bulk material comprising the nucleus.

Contrary to popular belief, the optical depth, τ, of most cometary comae is generally small enough to allow direct detection of the nucleus, in principle. Possible exceptions are unusually active comets, such as C/1995 O1 (Hale-Bopp), for which τ may approach unity. For most comets, the real problem lies with the intrinsic faintness of the nucleus relative to the light scattered from dust grains in the coma, i.e., the *contrast* is usually too small to distinguish the nucleus clearly. Historically, planetary astronomers have attempted to overcome this obstacle by observing comets at large heliocentric distances, when the nucleus was *assumed* to be inactive and coma-free. On the one hand, the activity level at large heliocentric distances is often so low that most of the observed light can be attributed to reflection from the nucleus. On the other hand, many comets are known to be conspicuously active at large heliocentric distances, preventing such an observational approach. Another approach was to observe only relatively nearby, very low activity comets, whose dust production rates were so small that the nucleus clearly stood out even when the spatial resolution was only hundreds of kilometers, but this works well for only a handful of objects. Spacecraft encounters, of course, are the best way to obtain detailed information on the physical properties of cometary nuclei, and we have learned much from the spectacular encounter images of 1P/Halley and 19P/Borrelly (see *Keller et al.* 2004). While spacecraft encounters provide "ground truth" that cannot be obtained any other way, this approach is necessarily limited to a small number of objects and cannot be used to determine the properties of cometary nuclei as a population. Fortunately, recent improvements in the resolution capabilities and sensitivities of ground- and space-based telescopes now allow us to study the physical properties of a large number of cometary nuclei, even in the presence of substantial coma.

1.5. Scope of this chapter

Within the context of this chapter, "physical properties" refer to the size, shape, albedo, and color of the nucleus. All of these properties can be observed directly, and in §2 we describe in detail the techniques for doing so. In §3, we summarize the results for each individual comet for which data are available because a comprehensive and critical evaluation of the results cannot be obtained from any other reference. After discussing techniques and results, in §4 we synthesize all the data to estimate the distribution of sizes, shapes, colors, and rotational periods of cometary nuclei as a population. In §5 we discuss some outstanding, unresolved issues in the study of cometary nuclei and comment on the direction of future research on the physical properties of cometary nuclei. Some short, concluding remarks comprise §6.

Some physical properties of cometary nuclei are *not* covered in this chapter. The structure, strength, and bulk density are especially important, but, in general, these can only be estimated indirectly, as discussed by *Weissman et al.* (2004) and by *Boehnhardt* (2004). Although we summarize results on the rotational periods of cometary nuclei, mainly because they are obtained from the same light curve data used to measure shapes, a comprehensive discussion of the rotational properties is given by *Samarasinha et al.* (2004). The physical nature of the ice and dust contained within cometary nuclei (e.g., crystalline vs amorphous ice, thermal conductivities and heat capacities of the ice and dust, etc.) is very poorly constrained observationally and is discussed from a modeling perspective by *Prialnik et al.* (2004). Finally, the very interesting question of how comets are related to the other minor bodies in the outer solar system is not treated here, but, rather, is covered separately by *Jewitt* (2004).

2. TECHNIQUES FOR DETECTING AND CHARACTERIZING COMETARY NUCLEI

2.1. General Considerations

Cometary nuclei are certainly among the most difficult objects of the solar system to detect and characterize, usually suffering from the dual problem of being faint and immersed in a coma. The techniques for their study are those first developed for the investigation of asteroids, but with the additional complexity caused by the presence of a coma. The primary technique, visible-wavelength imaging, uses reflected sunlight and takes advantage of high–performance detectors like CCDs. This technique has been most successful for relatively large and/or very low activity nuclei at large heliocentric distances, and for comets observed at close range and with sufficient spatial resolution to separate unambiguously the nuclear and coma signals. The pros and cons of these two cases will be discussed below. A third method using this technique, the in-situ spacecraft investigation, is discussed by *Keller et al.* (2004) and will not be addressed here.

A second technique relies on the detection of thermal emission from the nucleus. The situation in this case is less favorable than for the reflected light because of the generally fainter signals, high thermal background with ground-based facilities, and inferior performance of IR detectors. Usually one has no choice but to observe the nuclei at close range, usually exploiting a close encounter with Earth. As with observations of reflected sunlight, a coma will usually be present and must be taken into account. Before the age of large–area infrared array detectors, this was difficult and so, again, very low activity comets were the most popular targets. New and improved thermal detectors, such as those on *SIRTF* will, however, relax the limitations of the technique.

The sample of objects for which the thermal emission at radio wavelengths may be

detected is even more restricted than in the infrared. The nucleus must be exceedingly close (e.g., C/1983 H1 IRAS-Araki-Alcock), or exceedingly large (e.g., C/1995 O1 Hale–Bopp). Radar observations additionally have a Δ^{-4} limitation, where Δ is the geocentric distance, and only rarely do comets pass close enough to the Earth to permit radar measurements of the nucleus (*Harmon et al.* 2004).

Finally, we discuss rarely–performed stellar occultation observations, which have the potential to provide detailed shape information on nuclei and their inner comae.

2.2. Using the Reflected Light

2.2.1. Observations

Detecting the solar light reflected by cometary nuclei remains the most powerful and efficient method to determine their size and to study their properties. However, this technique requires knowledge of the albedo and phase law, as discussed below.

At large heliocentric distances, say $r_h \gtrsim 4$ AU, the activity of most ecliptic comets is very weak, and the coma may become sufficiently faint, or possibly non-existent, to reveal the "bare" nucleus. Thus, the best strategy for these comets generally is to observe near aphelion. However, there are two main problems: (1) the geometric conditions (large r_h and Δ) usually result in a very faint nuclear signal, and (2) the criterion used to decide the non-existence of a coma, namely the stellar appearance of the nucleus, is not robust because an unresolved coma can still contribute substantially to the observed signal. The most well-known example is 2P/Encke, which has been anomalously bright at almost every observed aphelion (*Fernández et al.* 2000, and references therein).

For the nearly isotropic comets, cometary activity can continue well beyond this rough boundary for the ecliptic comets, probably due to the higher abundance of ices more volatile

than water, such as CO. Many comets are known to be active beyond 5 AU (e.g., *Szabo et al.* 2001; *Licandro et al.* 2000; *Lowry and Fitzsimmons* 2001) and even beyond 10 AU (*Meech* 1992), such as 1P/Halley (*West et al.* 1991) and C/1995 O1 Hale–Bopp. The poor spatial resolution when observing such objects at these distances makes accounting for the coma's contribution highly problematic. Once these long-active comets finally do de-activate, the intrinsic faintness of the nuclear signals generally limits the observations to snapshots in one (R) or two (V, R) bands, often with large uncertainties on the ($V - R$) color index.

Nevertheless, in a few cases multiple observations have been secured allowing the construction of a (sometimes partial) light curve, which can be used to investigate the shape and rotational state of the nucleus. Despite these limitations, this approach has been pursued by several groups of ground-based observers and has produced valuable data on the physical properties of cometary nuclei. In addition, and quite recently, near-infrared spectra of a few weakly-active nuclei have been obtained using large telescopes in an attempt to detect spectral signatures (e.g., water ice and minerals). Currently, only Centaurs (e.g., Chiron, Chariklo) present convincing cases of detection of water ice on their surface.

An entirely different approach has been pioneered by Lamy and co-workers (e.g., *Lamy et al.* 1995, 1998a,b, 1999, 2001, 2002) and is based on the very high spatial resolution offered by the *Hubble Space Telescope (HST)*. The basic rationale is that, while the nuclear signal is preserved in the point spread function (PSF) of the telescope, the signal from the coma, an extended source, is diluted as the spatial resolution increases. The contrast between the nucleus and the coma is maximized by observing comets at their minimum geocentric distance. A model for the surface brightness distribution of the nucleus plus coma is constructed and compared to the observed brightness distribution to estimate the

signal from the nucleus. The brightness distribution of the comet is modeled as

$$B(\rho) = [k_n \delta(\rho) + coma] \otimes PSF \tag{1}$$

where ρ is the projected distance from the nucleus, $\delta(\rho)$ is the Dirac delta function, $\otimes$ is the convolution operator, and PSF is the point spread function of the telescope. The first term is the contribution of the nucleus, i.e., the PSF scaled by the factor k_n. The coma can be modeled by any function that provides a reasonable representation of the real coma, for example the canonical k_c/ρ inverse power law, where k_c is a scaling factor, or a generalized k_c/ρ^a, or a more complex function containing radial and azimuthal variations such as implemented for the asymmetric and structured comae of 19P/Borrelly and Hale-Bopp (C/1995 O1). The scaling factor k_n, the sub-pixel locations of the nucleus (x_n, y_n), and the parameters of the coma model (e.g., k_c, a) are determined individually on each image by minimizing the residuals between the synthetic and the observed images. The fits are performed either on the azimuthally averaged radial profiles, or on X and Y profiles, or on the full image. The instrumental magnitudes are calculated by integrating the scaled PSFs and are transformed to Johnson-Kron-Cousins magnitudes.

2.2.2. Interpretation of the Observations

Once the magnitude, m, of the nucleus has been determined, the standard technique introduced by *Russell* (1916) is used to retrieve its physical properties. Russell's original formula, devised for asteroids observed at large phase angles, has been conveniently reformulated by *Jewitt* (1991) and, in the case of a spherical object, is given by

$$p\Phi(\alpha) r_n^2 = 2.238 \times 10^{22} r_h^2 \Delta^2 10^{0.4(m_\odot - m)} \tag{2}$$

where m, p, α, and $\Phi(\alpha)$ are, respectively, the apparent magnitude, the geometric albedo, the phase angle (sun-comet-observer angle) and the phase function $\Phi(\alpha)$ of the nucleus

in the same spectral band (e.g., V or R), $m_\odot$ is the magnitude of the Sun ($V = -26.75$, $R = -27.09$) in the same spectral band, r_h and Δ are, respectively, the heliocentric and geocentric distances of the nucleus (both in AU) and r_n is the radius of the nucleus (in meters). Observers often proceed in two steps, introducing first the absolute magnitude, H, of the nucleus (i.e., the magnitude at $r_h = \Delta = 1$ AU, $\alpha = 0°$):

$$H = m - 5 \log r_h \Delta - \alpha\beta \tag{3}$$

where the phase function is given by:

$$-2.5 \log(\Phi(\alpha)) = \alpha\beta \tag{4}$$

and then incorporating the relationship between r_n (in meters) and p:

$$r_n = \frac{1.496 \times 10^{11}}{\sqrt{p}} 10^{0.2(m_\odot - H)} \tag{5}$$

A linear phase coefficient $\beta = 0.04$ mag/deg is generally used, with an estimated uncertainty of ± 0.02 mag/deg. In fact, a value $\beta = 0.06$ mag/deg has been obtained for 2P/Encke (*Fernández et al.* 2000) and 48P/Johnson (*Jewitt and Sheppard* 2003). For observations at small phase angles, the impact of the phase angle effect on the nuclear magnitude is small, but it becomes overwhelming at large phase angles (e.g., a correction of 2 mag to the nuclear magnitude and a factor 2.5 to the radius at $\alpha = 50°$). Finally, once an albedo is assumed (generally $p_V = p_R = 0.04$), or is independently determined, the radius r_n of the nucleus can be calculated. An uncertainty of ± 0.017 on the albedo appears realistic, at least for ecliptic comets (see section 4.3 below), and has an impact of $\sim$20% on the value of the radius. In summary, for nuclei observed at small phase angles and whose physical properties are not too unusual ($\beta = 0.04 \pm 0.02$ mag/deg and $p = 0.04 \pm 0.017$), the measurement of its magnitude offers a robust determination of its radius, at least of one of its cross-sections in the case of single (i.e., "snapshot") observations.

2.3. Using the Thermal Emission

2.3.1. Observations.

The asteroid community has been using radiometry for over 30 years (e.g., *Allen* 1971) to derive robust sizes and albedos. The application of this method to cometary nuclei began in 1984, i.e., *before* the 1P/Halley apparition (*Campins et al.* 1987), and has been used in earnest since the mid-1990s with the advent of array-detectors sensitive to radiation in the 10 to 20 μm range.

For datasets of outstanding quality – high signal and multiple wavelengths – it is also possible to constrain various fundamental parameters of the the nucleus, such as thermal inertia and surface roughness (see *Campins and Fernández* 2003). If multi-epoch data are obtained, the thermal phase behavior of the nucleus may be deduced. If time series of IR data are taken simultaneously with visible-wavelength photometry, the existence of large-scale albedo spots on the surface may be discovered. Observations at very long (mm or cm) wavelengths provide clues on the emissivity of the bulk material in the nucleus (i.e., sub-surface).

Unfortunately, the difficulties of observing cometary nuclei usually prevent one from obtaining such a robust dataset. The two main problems are related to the usual observational paradigm: when the nucleus is close to Earth and bright, it is often shrouded in coma, but when it is far from the Sun and less active, it is often too faint. Thus, traditionally the best nuclei to observe are those that are weakly active and/or large or nearby. Work by *Campins et al.* (1987), *Millis et al.* (1988), and *A'Hearn et al.* (1989) are excellent examples of successful observations of just such special comets.

The techniques applied at visible wavelengths to deal with the effects of the coma can also be applied to the thermal IR images. Both cases require excellent spatial resolution, but

a complication is that, for the ideal case of diffraction-limited observations where the width of the PSF is proportional to wavelength, the thermal radiation and reflected light sample different scales of the inner coma. Thus, in this case when the dust opacity is constant with wavelength, or decreases with wavelength slower than λ^{-1}, the nucleus-to-coma contrast ratio will generally be larger for the observations at visible wavelengths compared to those made at thermal wavelengths. Since ground-based data in the two wavelength regimes often have similar spatial resolutions owing to the effects of atmospheric seeing, the problem of sampling different spatial scales of the coma usually only applies to spacecraft data. Despite these difficulties, *Jorda et al.* (2000), *Lamy et al.* (2002a) and *Groussin et al.* (2003a) successfully used the *Infrared Space Observatory (ISO)* to detect and characterize several nuclei in the 10 μm region taking advantage of the much better sensitivity to thermal emission resulting from the absence of the warm terrestrial atmosphere.

While typical ground-based thermal measurements are made in the 10 μm atmospheric window (and, less frequently, in the 5 and 20 μm windows), the submillimeter, millimeter, and centimeter windows have been exploited to detect the thermal radio continua of a few very bright nuclei – namely Hale-Bopp (reviewed by *Fernández* 2003), and IRAS-Araki-Alcock (*Altenhoff et al.* 1983).

2.3.2. Interpretation and Analysis.

Once the thermal continuum flux density F_{th} has been measured, it can be interpreted via the equation

$$F_{th}(\lambda) = \epsilon_{th} \int\int B_\nu[T(r_h, pq, \eta, \epsilon_{th}, \theta, \phi), \lambda] d\phi d\cos\theta \; r_n^2 \; \frac{\Phi_{th}}{\pi\Delta^2} \tag{6}$$

where Φ_{th} is the phase function at thermal wavelengths, p is the geometric albedo at reflected wavelengths, B_ν is the Planck function, ϵ_{th} is the emissivity at thermal wavelengths, η is a factor to account for infrared beaming (see *Spencer et al.* 1989), and T is the temperature. The temperature itself is a function of r_h, p, η, ϵ_{th}, the surface cometographic coordinates, θ and ϕ, and the phase integral q, which links the geometric and Bond albedos. Buratti *et al.* (2004) derived $q \simeq 0.3$ for 19P/Borrelly. Traditionally the largest sources of error in this modeling effort came from Φ_{th} and η. Φ_{th} was often parametrized as a function of phase angle, α, such that $-2.5 \log \Phi_{th} \propto \alpha$, but recently the more sophisticated approach of explicitly calculating the surface integral of Planck emission over the Earth-facing hemisphere has become preferable (*Harris* 1998; *Lamy et al.* 2002). The beaming parameter η however is still largerly unconstrained for comets and remains the largest uncertainty; we are only beginning to understand the variety of values possible for near-Earth asteroids comparable in size to the cometary nuclei (e.g. *Delbo et al.* 2003).

For objects with low albedos, such as cometary nuclei, r_n can be determined to good accuracy from their thermal flux density, provided the observations are secured at low phase angles. This is because the thermal emissivity is close to 1, so the thermal emission does not depend strongly on the assumed value for ϵ_{th}. This is to be contrasted with the visible case, where the flux is proportional to the geometric albedo, which is very small and can, in principle, vary by a large factor. Fortunately, the range of values measured for the geometric albedo seems to be rather limited (see the previous section), which means that accurate values for the nuclear radius can be derived solely from the visible data as well. In §2.7, we discuss the measurements of the albedo.

One important caveat to this formulation is that it assumes the nucleus is spherical. Not only does this make r_n an "effective" radius instead of a true radius, but r_n applies only to the Earth-facing cross section at the time the data were taken. Observations over

a rotation period are generally needed to constrain the "mean" effective radius. It is, of course, possible to implement the equations to handle a nucleus of ellipsoidal or even arbitrary shape, although frequently the quality of the data does not warrant such an action. Early work by *Brown* (1985) demonstrated how ellipticity of the nucleus can affect the measured fluxes. More recently, *Gutierrez et al.* (2001) have investigated how arbitrary shapes and variegated surface-ice/surface-dust ratios can affect the thermal behavior of nuclei.

The critical step for this method is to calculate a surface temperature map $T(\theta, \phi)$ of the nucleus for the time at which it was observed. This can be done using a thermal model, the fundamental parameters of which are the rotation period and the thermal inertia (the square root of the product of the conductivity, heat capacity, and bulk density). For most datasets, one of two commonly-used thermal models are usually employed. One, for slow-rotators (a.k.a. "standard thermal model"), applies if the rotation is so slow, or the thermal inertia is so low, that every point on the surface is in instantaneous equilibrium with the impinging solar radiation. The other, for rapid-rotators (a.k.a. "isothermal latitude model"), applies if the rotation is so fast, or the thermal inertia is so high, that a surface element does not appreciably cool as it spins away from local noon and out of sunlight. This model also assumes that the rotation axis is perpendicular to the Sun-Earth-object plane. (For an axis that points at the Sun, the two models predict the same temperature map.) Note that the terms "slow-" and "rapid-rotator" are slightly misleading, in that the thermal inertia is usually the physical quantity that determines the thermal behavior. Thus, two cometary nuclei with identical and long rotation periods, but vastly different thermal inertias, may not necessarily both be "slow-rotators."

Furthermore, small bodies in the outer planets region, at $\sim$10 AU or beyond, can behave like rapid-rotators even if their rotational periods are long. This is because thermal

radiation scales as T^4 and when T is low enough, those bodies do not cool substantially during night time.

In practice, there are few objects in the inner solar system that behave thermally as rapid-rotators, so the slow-rotator model is often employed as the default. Of the cometary nuclei that have been studied, nearly all appear to behave as slow-rotators. The only possible (unconfirmed) exception so far is the very low activity comet 107P/Wilson-Harrington (*Campins et al.* 1995). Among the asteroids, one notable rapid-rotator is (3200) Phaethon (*Green et al.* 1985), which may be a dormant or extinct cometary nucleus. Whether or not the thermal inertias of all highly-evolved comets are low remains to be seen. *Campins and Fernández* (2003) give some upper limits to the thermal inertias of a few nuclei, but, for the most part, these limits are roughly an order of magnitude higher than the expected values.

The applicability of the slow- or rapid-rotator model can be quantified by the parameter Θ, introduced by *Spencer et al.* (1989), which is

$$\Theta = \frac{\Gamma\sqrt{\omega}}{\epsilon\sigma T_{ss}^3}, \tag{7}$$

where Γ is the thermal inertia, ω is the rotational angular frequency, σ is the Stefan-Boltzmann constant, and T_{ss} is the temperature at the subsolar point. Ideal slow-rotators have $\Theta = 0$; rapid-rotators, $\Theta = \infty$. Since Θ depends so steeply on the subsolar temperature, cometary nuclei that mimic slow-rotators near perihelion could conceivably act more like rapid-rotators at aphelion. Due to sensitivity limitations in the mid-IR, at the time of this writing there have been no detections of cometary nuclei at large heliocentric distances, so currently the problem is moot. However, *SIRTF* is expected to detect comets out to $\sim$5 AU from the Sun, so the interpretation of radiometry must proceed with caution.

Enhancements to the thermal modeling can be made and are justified when there are measurements of the nucleus's thermal continuum at many wavelengths. At the very minimum, the 10 μm vs. 20 μm color can be used to discriminate between slow-rotators

and fast-rotators. A further tack is to recognize that comets have a significant near-surface ice component (unlike the asteroids) that is sublimating away and, thus, probably affects their thermal behavior. The "mixed model" introduced by Lamy and co-workers (*Lamy et al.* 2002; *Groussin and Lamy* 2003) employs a water-ice sublimation term when calculating the surface temperature map. The effect is to provide a generally cooler nucleus than otherwise implied by the standard slow-rotator model. The thermal inertia itself can be roughly constrained with this method. For example, very low values of the thermal inertia, about one-fifth that of the Moon, have been derived for Centaurs Chiron and Chariklo by *Groussin et al.* (2003b). Naturally, even more detailed models of nuclear structure and thermal behavior are possible, and these are discussed in the chapter by *Prialnik et al.* (2004).

2.4. Combining Reflected Light and Thermal Emission

If visible and thermal IR observations are performed simultaneously, then it is possible to solve independently for the radius and the albedo of the nucleus using equations 2 and 6 as system with two unknowns, p and r_n. This method has been implemented for a handful of nuclei (see §3.3). In practice, and as emphasized in the above section, r_n is determined by the thermal constraint (i.e., equation 6); consequently the visible constraint (i.e., equation 2) yields the albedo. An illustration of this practical implementation is given by *Lamy et al.* (2002) for the case of 22P/Kopff.

2.5. Light Curves

The light curve (by which we mean the short–timescale series of photometric measurements, not the orbit–timescale study of activity as a function of r_h) provides

information on the shape and rotational period of a cometary nucleus. Only observations at visible (reflected light) and infrared (thermal emission) wavelengths are presently capable of producing such light curves. Very much like the case for asteroids, the periodic temporal variation of the brightness is interpreted in terms of the rotation of an elongated body. Light curves of sufficient length have been obtained for only a few comets (e.g., 2P/Encke), and the interpretation is frequently difficult (e.g., multiple solutions for the rotational period may be found), but the situation has improved with recent data sets that show periods much more clearly (e.g., *Lowry and Weissman* 2003; *Jewitt and Sheppard* 2003). *Samarasinha et al.* (2004) discuss these problems in some detail.

One extra complication is the possibility that the nucleus has a non-uniform albedo, which would add a non-shape related component to the temporal brightness variations. Indeed, spacecraft imaging of 19P/Borrelly revealed some evidence of surface variations (*Soderblom et al.* 2001), although they are difficult to separate from topography effects because of the modest spatial resolution of the images; see *Nelson et al.* (2004) for a discussion of this problem. The possibility of large-scale albedo features on the surface of the nucleus can be ruled out if visible and thermal light curves are obtained simultaneously. Such light curves will be in-phase for shape-dependent rotational modulation and out-of-phase for albedo-dependent modulation. Generally, however, the subject is often disregarded simply because datasets are rarely of sufficient quality to draw definite conclusions.

The default case is to analyze the temporal variation in terms of the varying apparent cross-section of a rotating, elongated nucleus. All observations available so far are consistent with, and interpreted as, rotation of a prolate spheroid (with semiaxes a and $b = c$) around one of the short axes. In a few cases, independent constraints on b and c have been obtained. The projected area of a spheroid in simple rotation is given by

$$S = \pi a b^2 [(\sin^2\phi/a^2 + \cos^2\phi/b^2)\sin^2\epsilon + \cos^2\epsilon/b^2]^{1/2} \quad (8)$$

where ϕ is the rotation angle and ϵ is the angle between the spin vector of the nucleus and the direction to the Earth. Figure 1 displays the ratio S_{min}/S_{max} (also expressed in magnitude variation, Δm) as a function of a/b and ϵ. If the orientation of the spin axis is independently constrained, for example by the shape of the coma (*Sekanina* 1987), the amplitude of the light curve yields the a/b ratio. Together with the absolute magnitude, corresponding to either the minimum or maximum projected areas, one can obtain a solution for the spheroidal shape of the nucleus. Generally, ϵ is not known, so that only a minimum value of a/b can only be obtained, corresponding to $\epsilon = 90°$. The situation is even more difficult for "snapshot" observations, as the effective radius, $r_{n,a}$, which represents the instantaneous projected area, will range between $\sqrt{ab}$ and b. For an axial ratio of 2, $r_{n,a} = 0.707\sqrt{ab}$, i.e., within 30% of the maximum value. The problem is, however, less serious than the above simple analysis tends to imply because the temporal aspect very much helps. As illustrated by the light curve of 19P/Borrelly (Fig. 8 of *Lamy et al.* 1998b), the fraction of time during which the small cross-section is seen is comparatively very short and may even be missed if the time resolution of the observations is not adequate. Consequently, a rotating spheroid displays a cross-section close to its maximum most of the time. As discussed by *Weissman and Lowry* (2003), the integration over all possible (random) orientations and rotational phases shows that the average projected area remains a large fraction $\kappa_n \pi ab$ of its maximum value πab: $\kappa_n = 0.924$ for $a/b = 1.5$, $\kappa_n = 0.892$ for $a/b = 2$, and $\kappa_n = 0.866$ for $a/b = 3$. For the effective radius, $r_{n,a}$, given by the instantaneous projected area, the scaling varies as $\sqrt{\kappa_n}$. For a typical axial ratio $a/b = 2$, a snapshot observation will, on average, lead to $r_{n,a} = 0.945\sqrt{ab}$, i.e., within 5.5% of the maximum value $\sqrt{ab}$. Even more important for questions such as the size distribution function is the *effective* radius, $r_{n,v}$, that of the sphere having the same volume (or mass) as the spheroid, via $r_{n,v}^3 = ab^2$. The ratio $r_{n,v}/r_{n,a}$ remains close to 1 with value of 0.972 for $a/b = 1.5$, 0.943 for $a/b = 2$, and 0.895 for $a/b = 3$. To summarize, the radius calculated

from an observed, apparent projected area will give, on average, an excellent estimate of the effective radius of the equivalent sphere. Note that the averaging with respect to rotational phase is implicitly done when authors average their data values that are too scarce to construct a credible light curve.

A light curve does not strictly gives access to a projected area. In the visible, the bidirectional reflectance comes into play but will not be a problem if the scattering properties are homogeneous over the nuclear surface. In the thermal infrared, it is the 2-dimensional distribution of temperature over the surface that comes into play, and that is certainly not homogeneous. For example, *Brown's* (1985) non-spherical thermal model predicts that the amplitude of the light curve will be larger in the infrared than in the visible, an effect apparently observed on 10P/Tempel 2 (*A'Hearn et al.* 1989). With the whole question of how to interpret the light curve of cometary nuclei still in its infancy, interpretations beyond the simple spheroidal model discussed above are not warranted. Complex effects, such as shadowing and unilluminated areas, cannot yet be handled properly but have already been noted (e.g., the skewness of the light curve of 9P/Tempel 1, *Lamy et al.* 2001).

2.6. Radar Observations

Studies of cometary nuclei using radar are discussed by *Harmon et al.* (2004). For completeness, we provide here a brief outline of the method. Basically, one sends a burst of microwaves of known power towards a nucleus and measures the power of the returned echo. There have been 6 such detections of nuclei, although in only two cases, C/1983 H1 (IRAS-Araki-Alcock) and C/1996 B2 (Hyakutake), is the signal-to-noise better than 4. There are as yet no delay-Doppler "images" of a cometary nucleus, as are now being routinely created for close-approaching near-Earth asteroids. The main reason is the

scarcity of comets that can overcome the Δ^{-4} dependence for detectability. In terms of the properties of nuclei, the radar data have mostly been used to constrain the radar-albedo and density, via arguments related to the bulk dielectric properties of cometary nuclei and their response to microwaves. The radar albedos are apparently similar to the visible-wavelength albedos. The bulk densities range between 0.5 to 1.5 times that of water, values that are not unexpected.

2.7. Occultations

Occultations are frequently used to constrain the shape and size of asteroids, and can provide a direct test of the validity of other methods, such as radiometry (§2.3). In principle, the same could be done for comets. An occultation trace may also have wings, owing to non-negligible optical depth in the inner coma, and this could provide information on dusty gas hydrodynamics in the inner coma and the location of active regions on the surface. In practice, this method is limited by the difficulty of locating a nucleus accurately within a surface brightness distribution that is dominated by coma for most astrometric observations, and in finding suitable stars that are occulted. Even a subarcsecond positional error perpendicular to the proper motion can shift the path of the comet's shadow on Earth by hundreds or thousands of kilometers. Given that the nucleus in question is typically on the order of 1 to 10 km across, the difficulty of obtaining a successful observation becomes apparent. Moreover, obtaining the ideal dataset with multiple chords through the nucleus requires tight spatial sampling across the predicted path, which can be logistically difficult with limited labor resources and equipment.

Currently the most useful occultation event observed is one by (the weakly-active and large) Centaur Chiron (*Bus et al.* 1996). One chord through most of the nucleus and one possibly grazing chord were observed, and this constrained the radius to be at least

90 ± 7 km. Chiron's ellipsoid is within 10% of spherical, so this is thought to be a robust lower limit. Ground-based radiometric data (*Campins et al.* 1994; *Fernández et al.* 2002) currently imply a radius of ∼80 km while space (ISO) data give 71 ± 5 km (*Groussin et al.* 2003b), so the agreement is not really satisfactory.

Another occultation event, this one by C/1995 O1 Hale-Bopp, was reported by *Fernández et al.* (1999b). Only one chord was measured, and, if real, it is impossible to tell if this chord went through the nucleus, grazed the nucleus, or passed near by. The optical depth of the inner coma may have been significant (i.e., approaching unity) for several tens of kilometers (cf., *Weaver and Lamy* 1997). With some reasonable assumptions about the dust outflow, the occultation constrained the (assumed-spherical) radius of the nucleus to be no larger than 48 km. With further restrictive assumptions, the upper limit is ∼30 km.

There are several other occultations by comets mentioned in the literature, but none of them have probed the nucleus.

2.8. Measuring the Albedo

One must be careful to specify what is meant by the term "albedo" because many different definitions are used. In this paper, we report values for the geometric albedo (p), which is defined as the zero-phase, disk-integrated reflectance relative to that produced by a "perfect" diffusing disk (cf., *Hanner* 1981). Sometimes the Bond albedo (A) is used instead of the geometric albedo; this is just the fraction of incident light that is scattered in all directions and is related to the geometric albedo by:

$$A = pq \tag{9}$$

where q is the phase integral, which is given by (cf., *Allen* 1973):

$$q = 2 \int \Phi(\alpha) \sin(\alpha) d\alpha, \tag{10}$$

where $\Phi(\alpha)$ is the disk–integrated, normalized phase function and α is the phase angle. Note that both albedos are functions of wavelength. In the energy balance equation for the surface of the nucleus, one must calculate the quantity:

$$\frac{\int F_{\odot}(\lambda)A(\lambda)d\lambda}{\int F_{\odot}(\lambda)d\lambda}, \tag{11}$$

which *Clark et al.* (1981) defines as the bolometric Bond albedo A_B, and which is wavelength independent. However for A that varies only slightly with wavelength, say for a grey object, the value at a particular wavelength will suffice and $A \simeq A_B$.

Various complications arise when attempting to derive photometric properties from disk-resolved imagery of the nucleus. So far, we have such data on comets 1P/Halley and 19P/Borrelly. For an unresolved image of a nucleus, we work with a body that has a subsolar point, and the geometric albedo is simply the true albedo at that point. In that case, we also employ a phase-darkening function to describe the photometric behavior from our (non-zero phase) vantage. For a resolved element of area on the surface of a nucleus, there is likely no subsolar point, and we must account for sunlight impinging on the element with some non-zero zenith angle. Thus, an understanding of the scattering is crucial to disentangle albedo and scattering effects. In a few cases (e.g., asteroid Eros [*Clark et al.* 2002]), one has a full shape model of the object in question, and then one can use (a) the observed disk-resolved photometry, and (b) the known scattering geometry as a function of position on the nucleus, to derive fundamental scattering parameters. Most commonly, the formulation presented by *Hapke* (1986) is used.

The most straightforward, assumption-free way to obtain the geometric albedo from resolved imaging of the nucleus is to combine the projected area S known from resolved images with remote photometry of the unresolved nucleus which gives pS as discussed in §2.2. Then the ratio unambiguously yields the geometric albedo p of the nucleus. In practice, this does usually require a good understanding of the rotational state, shape and

phase function of the nucleus, since in most cases the resolved imaging and the ground-based data will have been obtained at different epochs. The resolved imaging must be matched to the remote viewing, which may be at a different aspect angle, and certainly one needs to match the rotational state and the projected area. Application of this procedure to the nucleus of 19P/Borrelly will be discussed in §3.3.1 below.

Returning to disk-integrated (unresolved) data on a cometary nucleus, the radiometric method (§2.3) is currently the most common way to derive the visible and near-IR geometric albedo. Whereas one usually only needs the IR equation to obtain a good estimate of the nuclear radius (since almost all of the incident energy is absorbed and then thermally re-radiated), the full method – solving both equations for the two unknowns – is required in order to have a confident, robust albedo measurement. Simultaneity, or an understanding of the rotation state, is also critical.

Another method involves deriving the radar albedo from radar echoes, and assuming that the reflectivity of the nucleus at centimeter wavelengths is similar to that at visible wavelengths. The existing radar data are discussed by *Harmon et al.* (2004). Generally, radar albedos seem to be as dark as their visible counterparts, but the quality of the radar data on cometary nuclei are not yet good enough to make a robust comparison between albedos in the two wavelength regimes.

3. PROPERTIES OF COMETARY NUCLEI

We now present a detailed discussion of the available data on the physical properties of cometary nuclei: size, shape, albedo, color and rotational period. The bulk of these data comes from six sources, which we briefly describe below. Additional sources will be introduced when discussing individual comets.

3.1. The Main Sources of the Data

3.1.1. Scotti (unpublished)

The largest data set obtained by a single observer with the same instrument (the 91 cm *Spacewatch* Schmidt-telescope at Kitt Peak equipped with a CCD camera) has, unfortunately, never been published, but a short note entitled *Comet Nuclear Magnitudes* dated January 14, 1995 (hereafter denoted *Sc*) has been widely circulated in the cometary community. Scotti applied a rudimentary technique to subtract the coma assuming a constant surface brightness inward from a thin annulus having a radius of a few times the radius of the seeing disk (a more detailed description and an evaluation of this method are given by *Tancredi et al.* 2000). This is obviously an oversimplification, and it always leads to an overestimation of the brightness of the nucleus by an amount that depends entirely on its activity. Scotti produced a table giving the absolute magnitude of 62 cometary nuclei from which he calculated a radius, assuming an albedo of 0.03 (they are reproduced here but scaled to an albedo of 0.04), convincingly demonstrating that the bulk of them are very small bodies with sizes of a few km. These results have further been very useful to estimate the exposure times for space-based observations.

3.1.2. Lamy et al. (1995, 1996, 1998a,b, 1999, 2000, 2001, 2002a,b), Jorda et al. (2000), Groussin et al. (2003a, 2004), Toth et al. (2003):

The approach employed by this group (hereafter denoted *La+*), which is to use the high spatial resolution of the *HST* to photometrically resolve the nucleus, has already been described in §2.2.1. Except for the few cases of complex comae, such as that of Hale-Bopp (C/1995 O1), the residuals between the observed and modeled images are usually very small, typically a few percent of the signal in the brightest pixel. Figure 2 illustrates the solution

obtained from the *HST* observations of 19P/Borrelly (a spheroid), in comparison with the best in-situ image obtained by the camera on the *Deep Space 1* spacecraft. Thirty one nuclei have been detected during the *HST* observations, all active except for 9P/Tempel 1, which was observed at $r_h = 4.48$ AU. For 18 comets only snapshot observations were obtained (i.e., one *HST* orbit per comet), while light curves were measured for 13 nuclei (8 *HST* orbits per comet, except 6 for 19P/Borrelly and 11 for 67P/Churyumov–Gerasimenko). The derived nuclear magnitudes were converted to standard R-band values, which were then used to derive sizes by adopting an albedo of $p_R = 0.04$ and a phase coefficient of $\beta = 0.04$ mag deg^{-1}.

3.1.3. Licandro et al. (2000)

This group (hereafter denoted *Li+*) has used several ground-based telescopes to observe 18 comets at large heliocentric distances to minimize possible coma contributions. No attempt has been made to subtract the contribution from the coma, although 7 comets were conspicuously active (6 of them at $r_h > 4$ AU). The 11 others were deemed inactive on the basis of their stellar appearance. The nuclear sizes were derived from the V magnitudes assuming $p_V = 0.04$ and $\beta = 0.04$ mag deg^{-1}. For reasons of consistency, we prefer using R magnitudes in the discussion below and in the tables presented later. Accordingly, we converted V magnitudes to R values assuming $(V - R) = 0.5$, the median value for the ecliptic comets (*Toth and Lamy* 2000), with the following exceptions: (i) 52P/Harrington–Abell, which was observed in the R band, (ii) 49P/Ashbrook–Jackson, 74P/Smirnova–Chernykh and 96P/Machholz 1, for which $(V - R)$ was independently determined.

3.1.4. Lowry et al. (1999), Lowry and Fitzsimmons (2001), Lowry et al. (2002), Lowry and Weissman (2003):

This group (hereafter denoted *Lo+*) uses a method similar to that described above, i.e., ground-based observations at large r_h. Out of 73 comets targeted, only 28 were deemed inactive on the basis of their stellar appearance, and the measured R magnitudes were converted to sizes using $p_R = 0.04$ and $\beta = 0.035$ mag deg^{-1}. As most of the comets were observed at small phase angles, the difference between using $\beta = 0.035$ and $\beta = 0.04$ is usually small (e.g., a 2.3% increase in the radius for $\alpha = 10°$), but will be applied for consistency. The remaining 45 comets were either active or were not detected, so that only an upper limit on the size of the nucleus could be obtained.

3.1.5. Meech et al. (2004)

This group (hereafter denoted *Me+*) observed 16 Jupiter family (JF) comets and 1 Halley type (HT) comet (109P/Swift–Tuttle) with the *Keck* telescope using the method described above. They concluded that 11 JF comets, as well as 109P, were inactive based on their stellar appearance. Their V and R magnitudes were converted to sizes using $p_V = p_R = 0.04$ and $\beta = 0.04$ mag deg^{-1}. This leads to two different values for the radius (except for 9P/Tempel 1), and we only compiled those corresponding to the R magnitudes for reasons of consistency. For 9P, we transformed the V to R magnitudes using $(V - R) = 0.5$ and obtained $r_n = 3.04$ km. The remaining 5 comets were active and only an upper limit to the size could be obtained. In a separate program, this group used the Wide-Field camera of the *HST* to search for five NICs at geocentric distances ranging from 20 to 29 AU, but none were detected and only upper limits could be placed on the sizes of their nuclei.

3.1.6. Tancredi et al. (2000)

This group (hereafter denoted *Ta+*) has compiled a set of 3990 measurements of "nuclear" magnitudes obtained from a variety of sources, mainly the Comet Light Curve Catalogue of *Kamél* (1990, 1992), the Minor Planet Center data base (thus including the results of Scotti presented above), the IAU Circulars, the International Comet Quarterly, and various scientific articles. The bulk of their analysis consisted of scrutinizing these inhomogeneous data and making sense of them. They rejected all magnitudes determined visually, performed various corrections, and plotted the resulting heliocentric brightnesses. Their "best estimates" of the absolute visual magnitudes $H_N = V(1, 1, 0)$ generally corresponds to the faintest observed magnitudes and were used to derive sizes using $p_V = 0.04$ and a coefficient $\beta = 0.04\,\mathrm{mag\,deg^{-1}}$ to correct for phase angle. They have introduced four quality classes (QC) which roughly quantifies the uncertainties affecting the nuclear magnitudes, from ± 0.3 mag (QC1) to ± 1 mag (QC4). The respective numbers of nuclei are 9 for QC1, 18 for QC2, 37 for QC3 and 41 for QC4 for a total of 105 nuclei. It is readily seen that the bulk of the sizes belongs to the lowest quality classes. An updated version of this catalog has been presented by *G. Tancredi* at the *Asteroids, Comets, Meteors 2002* conference and has been kindly made available to us. Those results are included in Table 1, but we have no means of assessing the quality of these improved determinations.

3.2. Sizes, Shapes, and Rotational Properties

In this section, we provide short summaries of the physical properties of individual comets. First we treat the *ecliptic* comets, and then we discuss the *nearly–isotropic* comets. Unless otherwise stated, r_n refers to the "effective radius", i.e., the value for the sphere having the same volume as the observed object. The albedo measurements are discussed separately in the next section.

3.2.1. Ecliptic Comets (ECs)

2P/Encke: A robust radiometric measurement of the size is reported by *Fernández et al.* (2000): 2.4 ± 0.3 km. This number is consistent with an earlier radiometrically–derived upper–limit of 2.9 km by *Campins* (1988). Visible-wavelength estimates of the size have frequently suffered from the spatially–unresolved coma that this comet displays at nearly every aphelion. *Fernández et al.* (2000), updating a compilation by *Sekanina* (1976), review the "nuclear" magnitudes that have been published since the 1960s and find that the data having the least coma contamination are: from *HST* in 1997 (published in that same paper), by *Garradd* (1997) in 1997, and by *Jewitt and Meech* (1987) in 1986. *Jewitt and Meech* (1987) state that the maximum radius of the nucleus is $2.8 \leq r_n \leq 6.4$ km, assuming albedos between 0.02 and 0.10, which is consistent with the later radiometric observations. Some photographic photometry was useful in constraining the absolute magnitude of the nucleus: for example, observations by *Van Biesbroeck* (1962) in 1960, and by Roemer in 1973 (reported by *Marsden* 1974) and 1974 (reported by *Marsden and Roemer* 1978). Finally *Fernández et al.* (2000) report an attempt to reconcile all published light curves to derive a shape; the lower limit on one of the axial ratios was found to be 2.6, indicating a very elongated nucleus. The rotational period was constrained in the 1980s by *Jewitt and Meech* (1987) and *Luu and Jewitt* (1990a), using time series of CCD photometry. A period of $P = 15.08$ hours (or possibly $\frac{3}{2}P = 22.62$ hours) satisfied all the data. However, more recent data from 2001 and 2002 presented by *Fernández et al.* (2002b) and *Lowry et al.* (2003) indicate that the dominant periodicity may have changed in the intervening years (or was poorly measured in the past). Currently, a period near $P = 11.01$ or $2P = 22.02$ hours (close to the above value of 22.62 hours) fits the data best. Furthermore, the dominant periodicities from the 1980s are not consistent with the most recent data. The situation hints that the nucleus of 2P/Encke may perhaps be in a complex rotation state (cf., *Belton*, 2000), although further investigations are necessary before a definite conclusion can be

drawn.

4P/Faye: Observed with the HST by *La+* in October–November 1991 and in February 2000. We favor the value $r_n = 1.8\,\mathrm{km}$ obtained in 2000 with the aberration–free *HST* . Re-examination of the 1991 observations obtained with the aberrated *HST* indicates that the signal from the nucleus was overestimated.

6P/d'Arrest: A snapshot observation by *Me+* at $r_h = 5.4\,\mathrm{AU}$ of the inactive nucleus yields $r_n = 1.71\,\mathrm{km}$. *Lo+* first determined an upper limit of 2.1 km and later obtained a partial light curve. They derived a mean effective radius of $r_{n,v} = 1.6 \pm 0.06\,\mathrm{km}$ (scaled to $\beta = 0.04\,\mathrm{mag\,deg^{-1}}$), and $a/b > 1.18 \pm 0.08$. The size determinations from *Me+*, *Lo+*, and *Ta+* (1.5 km) are in good agreement but are considerably smaller than previous estimates of 3.5 km by *Campins and Schleicher* (1995) using IR photometry and of 2.7 km by *Meech* (unpublished). Determinations of the rotational period have been reported by *Fay and Wisniewski* (1978): 5.17 hr, *Lowry and Weissman* (2001): $7.2 \pm 0.12\,\mathrm{hr}$ and *Gutiérrez et al.* (2003): $6.67 \pm 0.03\,\mathrm{hr}$. The apparent discrepancies have been thoroughfully analyzed by the last authors who concluded that, if all these measurements are correct, a change in the period has taken place or the nucleus is in a complex rotational mode. We adopt 7.0 hr as a reasonable estimate for the present period of 6P.

7P/Pons–Winnecke: A snapshot observation by *Lo+*, when the comet was apparently inactive at $r_h = 5.58\,\mathrm{AU}$ yields $r_n = 2.6 \pm 0.1\,\mathrm{km}$.

9P/Tempel 1: The two extreme cross-sections observed by *La+* give $r_n = 2.8$ and 3.3 km. Converting the V magnitude measured by *Me+* to an R magnitude using an average $(V - R) = 0.52$, yields $r_n = 3.07\,\mathrm{km}$, in excellent agreement with the above range and with the upper limit of $3.2 \pm 0.1\,\mathrm{km}$ determined by *Lo+* without any correction. We very much doubt that the subsequent comatic correction introduced by *Lo+* and the resulting $r_n = 2.3\,\mathrm{km}$ are correct. As discussed above, comatic corrections of ground-based

images remain highly problematic. The brightness obtained by *La+* and *Weissman et al.* (1999) lead to spheroidal solutions for the nucleus, assuming an aspect angle of ∼90°, that are in remarkable agreement: $a = 3.8 - 3.9\,\mathrm{km}$ and $b = 2.8 - 2.9\,\mathrm{km}$. *Fernández et al.* (2003) obtained simultaneous visible and near-infrared observations at $r_h = 2.55\,\mathrm{AU}$ outbound while the comet was still quite active. Two different methods were used to correct for the contribution of the coma ($\simeq 15\%$) in their mid-infrared measurements and their interpretation using the standard thermal model leads to a radius of the maximum cross-section of the nucleus of $3.0 \pm 0.2\,\mathrm{km}$. Combining this result with that of *La+* gives $p_R = 0.048 \pm 0.007$, significantly different (but still within the respective uncertainties) from the value $p_R = 0.072 \pm 0.016$ derived by *Fernández et al.* (2003). Their large albedo is probably a consequence of their inability to properly account for the large coma contribution in their visible observations. Combining the above albedo $p_R = 0.048$ with the measurements of *La+* and *Weissman et al.* (1999) leads to a spheroidal solution with $a = 3.5\,\mathrm{km}$ and $b = 2.6\,\mathrm{km}$ and an effective radius $r_{n,v} = 2.9\,\mathrm{km}$. From their partial light curve, *La+* extrapolated a rotational period in the range of ∼25–33 hr. *Fernández et al.* (2003) found that a longer period ∼41 hr (1.71 d) does not contradict their observations obtained at three different epochs.

10P/Tempel 2: An early, in-depth investigation led *Sekanina* (1987) to constrain the orientation of the rotation axis of the nucleus and its gross physical properties. 10P was extensively observed by *A'Hearn et al.* (1989), who combined optical and infrared photometry, and by *Jewitt and Luu* (1989), who performed CCD photometry from aphelion (thus convincingly detecting a bare nucleus) to perihelion. Their interpretations converge to a spheroidal nucleus with $a = 8 - 8.15\,\mathrm{km}$ and $b = c = 4 - 4.3\,\mathrm{km}$ with an albedo $p_R = 0.024 \pm 0.005$ and a rotational period of ∼9 hr. The effective radii are $r_{n,a} = 5.7 - 5.9\,\mathrm{km}$ and $r_{n,v} = 5.0 - 5.3\,\mathrm{km}$ The revised values by *Campins et al.* (1995) remain in agreement with these results. Various snapshot observations are also in agreement

with these results assuming the above albedo of 0.024 except as noted: *Mueller* (1992), $r_n = 5.9\,\mathrm{km}$; *Mueller and Ferrin* (1996), $r_n = 5.2\,\mathrm{km}$ ($p = 0.022$); *La+*, $r_n = 5.9\,\mathrm{km}$; *Me+*, $r_n = 6.4\,\mathrm{km}$. The value of *Ta+* scaled to $p_R = 0.024$, i.e., $r_n = 3.7\,\mathrm{km}$, is inconsistent with the above results.

14P/Wolf: A snapshot observation by *Lo+*, when the comet was apparently inactive at $r_h = 3.98\,\mathrm{AU}$ yields $r_n = 2.33 \pm 0.12\,\mathrm{km}$. The enormous scatter of the data points of *Ta+* makes their estimate of $r_n = 1.3\,\mathrm{km}$ highly uncertain.

15P/Finlay, 16P/Brooks 2: The large scatter of the data points of *Ta+* makes their estimates highly uncertain.

17P/Holmes: A snapshot HST observation by *La+* yields $r_n = 1.71\,\mathrm{km}$.

19P/Borrelly: A complete solution was first proposed by *La+*: $a = 4.4 \pm 0.3\,\mathrm{km}$, $b = 1.8 \pm 0.15\,\mathrm{km}$ assuming an albedo of 0.04 (see section 3.3.1 for a discussion of this issue). The in-situ observations of Deep Space 1 (*Soderblom et al.* 2002; *Buratti et al.* 2003) yield $a = 4.0 \pm 0.05\,\mathrm{km}$ and $b = 1.6 \pm 0.04\,\mathrm{km}$. The above determination gives $r_{n,a} = 2.5\,\mathrm{km}$ and $r_{n,v} = 2.2\,\mathrm{km}$. The snapshot results of *Lo+* and *Weissman et al.* (1999) are consistent with the above solution. The rotational periods $P = 25.0 \pm 0.5\,\mathrm{hr}$ found by *La+* and that obtained by *Mueller and Samarasinha* (2001), $P = 26\,\mathrm{hr}$, are in excellent agreement.

21P/Giacobini–Zinner: A snapshot observations by *Mueller* (1992) at $R_h = 3.75\,\mathrm{AU}$ gives $r_n = 2.1\,\mathrm{km}$ (using an albedo of 0.04) and $a/b > 1.5$. The heliocentric light curve of *Ta+* indicates that the comet was still active at that distance and that their estimate $r_n = 1.0\,\mathrm{km}$ derived from observations beyond 4.5 AU is reasonable. A rotational period of $9.5 \pm 0.2\,\mathrm{hr}$ has been reported by *Leibowitz and Brosch* (1986).

22P/Kopff: Combined visible and infrared photometry (*La+*) leads to $r_n = 1.67 \pm 0.18\,\mathrm{km}$ and $p_V = 0.042 \pm 0.006$ ($p_R = 0.047$). The slightly different value of $r_n = 1.52\,\mathrm{km}$, reported

by *Jorda et al.* (2000), resulted from an early, less elaborate analysis of the same data. The visible light curve built from the eight *HST* observations spanning ∼12 hr had a small range of 0.14 ± 0.07 mag and could not constrain the rotational state. The snapshot observation at $r_h = 5.11$ AU by *Lo+*, when scaled to $p_R = 0.047$, gives $r_n = 1.65 \pm 0.1$ km, in remarkable agreement with the above results, as well as with the value estimated by *Ta+* ($r_h = 1.8$ km). A partial light curve recently obtained by *Lo+* at $r_h = 4.49$ AU clearly suggests a rotational period of 12.30 ± 0.8 hr and an amplitude range of 0.55 ± 0.07 mag, corresponding to a minimum axial ratio of 1.66 ± 0.11 and a mean effective radius $r_n = 2.76 \pm 0.12$ km (scaled to $p_R = 0.047$ and $\beta = 0.04$ mag deg−1). As discussed by *Lowry and Weissman* (2003), their solution is totally inconsistent with the above results (the pole-on view assumed for the *La+* observations must have resulted in a near-maximum cross section assuming a nucleus in simple rotation) but is consistent with unpublished results by *Meech* obtained at $r_h = 4.73$ AU: $r_n = 2.8$ km and $P_{rot} = 12.91$ hr. In an early study of 22P, *Sekanina* (1984) found $P = 9.4 \pm 1.3$ hr. At this stage, it is impossible to reconcile the two groups of observations without considering more complex solutions for the rotational state and the shape of the body. For the time-being, we keep the self-consistent solution of *La+* for the size and albedo and the values of a/b and P_{rot} from *Lo+*.

24P/Schaumasse: The large scatter in the data used by *Ta+* makes their estimate highly uncertain.

26P/Grigg–Skjellerup: A stellar–like nucleus was observed by *Boehnhardt et al.* (1999) and by *Li+*, and they derived radius values of 1.44 ± 0.05 and 1.57 km, respectively. However, a non-detection by *Lowry et al.* (1999) places an upper limit on the radius of 1.2 ± 0.1 km. The graph presented by *Ta+* suggests an inactive nucleus beyond ∼2 AU, and their estimated radius of 1.3 km seems reasonable. A spheroid with $a \sim 2.2$ km and $b \sim 1$ km (i.e., $a/b = 2.2$) would be consistent with all the above results. This solution corresponds to

$r_{n,v} = 1.3\,\mathrm{km}$. Radar observations yielded a lower limit $r_n > 0.4\,\mathrm{km}$ (*Kamoun et al.* 1982, 1999).

28P/Neujmin 1: This low activity nucleus has been extensively studied and is the second largest EC in the sample. *Campins et al.* (1987) combined visible and infrared photometry when the comet made a relatively close encounter with Earth but was at a large phase angle ($\sim 30°$). The maximum value of the infrared flux leads to $r_n = 10.6 \pm 0.5\,\mathrm{km}$ and $p_V = 0.026$. Their single minimum value is not consistent with a light curve having $P = 12.75\,\mathrm{hr}$ (*Delahodde et al.* 2001) and, in addition, brings the albedo down to an unrealistic value of $p_V = 0.016$. Visible photometry yields $r_n = 10.0\,\mathrm{km}$ (*Jewitt and Meech* 1988) with $p_R = 0.03 \pm 0.01$, and $r_n = 11.4\,\mathrm{km}$ (*Me+*). The visible albedo $p_V = 0.026$ and the color $(V - R) = 0.45$ leads to $p_R = 0.04$, so that the above values of r_n need not be scaled. Assuming that (*Me+*) observed the largest projected area πab, and that $a/b = 1.5$ (in fact, a lower limit obtained by *Delahodde et al.* 2001), we obtain $a = 14.0\,\mathrm{km}$, $b = 9.3\,\mathrm{km}$ and $r_{n,v} = 10.7\,\mathrm{km}$, which is our current best estimate A detailed analysis of a large set of observations led *Delahodde et al.* (2001) to determine a rotational period of $12.75 \pm 0.03\,\mathrm{hr}$, in good agreement with previous measurements.

29P/Schwassmann–Wachmann 1: This is the largest EC in our sample, but there is some confusion regarding the classification of this comet. With a Tisserand parameter $T_J = 2.983$, it qualifies as an EC but its orbit also satisfies the strict definition of Centaurs given by *Jewitt and Kalas* (1998): $q \geq 5\,\mathrm{AU}$ and $a \leq 30\,\mathrm{AU}$ (corresponding to the orbits of Jupiter and Neptune, respectively). Thus duality arises because the criteria for the two classifications are not consistent, T_J for ECs and q and a for the Centaurs. The current perihelion of 29P is less than 0.3 AU outside of Jupiter's aphelion, and it could easily be perturbed into a fully-crossing orbit in the near future. On the other hand, its albedo of 0.13 ± 0.04 (*Cruikshank and Brown* 1983), if correct, is totally atypical of cometary nuclei

(see §3.3) while being common among Centaurs (*Barucci et al.* 2004). Various estimates of its radius based on visible magnitudes range from 21 to 52 km assuming an albedo of 0.04. *Cruikshank and Brown* (1983) combined thermal measurements at 20 μm and visible photometry to obtain $r_n = 20.0 \pm 2.5$ km and $p_V = 0.13 \pm 0.04$. They correctly noted that the size is controlled by the infrared measurements, while the albedo is controlled by the visible magnitude, which was *estimated*. *Meech et al.* (1993) argued that 29P is probably never totally inactive and attempted to estimate the coma contribution by measuring the total nucleus+coma signal in apertures of different sizes. They determined a minimum axial ratio of 2.6 and, assuming $p_R = 0.04$ and $\beta = 0.04$ mag deg^{-1}, a rotationally averaged radius of $r_n = 15.4 \pm 0.2$ km, a value that we presently select. However, using an albedo of 0.13 reduces this value to 8.6 ± 0.1 km. For the rotational state of 29P, we adopt the simple rotation with a period of 14.0 hr (*Meech et al.* 1993), consistent with the rough estimate of 10 hr reported by *Luu and Jewitt* (1993). However, the former authors determined a second period of 32.2 hr implying a complex state of rotation.

31P/Schwassmann–Wachmann 2: Observed as a star-like object at $r_h = 4.58$ AU by *Luu and Jewitt* (1992), who derived a radius of 3.1 km, a minimum axial ratio of 1.6, and a rotational period of 5.58 ± 0.03 hr.

33P/Daniel: The value of *Ta+* looks questionable because of the large scatter in the data.

36P/Whipple: A snapshot observation of a star-like nucleus at $r_h = 4.43$ AU by *Lo+* give $r_n = 2.28 \pm 0.21$ km, which is consistent with the value quoted by *Ta+*, $r_n = 2.3$ km.

37P/Forbes: The stellar-like appearance at $r_h = 3.59$ AU led *Li+* to derive $r_n = 1.1$ km, close to the value of 1.0 km estimated by *Ta+*. *La+* obtained a slightly smaller value, $r_n = 0.81$ km. If the above authors observed different extreme cross–sections, the spheroidal solution leads to $a = 1.38$ km, $b = 0.8$ km (not unrealistic since $a/b = 1.73$), and

$r_{n,v} = 0.96\,\mathrm{km}$.

39P/Oterma: The heliocentric light curve reported by *Ta+* does not allow a reliable derivation of the size.

40P/Väisälä 1: Undetected by *Lo+*, thus giving an upper limit $r_n < 3.6 \pm 0.2\,\mathrm{km}$. The estimate of $r_n = 1.5\,\mathrm{km}$ by *Ta+* is reasonable, although an error bar of $\pm 1\,\mathrm{km}$ is warranted given the large scatter in the data.

41P/Tuttle–Giacobini–Kresák: The heliocentric light curve of *Ta+* indicates that this is a very small nucleus; $r_n = 0.7\,\mathrm{km}$ is probably a good estimate, but even this may only be an upper limit.

42P/Neujmin 3: There is too much scatter in the data used by *Ta+* to derive a reliable size of the nucleus. *Kresák et al.* (1984) reported that this comet and 53P/Van Biesbroeck are fragments from a parent comet that split in March 1845.

43P/Wolf–Harrington: Two determinations have been reported by *Lo+* from observations at $r_h = 4.87\,\mathrm{AU}$, $r_n = 3.3 \pm 0.7\,\mathrm{km}$, and at $r_h = 4.46\,\mathrm{AU}$, $r_n = 3.4 \pm 0.2\,\mathrm{km}$, when the comet had a stellar appearance. At $r_h = 3.04\,\mathrm{AU}$ outbound, the comet was very active, displaying both a coma and a tail, leading *Li+* to impose $r_n \ll 3.1\,\mathrm{km}$. On the following inbound branch, the comet was reported active at $r_h = 3.9\,\mathrm{AU}$ (*Hainaut et al.* 1996). The graph of *Ta+* convincingly shows a monotonic decrease of brightness as r_h increases up to 4 AU, the faintest value yielding $r_n = 1.8\,\mathrm{km}$. A spheroidal solution based on the two above extreme cross-sections leads to $a = 6.4\,\mathrm{km}$, $b = 1.8\,\mathrm{km}$, and $a/b = 3.6$, which would be unusually large. Pending further observations, we are inclined to think that the large values of *Lo+* are not correct and that $r_n = 1.8\,\mathrm{km}$ (*Ta+*) is a realistic estimate. Finally, it must be noted that 43P has undergone major orbital changes in the recent past (e.g., q decreased from 2.5 to 1.5 AU in 1936) and this could explain surges of vigorous

activity thereafter.

44P/Reinmuth 2: A snapshot observation by *La+* gives $r_n = 1.61$ km. The estimate of 1.5 km by *Ta+* (but with considerable scatter in the data), and the upper limit of 3.1 km from *Lo+*, are consistent with that choice.

45P/Honda–Mrkos–Pajdusakova: La+ obtained a mean value of $r_n = 0.34 \pm 0.01$ km from observations performed on two consecutive days, making this nucleus one of the smallest ever observed. However, they pointed out that the potentially large systematic error because of the large phase angle ($\alpha \simeq 90°$) during the observations. In fact, if 45P/HMP is as phase darkened as 2P/Encke and 48P/Johnson, then a linear phase coefficient $\beta = 0.06\,\mathrm{mag\,deg^{-1}}$ should be applied instead of the standard value of $0.04\,\mathrm{mag\,deg^{-1}}$, and this leads to $r_n = 0.78$ km. The snapshot observation of *Lo+* gives a much larger value of $r_n = 1.34 \pm 0.55$ km, but the large error bar means that r_n could be as small as 0.79–0.82 km if $\beta = 0.06\,\mathrm{mag\,deg^{-1}}$ is applied, in agreement with the above revised value. We conclude that $r_n = 0.8$ km is probably the best estimate for the time–being.

46P/Wirtanen: It was marginally detected on CCD frames by *Boehnhardt et al.* (1997) at $r_h = 4.6$ AU giving an upper limit of the radius of 0.8 km (assuming $p = 0.04$) and a probable value of 0.69 km. The first unambiguous detection of the nucleus was by *La+*, giving $r_n = 0.62 \pm 0.02$ km (R band), $a/b \geq 1.2$, and $P_{rot} = 6.0 \pm 0.3$ hr. VLT observations by *Boehnhardt et al.* (2002) gave $r_n = 0.56 \pm 0.04$ km, $a/b \geq 1.4 \pm 0.01$, and a partial light curve in agreement with the above period. A slightly larger value of $r_n = 0.7$ km is reported by both *Meech et al.* (2000) and *Ta+*, while upper limits are given by *Lo+* and *Me+*. CCD photometry of the already active comet suggested a possible period of 7.6 hr (*Meech et al.* 1997).

47P/Ashbrook–Jackson: A partial light curve was obtained by *La+* (2001), giving a mean radius $r_n = 2.8$ km, $a/b \gtrsim 1.4$, and $P_{rot} \gtrsim 44.5$ hr. The nucleus appears inactive near

aphelion (stellar appearance), so that the determination of *Li+*, $r_n = 3.1\,\mathrm{km}$, and the estimate of *Ta+*, $r_n = 2.9\,\mathrm{km}$, are in agreement taking into account the fact that this nucleus is elongated.

48P/Johnson: The nucleus was reported active at $r_h = 3.36\,\mathrm{AU}$ by *Lo+*, thus only giving $r_n \leq 3.5\,\mathrm{km}$. Measurements by *Li+* at smaller r_h were certainly contaminated by a coma, although they claimed a stellar appearance, and this would explain their large value of $r_n = 3.7\,\mathrm{km}$. Several months of observations of a star-like nucleus at $r_h \sim 4\,\mathrm{AU}$ allowed *Jewitt and Sheppard* (2003) to secure a fairly complete lightcurve and to derive a spheroidal solution with $a = 3.5$ and $b = 2.6\,\mathrm{km}$ yielding $r_{n,v} = 2.87\,\mathrm{km}$) and $a/b \gtrsim 1.35$ and $P_{rot} = 29.0 \pm 0.04\,\mathrm{hr}$.

49P/Arend–Rigaux: This is a nearly–extinct nucleus that has been extensively studied by combined visible and infrared photometry. *Tokunaga and Hanner* (1985) reported a size of $r_n = 4.8 \pm 0.4\,\mathrm{km}$ and a geometric albedo of 0.05 ± 0.01 at $1.25\,\mu\mathrm{m}$. *Brooke and Knacke* (1986) determined $r_n = 5.1 \pm 1.1\,\mathrm{km}$ and $p_V = 0.02 \pm 0.01$. *Veeder et al.* (1987) found the nucleus to be elongated with equivalent radii of 5.1 and 3.8 km and $p_V = 0.03$. The in-depth investigation by *Millis et al.* (1988) resulted in a more accurate determination of the size and shape: $a = 6.5\,\mathrm{km}$ and $b = 4\,\mathrm{km}$ ($a/b = 1.63$), an albedo of $p_V = 0.028$, and a rotational period of $P = 13.47\,\mathrm{hr}$. The observational data have been reanalyzed by *Campins et al.* (1995) using new parameters for the thermal model and they give an effective radius of $4.6 \pm 0.2\,\mathrm{km}$ for a sphere having the maximum projected area πab and a geometric albedo of 0.04 ± 0.01. Keeping $a/b = 1.63$ from *Mueller et al.* (1998), we obtained $a = 5.9\,\mathrm{km}$ $b = 3.6\,\mathrm{km}$ and $r_{n,v} = 4.24 \pm 0.2\,\mathrm{km}$. From R band CCD photometry, *Lo+* reported two determinations of the radius, 3.8 ± 0.1 and $4.0 \pm 0.11\,\mathrm{km}$, assuming an albedo of 0.04. With the exception of the value reported by *Ta+* all the above results are consistent, the results of *Millis et al.* (1988) corrected by *Campins et al.* (1995) providing

the most detailed description. Thus, we use $r_{n,v} = 4.24\,\mathrm{km}$ and $p_V = 0.04 \pm 0.01$. *Jewitt and Meech* (1985) obtained a light curve from which they obtained two possible rotational periods, 9.58 ± 0.8 and $6.78 \pm 0.08\,\mathrm{hr}$.

50P/Arend: A snapshot observation by *La+* gave $r_n = 0.95\,\mathrm{km}$. The revised estimate of *Ta+*, $r_n = 1.0\,\mathrm{km}$ (compared to the original value of 3.0 km), is in good agreement with the above result.

51P/Harrington: Lo+ give an upper limit of 1.9 km. Although consistent with it, the value of $r_n = 1.4\,\mathrm{km}$ by *Ta+* cannot be considered reliable because of the large scatter in the data. Recent CCD images taken by *Manteca* (2002) show that this comet has split again into two components. A similar splitting was recorded at the 1994 apparition by *Scotti* (1994), who found a double nucleus on Spacewatch images. A detailed analysis of the astrometric data and of the circumstances of the splitting is still in progress (*Sekanina*, 2001).

52P/Harrington–Abell: Li+ obtained $r_n = 1.4\,\mathrm{km}$ from two images of a star-like nucleus at $r_h = 2.83\,\mathrm{AU}$. The fainter magnitude reported by *Carlson* (1990) corresponds to $r_n = 1.0\,\mathrm{km}$, in close agreement with the value selected by *Ta+*, $r_n = 1.1\,\mathrm{km}$. A spheroidal solution assuming that the above observations correspond to extreme cross-sections, yields $a = 2$, $b = 1\,\mathrm{km}$ (i.e., $a/b = 2$), and $r_{n,v} = 1.3\,\mathrm{km}$.

53P/Van Biesbroeck: Me+ derived $r_n = 3.33\,\mathrm{km}$ from a snapshot observation at $r_h = 8.31\,\mathrm{AU}$ (i.e., close to aphelion) in agreement with the result $r_n \ll 6.7\,\mathrm{km}$ of *Li+*. The comet is known to be active out to 6 AU, as illustrated by the very erratic heliocentric light curve of *Ta+*. *Krešák et al.* (1984) reported that this comet and 42P/Neujmin 3 are fragments of a parent comet that split in March 1845.

54P/de Vico–Swift: Undetected by *Lo+* at $r_h = 5.39$ AU (aphelion), they obtained an upper limit of 2.1 km.

56P/Slaughter–Burnham: A snapshot observation at $r_h = 7.42$ AU by *Me+* of the inactive nucleus gives $r_n = 1.56$ km. This is in good agreement with the estimate of *Ta+*, $r_n = 1.5$ km.

57P/du Toit–Neujmin–Delporte: Lo+ determined an upper limit of 1.1 km. The considerable scatter in the heliocentric light curve of *Ta+* makes their estimate of $r_n = 1.6$ km unreliable. The comet has recently split: two fragments were first discovered (IAUC 7934, 2002) followed by eighteen more (*Fernández et al.* 2002b). A preliminary analysis of this event has been reported by *Sekanina* (2002a,b).

58P/Jackson–Neujmin: There is too much scatter in the light curve of *Ta+* to estimate a size.

59P/Kearns–Kwee: A snapshot observation by *La+* yields $r_n = 0.79$ km. Such a small nucleus, active out to at least 4.2 AU, would be very difficult to detect from the ground.

60P/Tsuchinshan 2: Certainly a very small nucleus ($r_n < 1$ km) and *Ta+* estimated $r_n = 0.8$ km, but the compiled data in their plot have wide scatter. The nucleus may be as small as $\sim$0.5 km.

61P/Shajn–Schaldach: A partial rotational light curve has been obtained by *La+* giving a mean radius $r_n = 0.64$ km, $a/b > 1.3$, and $P_{rot} \gtrsim 18$ hr. At the time of the *HST* observations, $r_h = 2.96$ AU, the comet was still very active, the nucleus and the coma contributing equally to the signal in the peak pixel. The snapshot observation of *Lo+* at $r_h = 4.4$ AU, performed under non–photometric conditions, gives $r_n = 0.92 \pm 0.24$ km. The low end, $r_n = 0.68$ km, is consistent with the result of *La+*. The comet may still have been weakly active at 4.4 AU.

62P/Tsuchinshan 1: Certainly a very small nucleus ($r_n < 1\,\mathrm{km}$) and (*Ta+*) estimated $r_n = 0.8\,\mathrm{km}$ but the compiled data in their plot have wide scatter, likewise 60P.

63P/Wild 1: A snapshot observation by *La+* gives $r_n = 1.45\,\mathrm{km}$. The non-detection by *Lowry and Fitzsimmons* (2001), which results in an upper limit $r_n \leq 0.6\,\mathrm{km}$, is therefore puzzling. Invoking a highly–elongated spheroid to reconcile the two observations would be rather artificial.

64P/Swift–Gehrels: A star-like nucleus detected at $r_h = 3.63\,\mathrm{AU}$ by *Li+* gave $r_h = 1.6 \pm 0.1\,\mathrm{km}$, which is consistent with the upper limit $r_h \leq 1.9\,\mathrm{km}$ obtained by *Lo+* and with the estimate by *Ta+* of $r_n = 1.7\,\mathrm{km}$.

65P/Gunn: This comet is very active out to aphelion, so that only upper limits were obtained, $r_n \ll 11.7\,\mathrm{km}$ (*Li+*) and $r_n \leq 8.8\,\mathrm{km}$ (*Lo+*). The estimate proposed by *Ta+* is $r_n = 4.8\,\mathrm{km}$.

67P/Churyumov–Gerasimenko: A rotational lightcurve has been obtained by *La+* giving a mean radius $r_n = 1.98 \pm 0.02\,\mathrm{km}$, $a/b > 1.3$ and $P_{rot} = 12.3 \pm 0.27\,\mathrm{hr}$. This comet was undetected by *Lo+* at aphelion (5.72 AU), thus imposing $r_n \leq 2.9\,\mathrm{km}$. Observations at 4.87 and 4.97 AU by Mueller (1992) give $r_n = 2.8 \pm 0.1\,\mathrm{km}$ (scaled to $p_R = 0.04$) and $a/b > 1.7$. The heliocentric light curve is well–behaved and shows that the comet is inactive beyond 4.5 AU and the revised estimate $r_n = 2.0\,\mathrm{km}$ by *Ta+* agrees with the result of *La+*.

68P/Klemola: The well-behaved heliocentric light curve produced by *Ta+* suggests that their value $r_n = 2.2\,\mathrm{km}$ is a good estimate.

69P/Taylor: This comet was found to be active at $r_h = 4.03\,\mathrm{AU}$ by *Lo+*, who obtained an upper limit of 3.4 km.

70P/Kojima: A partial rotational light curve was obtained by *La+*, giving a mean radius $r_n = 1.86\,\mathrm{km}$, $a/b > 1.1$, and $P_{rot} \gtrsim 22\,\mathrm{hr}$. The large scatter in the data at $r_h > 3.4\,\mathrm{AU}$

makes the estimate of *Ta+*, $r_n = 1.2\,\mathrm{km}$, rather arbitrary.

71P/Clark: A snapshot observation by *La+* at $r_h = 2.72\,\mathrm{AU}$ gives $r_n = 0.68 \pm 0.07\,\mathrm{km}$, which is consistent with the non–detection at $r_h = 4.4\,\mathrm{AU}$ by *Lo+* ($r_n \leq 0.9\,\mathrm{km}$). The observations by *Me+* at aphelion ($r_h = 4.67\,\mathrm{AU}$) yields $r_n = 1.31 \pm 0.04\,\mathrm{km}$, similar to the value estimated by *Ta+*. A spheroid with $a = 2.13\,\mathrm{km}$ and $b = 0.75\,\mathrm{km}$ could reconcile the two determinations within the error bars, but has a very large axis ratio, $a/b \geq 2.85$, and further requires that *La+* and *Lo+* observed the smallest cross-section while *Me+* the largest one. This nucleus certainly deserves further observations.

73P/Schwassmann–Wachmann 3: The nucleus was reported as split into two components by *Schuller* (1930) but there was no other independent report. In 1994, the comet was reported active at $r_h = 3.03\,\mathrm{AU}$, and *Boehnhardt et al.* (1999) derived $r_n < 1.26\,\mathrm{km}$. The principal nucleus further split into at least 3 components in the autumn of 1995. Undetected in 1998 by *Lowry and Fitzsimmons* (2001) at $r_h = 5.03\,\mathrm{AU}$, they obtained an upper limit for the largest component of $r_n < 0.9\,\mathrm{km}$. Fragment B was detected by the HST at $r_h = 3.25\,\mathrm{AU}$ and *Toth et al.* (2003) derived $r_n = 0.68 \pm 0.04\,\mathrm{km}$ and $a/b > 1.16$.

74P/Smirnova–Chernykh: A partial rotational light curve was obtained by *La+* giving a mean radius of $r_n = 2.23 \pm 0.1\,\mathrm{km}$, $a/b > 1.14$, and $P \sim 20\,\mathrm{hr}$. At $r_h = 3.56\,\mathrm{AU}$, the comet was still very active, the nucleus and the coma contributing equally to the signal in the peak pixel. This explains why *Li+* ($r_h = 4.57\,\mathrm{AU}$) and *Lo+* ($r_h = 4.61\,\mathrm{AU}$) obtained only upper limits, $r_n \ll 11.2\,\mathrm{km}$ and $r_n \leq 7.1 \pm 1.1\,\mathrm{km}$, respectively. The value $r_n = 6\,\mathrm{km}$ estimated by *Ta+* is totally arbitrary.

75P/Kohoutek: A non-detection by *Lo+* gives $r_n \leq 1.5\,\mathrm{km}$, while the estimate by *Ta+* is $r_n = 1.8\,\mathrm{km}$.

76P/West–Kohoutek–Ikemura: A partial rotational light curve was obtained by *La+* at $r_h = 3.09\,\mathrm{AU}$ giving a mean radius $r_n = 0.33 \pm 0.03\,\mathrm{km}$, $a/b > 1.47$, and $P_{rot} \sim 13\,\mathrm{hr}$. The comet was still active, explaining the much larger value estimated by *Ta+*.

77P/Longmore: There is too much scatter in the data of *Ta+* to obtain a reliable estimate.

78P/Gehrels 2: A snapshot observation of a star-like nucleus at $r_h = 5.46\,\mathrm{AU}$ *Lo+* yields $r_n = 1.42 \pm 0.12\,\mathrm{km}$. The heliocentric light curve of *Ta+* displays a lot of scatter at 3.5 AU, suggesting that the comet is still active at that distance.

79P/duToit–Hartley: A snapshot observation at $r_h = 4.74\,\mathrm{AU}$ by *Lo+* revealed an inactive nucleus whose radius is $r_n = 1.4 \pm 0.3\,\mathrm{km}$.

81P/Wild 2: Observed while the nucleus was inactive at $r_h = 4.7\,\mathrm{AU}$ by *Meech and Newburn* (1998), they determined $r_n = 2.0 \pm 0.04\,\mathrm{km}$ and that the nucleus is fairly spherical, or has a relatively long period. Still inactive at $r_h = 4.25\,\mathrm{AU}$ inbound, *Lo+* obtained $r_n = 2.0 \pm 0.3\,\mathrm{km}$. The comet was, however, found active at $r_h = 4.34\,\mathrm{AU}$ outbound, so that *Li+* put an upper limit $r_n \ll 5.7\,\mathrm{km}$. Finally, *Fernández* (1999) obtained infrared images at $10.6\,\mu\mathrm{m}$ when the comet was at $r_h = 1.85\,\mathrm{AU}$, and therefore active. Although the measured flux was probably dominated by coma, that author applied the Standard Thermal Model for asteroids to derive $r_n < 3.0 \pm 0.6\,\mathrm{km}$. A nearly spherical nucleus with $r_n = 2\,\mathrm{km}$ is the most probable solution. This comet is the target of the *Stardust* mission, which will fly by its nucleus in January 2004.

82P/Gehrels 3: A partial rotational light curve was obtained by *La+* at $r_h = 3.73\,\mathrm{AU}$ giving a mean radius $r_n = 0.73 \pm 0.02\,\mathrm{km}$, $a/b > 1.6$, and $P_{rot} \sim 50\,\mathrm{hr}$. The comet appears to be active all along its orbit, so that *Li+* could only determine $r_n < 3.0\,\mathrm{km}$.

83P/Russell 1: A non-detection by *Lo+* at $r_h = 3.01\,\mathrm{AU}$ gives $r_n \leq 0.5\,\mathrm{km}$.

84P/Giclas: A snapshot observation by *La+* gives $r_n = 0.90 \pm 0.05$ km.

86P/Wild 3: A partial rotational light curve was obtained by *La+* at $r_h = 2.32$ AU giving a mean radius $r_n = 0.43 \pm 0.02$ km, $a/b > 1.35$, and an ill–defined period. A snapshot observation at 4.95 AU by *Me+* gives $r_n = 0.65 \pm 0.03$ km. These two determinations are inconsistent but satisfy the condition $r_n \leq 0.9$ km (*Lo+*). The unpublished value of 3.1 km suggested by Meech is apparently unjustified.

87P/Bus: The light curve obtained by *La+* at $r_h = 2.45$ AU gives a mean radius $r_n = 0.28 \pm 0.01$ km, $a/b > 2.20$, and $P_{rot} = 25$ hr. Two upper limits have been reported, $r_n \leq 0.6$ km at $r_h = 4.32$ AU (undetected) by *Lo+* and $r_n < 3.42$ km at $r_h = 4.77$ AU (close to aphelion) by *Me+* (a coma was present). It is probably impossible to detect this nucleus from the ground.

88P/Howell, 89P/Russell 2, 90P/Gehrels 1, 91P/Russell 3, 94P/Russell 4: There is too much scatter in the data presented by *Ta+* to obtain reliable size estimates. 89P was found active at $R_h = 3.04$ AU by *Lo+* leading to $r_n < 2.2$ km, and possibly $r_n \leq 1.3 \pm 0.3$ km after removing the comatic contribution.

92P/Sanguin: Two snapshot observations of a star–like nucleus, one at $r_h = 8.57$ AU by *Me+*, the other at $r_h = 4.46$ AU by *Lo+*, give $r_n = 1.19$ km and $r_n = 1.7 \pm 0.63$ km, respectively. These values are consistent owing to the large uncertainty in the latter value.

97P/Metcalf–Brewington: A star-like nucleus (with possibly a faint coma) detected at $r_h = 3.67$ AU by *Li+* gives $r_n = 1.5 \pm 0.16$ km, which, strictly speaking, should be considered an upper limit. Observed at 4.76 AU inbound by *Lo+*, it was found inactive resulting in $r_n = 2.18 \pm 0.41$ km. An intermediate size of $r_n = 1.7$ km is compatible with these two determinations, taking into account the error bars.

98P/Takamizawa: Observed at $r_h = 3.78\,\mathrm{AU}$ by *Li+* as a trailed object, their determination of $r_n = 3.7\,\mathrm{km}$ cannot be considered reliable. The heliocentric light curve of *Ta+* suggests that this comet is weakly active; their radius $r_n = 2.4\,\mathrm{km}$ has now been revised to $r_n = 3\,\mathrm{km}$.

99P/Kowal 1: There is too much scatter in the data presented by *Ta+* to obtain a reliable estimate.

100P/Hartley 1: Undetected by *Lo+* at $R_h = 3.94\,\mathrm{AU}$, they derived an upper limit $r_n < 1.2\,\mathrm{km}$.

101P/Chernykh: There is two much scatter in the data presented by *Ta+* to obtain a reliable estimate. *Luu and Jewitt* (1991) discovered that this comet has split.

103P/Hartley 2: The thermal flux of the nucleus was measured at $11.5\,\mu\mathrm{m}$ using ISOCAM on *ISO* . The preliminary determination $r_n = 0.58\,\mathrm{km}$ (*Jorda et al.* 2000) has now been revised to $r_n = 0.71 \pm 0.13\,\mathrm{km}$ by *Groussin et al.* (2003a), which is consistent with the upper limits of *Li+*, $r_n \ll 5.3$ and of *Lo+* $r_n \leq 5.8\,\mathrm{km}$.

104P/Kowal 2: A snapshot observation of a star-like nucleus at $r_h = 3.94\,\mathrm{AU}$ by *Lo+* gives $r_n = 1.0 \pm 0.5\,\mathrm{km}$.

105P/Singer–Brewster: There is too much scatter in the data presented by *Ta+* to obtain a reliable estimate.

106P/Schuster: A snapshot observation by *La+* gives $r_n = 0.94 \pm 0.05\,\mathrm{km}$, which is quite close to the value in the revised catalog of *Ta+*, $r_n = 0.8\,\mathrm{km}$.

107P/Wilson–Harrington: The identification of this object as a comet remains problematic as discussed by *Weissman et al.* (2003) and it was in fact first classified as a Near-Earth Asteroid. It has a Tisserand parameter slightly in excess of 3 ($T_J = 3.084$) but

an orbit typical of ECs ($a = 2.643\,\mathrm{AU}$, $e = 0.621$, $i = 2.78°$). In their dynamical analysis, *Bottke et al.* (2002) assign it only a 4% probability of being of cometary origin; they find the most probable source to be the outer main belt (65%). Its activity was observed on only one night, on two Palomar photographic plates taken in 1949, and the object is trailed on both images; no activity was detected on plates taken three nights later. Subsequent searches for cometary activity have all been negative (e.g., *Chamberlin et al.* 1996). 107P was observed simultaneously in the near and thermal infrared by *Campins et al.* (1995). Using first the STM, they obtained $r_n = 1.3 \pm 0.16\,\mathrm{km}$ and $p_J = 0.10 \pm 0.02$, a somewhat surprising value. Thus, they favored the ILM solution which gives $r_n = 2.0 \pm 0.25\,\mathrm{km}$ and $p_J = 0.05 \pm 0.01$. Since the color is very neutral, this value holds as well for the V and R bands. Visible snapshot observations have been reported by *Lo+* giving $r_n = 1.78 \pm 0.03\,\mathrm{km}$ and *Me+* giving $r_n = 1.96 \pm 0.02\,\mathrm{km}$. There exists also and an unpublished value $r_n = 2.0\,\mathrm{km}$ by *Meech*. The rotational state has been investigated by *Osip et al.* (1995), who found $P_{rot} = 6.1 \pm 0.05\,\mathrm{hr}$ and $a/b \geq 1.2$. If we scale the above *Lo+* and *Me+* values to $p_R = 0.05$, we get $r_n = 1.59 \pm 0.03$ and $r_n = 1.75 \pm 0.02$, respectively. A spheroidal solution with $a = 1.9\,\mathrm{km}$ and $b = 1.6\,\mathrm{km}$ with $p_R = 0.05$ is then compatible with all above results, implying an obliquity of 90°, and that *Campins et al.* (1995) and *Me+* observed the largest cross-section while *Lo+* the smallest. We then obtain $r_{n,v} = 1.7\,\mathrm{km}$.

110P/Hartley 3: A complete rotational light curve has been obtained by *La+* giving a mean radius $r_n = 2.15 \pm 0.05\,\mathrm{km}$, $a/b > 1.3$, and $P_{rot} \sim 10\,\mathrm{hr}$.

111P/Helin–Roman–Crockett: This comet was undetected by *Lo+* at $r_h = 4.35\,\mathrm{AU}$, thus imposing $r_n \leq 1.5\,\mathrm{km}$. *NTT* observations made at $r_h = 4.56\,\mathrm{AU}$ by *Delahodde et al.* (2003) give a subkilometer radius of $r_n = 0.6 \pm 0.3\,\mathrm{km}$.

112P/Urata–Niijima: A snapshot *HST* observation at $r_h = 2.30\,\mathrm{AU}$ by *La+* gives $r_n = 0.90 \pm 0.05\,\mathrm{km}$. The estimate by *Ta+* is 0.7 km, but the compiled data in their plot

have wide scatter.

113P/Spitaler: This comet was undetected by *Lo+* at $r_h = 4.22\,\mathrm{AU}$, thus imposing $r_n \leq 2.0\,\mathrm{km}$. The estimate of *Ta+*, $r_n = 1.1\,\mathrm{km}$ seems plausible.

114P/Wiseman–Skiff: A snapshot *HST* observation at $r_H = 1.57\,\mathrm{AU}$ by *La+* gives $r_n = 0.78 \pm 0.04\,\mathrm{km}$.

115P/Maury: Me+ observed a star–like nucleus at $r_h = 5.34\,\mathrm{AU}$ and give r_n =1.11 km.

116P/Wild 4: The heliocentric light curve of *Ta+* suggests that the comet could be inactive at $r_h = 4\,\mathrm{AU}$. A radius of 3.5 km, recently revised to 3.0 km, is probably a good estimate, pending further observations.

117P/Helin–Roman–Alu: The value of *Ta+*, $r_n = 3.5\,\mathrm{km}$, comes from measurements at aphelion. It is unclear whether the comet is inactive then.

118P/Shoemaker–Levy 4: A star-like nucleus detected at $r_h = 4.71\,\mathrm{AU}$ by *Lo+* gives $r_n = 2.4 \pm 0.2\,\mathrm{km}$ similar to the value estimated by *Ta+*, but the compiled data in their plot have wide scatter.

119P/Parker–Hartley: This comet was still very active at $r_h = 3.42\,\mathrm{AU}$ when observed by *Lo+*, who obtained an upper limit $r_n < 7.4 \pm 0.2\,\mathrm{km}$ and then refined that to $r_n < 4.0 \pm 0.6\,\mathrm{km}$ after estimating the comatic contribution. As illustrated by the heliocentric light curve of *Ta+*, the comet is simply too active out to 4 AU to make a sensible estimate of r_n.

120P/Mueller 1: A star–like nucleus detected at $r_h = 3.08\,\mathrm{AU}$ by *Lo+* gives $r_n = 1.5\,\mathrm{km}$. The plot of *Ta+* shows considerable scatter of the magnitudes at that distance, indicating that the comet could well be active.

121P/Shoemaker–Holt 2: A star–like nucleus detected at $r_h = 5.03\,\mathrm{AU}$ by *Lo+* gives $r_n = 1.62 \pm 0.57\,\mathrm{km}$.

123P/West–Hartley, 124P/Mrkos, 125P/Spacewatch: There is too much scatter in the data presented by *Ta+* to obtain reliable estimates.

128P/Shoemaker–Holt 1: Two snapshot observations of a star-like nucleus at $r_h = 4.99\,\mathrm{AU}$ by *Lo+* give compatible results, $r_n = 2.48 \pm 0.1\,\mathrm{km}$ and $r_n = 2.12 \pm 0.18\,\mathrm{km}$, which are both consistent with the upper limit $r_n < 4.0\,\mathrm{km}$ when the comet was observed at $r_h = 3.66\,\mathrm{AU}$ by *Lo+*, when it was still active. We adopt an average value $r_{n,v} = 2.3\,\mathrm{km}$.

130P/McNaught–Hughes, 131P/Mueller 2, 132P/Helin–Roman–Alu 2, 134P/Kowal–Vavrová, 135P/Shoemaker–Levy 8, 136P/Mueller 3: There is too much scatter in the data presented by *Ta+* to extract reliable estimates.

137P/Shoemaker–Levy 2: This comet was observed at $r_h = 4.24\,\mathrm{AU}$ by *Li+*, but various technical problems make their determination $r_n = 4.5\,\mathrm{km}$ questionable. This is confirmed by the upper limit $r_n \leq 3.4\,\mathrm{km}$ found by *Lo+* when they observed the comet at $r_h = 2.29\,\mathrm{AU}$, while it was still active. The heliocentric light curve of *Ta+* indicates that the magnitude at $r_h = 5\,\mathrm{AU}$ may provide a good estimate, $r_n = 2.9\,\mathrm{km}$.

138P/Shoemaker–Levy 7: There is too much scatter in the data presented by *Ta+* to extract a reliable estimate.

43P/Kowal–Mrkos: A star-like nucleus was observed by *Jewitt et al.* (2003) from $r_h = 3.4$ to $4.0\,\mathrm{AU}$ and their almost complete lightcurve clearly suggests a rotational period of $17.21 \pm 0.1\,\mathrm{hr}$ and an amplitude range of $0.45 \pm 0.05\,\mathrm{mag}$, corresponding to a minimum axial ratio of 1.49 ± 0.05. Assuming an albedo of 0.04 and using the phase coefficient determined by these authors $\beta = 0.043 \pm 0.014\,\mathrm{mag\,deg}{-1}$, the spheroidal solution has semiaxes $a = 7.0$ and $b = 4.7\,\mathrm{km}$ yielding $r_{n,v} = 5.4\,\mathrm{km}$. Note that the effective radius

$r_n = 5.7 \pm 0.6$ km reported by the above authors was derived using a *Bowell et al.* (1989) type phase curve having $G = 0.15$ which has an opposition effect of about 0.2 mag above the linear phase law.

147P/Kushida–Muramatsu: The nucleus of this comet is the smallest of all the objects catalogued to date. From observations with the *HST* at r_h =2.83 AU over a 13 hr time interval, *La+* found a very small, $r_n = 0.21 \pm 0.01$ km, highly active nucleus with $a/b > 1.53$, and a possible rotational period of 9.5 hr. It is therefore not surprising that *Lo+* could not detect the comet at $r_h = 4.11$ AU, thus imposing $r_n \leq 2.0$ km.

152P/Helin–Lawrence: This comet is still active at aphelion ($r_h = 5.85$ AU), and the smallest upper limit is presently $r_n \leq 1.74$ km (*Me+*).

P/1993 W1 (Mueller 5), P/1994 A1 (Kushida), P/1994 J3 (Shoemaker 4), P/1995 A1 (Jedicke), P/1996 A1 (Jedicke), P/1997 C1 (Gehrels), P/1997 G1 (Montani), P/1997 V1 (Larsen): There is too much scatter in the data presented by *Tancredi et al.* (2000) to extract a reliable estimate.

3.2.2. Nearly–Isotropic Comets (NICs)

1P/Halley: The size and shape of its nucleus were determined from in-situ imaging made by the *Vega* 1, 2 and *Giotto* spacecrafts in 1986 (*Sagdeev et al.* 1986a; *Keller et al.* 1986, 1987, 1994; *Keller* 1990; see also *Keller et al.* 2004). The nucleus is an elongated, irregularly–shaped body approximated by an ellipsoid with semi-axes ($a \times b \times c$) of $7.21 \pm 0.15 \times 3.7 \pm 0.1 \times 3.7 \pm 0.1$ km (*Giotto*) and $7.65 \pm 0.25 \times 3.61 \pm 0.25 \times 3.61 \pm 0.25$ km (*Vega* 1, 2). It is in non–principal axis rotation, and there was a long dispute over whether the nucleus rotates in the "short-axis mode" (SAM) or "long-axis mode" (LAM) (*Sagdeev et al.* 1989; *Peale and Lissauer* 1989; *Abergel and Bertaux* 1990; *Belton* 1990; *Belton et al.*

1991; *Samarasinha and A'Hearn* 1991). In the modes identified as most likely, the long axis conducts a 3.7 day precessional motion around the space–fixed vector of the total rotational angular momentum, while the nucleus also rotates around the long axis with a 7.3 day period.

8P/Tuttle: A single value $r_n = 7.8\,\mathrm{km}$ was reported by *Li+* when the comet was at $r_h = 6.29\,\mathrm{AU}$ and appeared inactive.

55P/Tempel–Tuttle: Its effective radius of 1.8 km and a minimum value of 1.5 for the axial ratio were derived from *HST* WFPC2 and *ISO* ISOCAM observations (*La+*). Ground–based observers determined similar sizes, e.g., *Hainaut et al.* (1998) *Weissman and Buratti* (personal communication) in the visible and *Fernández* (1999) in the mid-infrared. There is still no data published for the rotational period of the nucleus.

96P/Machholz 1: A star–like nucleus detected at $r_h = 4.83\,\mathrm{AU}$ by *Li+* gives $r_n = 3.5\,\mathrm{km}$. There are unpublished data by *Meech* giving $r_h = 2.8\,\mathrm{km}$, $a/b > 1.4$, and $P_{rot} = 6.38\,\mathrm{hr}$. A spheroid with $a = 4.3\,\mathrm{km}$ and $b = 2.8\,\mathrm{km}$ ($a/b \sim 1.5$) would be consistent with the two results above, yielding $r_{n,v} = 3.2\,\mathrm{km}$.

109P/Swift–Tuttle: A mean effective radius of 11.8 km was determined from ground-based CCD photometry (*O'Ceallaigh et al.* 1995) at $r_h = 5.3\,\mathrm{AU}$ outbound in the presence of a weak coma. Later, at $r_h \sim 5.8\,\mathrm{AU}$ outbound, the nucleus had a stellar appearance and *Boehnhardt et al.* (1996) determined two comparable values of the radius, 12.2 and $12.5 \pm 0.3\,\mathrm{km}$ at a time interval of 5 days. *Meech et al.* (2004) observed this comet at 14.5 AU and derived an effective radius of 13.7 km. A radius of $15.0 \pm 3.0\,\mathrm{km}$ was estimated from ground-based IR photometry (*Fomenkova et al.* 1995). An average radius of 13.0 km appears realistic. The rotational period of the nucleus has been determined by *Sekanina* (1981) from the recurrent pattern of coma jets on 1862 photographs, $P_{rot} = 66.5\,\mathrm{hr}$ and on 1992 CCD images by *Jorda et al.* (1992), $\sim 69.6\,\mathrm{hr}$, *Yoshida et al.* (1992), $69.4 \pm 0.24\,\mathrm{hr}$

and *Boehnhard and Birkle* (1994), 67.08 hr.

126P/IRAS: The thermal flux of the nucleus was measured at 11.5 μm using ISOCAM. The preliminary determination $r_n = 1.43$ km (*Jorda et al.* 2000) has now been refined to $r_n = 1.57 \pm 0.14$ km by *Groussin et al.* (2003a).

P/1991 L3 (Levy): A stellar appearance at $r_h = 3.1$ AU led *Fitzsimmons and Williams* (1994) to consider that they observed a bare nucleus, shortly after it had ceased outgassing. They determined $r_n = 5.8 \pm 0.1$ km, $a/b > 1.3$ and $P_{rot} = 8.34$ hr.

C/1983 H1 (IRAS–Araki–Alcock): Extensive observations in the visible, infrared, radio, and radar wavelength ranges were performed when it passed near the Earth on 11 May 1983. The radar and radio observations of *Altenhoff et al.* (1983), *Goldstein et al.* (1984), *Irvine et al.* (1984) and *Harmon et al.* (1989) converge to a non–spherical nucleus with a radius is in the range 2.5-6.0 km (the a/b ratio could not be determined) and a rotation period is in the range 24–72 hr. From a study of the temporal variation of its asymmetric coma, *Watanabe* (1987) and later *Pittichová* (1997) estimated that the period lies in the range 18–170 hr. From a synthesis of visible, infrared, and radar observations, *Sekanina* (1988) derived a prolate spheroid nucleus with $a = 8$, and $b = c = 3.5$ km and a rotational period of 51.3 hr. Infrared observations and a simple thermal model, assuming a constant temperature for the surface of the nucleus, were used to derive that the radius was in the range of 3.6–5.0 km (*Feierberg et al.*, 1984; *Hanner et al.*, 1995; *Brown et al.*, 1985). *Groussin et al.* (2004) re-examined the interpretation of all visible, infrared and radio observations and using their thermal model, they derived an equivalent radius $r_n = 3.5 \pm 0.5$ km.

C/1983 J1 (Sugano–Saigusa–Fujikawa): Hanner et al. (1987) obtained a value of 0.37 km for the average radius of the nucleus from infrared spectroscopic observations. This result was a clear indication that cometary nuclei, including NICs, could be

subkilometer–sized bodies.

C/1995 O1 (Hale–Bopp): *Weaver and Lamy* (1997) and *Fernández* (2003) reviewed all the data pertaining to the size of the nucleus. The former review discusses all wavelengths, while the latter focuses on infrared and radio observations. The dominant visible–wavelength dataset is from *HST*. The spatial resolution and image quality were sufficient to obtain photometric extractions of the nucleus, from which a radius of ∼35 km was derived (*Weaver and Lamy* 1997). The dominant radiometric datasets are from *ISO* (*Jorda et al.* 2000), the *Very Large Array (VLA)* (*Fernández* 1999), the *Owens Valley Radio Observatory (OVRO)* (*Qi* 1999), and the *Institut de Radioastronomie Millimétrique (IRAM)* (*Altenhoff et al.* 1999). Generally, the radio data suggest a smaller nucleus than implied by the infrared data. A compromise solution by *Fernández* (2003) was to argue that (a) the subsurface layer sampled by the radio observations was cooler and/or less emissive than expected, and (b) there was some excess dust not accounted for in the infrared photometry. This would shift the radii from the two wavelength regimes towards each other and leads to a radius of 30 ± 10 km, consistent with the *HST* results. The rotational period of the nucleus was determined by two different methods, 11.34 ± 0.02 hr was derived by *Licandro et al.* (1998) and 11.35 ± 0.04 hr by *Jorda et al.* (1999) (see *Samarasinha et al.* 2004). An extensive, ground–based CCD imaging observational campaign (*Farnham et al.* 1999) showed a systematic motion of the rotational pole of the nucleus, and this was interpreted as resulting from precession due to complex rotation. However, *Samarasinha* (2000) showed that there are no effects due to precession in the observed coma morphology.

C/1996 B2 (Hyakutake): Optical, infrared, and radar observations were performed during its close approach to Earth. *Lisse et al.* (1999) estimated a nuclear radius of 2.4 ± 0.5 km from the infrared and optical data. Radar observations revealed a clear detection of the nucleus, but an extremely small radar albedo of 0.011 is required to be

consistent with the infrared data (*Harmon et al.* 1997; see *Harmon*, 2004). If the radar albedo is 0.04, the radius of the nucleus derived from the radar detection drops to only ∼1.3 km. Early observations showed a fast rotation period of 6.30 ± 0.03 hr, which was later refined by *Schleicher and Osip* (2002) to 6.273 ± 0.007 hr. This NIC underwent a partial fragmentation as large fragments (∼10–20 m in diameter) were observed traveling away from the nucleus with a velocity of $\sim 10\,\mathrm{m\,s^{-1}}$ (*Lecacheux et al.* 1996; *Desvoivres et al.* 2000).

C/1983 O1 (Černis), C/1984 K1 (Shoemaker), C/1986 P1 (Wilson), C/1987 H1 (Shoemaker), C/1987 F1 (Torres), C/1988 B1 (Shoemaker), C/1997 T1 (Utsonomiya): Only upper limits are reported for the nuclear radii of these NICs by *Me+*. An upper limit for the radius of C/1997 T1 is also reported by *Fernández* (1999) from infrared measurements.

C/1999 S4 (LINEAR): This comet underwent catastrophic fragmentation in July 2000. Lower limits for the size of the nucleus prior to disruption were derived indirectly from the long-term monitoring of the water production rate: $r_n \geq 0.375$ km by *Makinen et al.* (2001), and $r_n \geq 0.44$ km by *Farnham et al.* (2001).

C/2001 OG108 (LONEOS): First classified as an asteroid of the Damocloid group, it developed a small amount of cometary activity as it approached perihelion and was subsequently reclassified as a comet. Simultaneous optical and thermal observations by *Abell et al.* (2003) give an effective radius of 8.9 ± 0.7 km and a visual albedo $p_V = 0.03 \pm 0.005$. Their composite lightcurve indicates a simple rotation with a period of 57.19 ± 0.5 hr and a minimum axial ration of 1.5. The spheroidal solution assuming $a/b = 1.3$ has $a = 10.1$ km and $b = c = 7.9$ km.

Essentially all the best data on the sizes and shapes of cometary nuclei are summarized in Tables 1, 2, and 3. The column labeled $r_{n,v}$ displays what we consider to be the most

reliable value of the effective radius, as defined in §3.2. An absence of value means that, in our opinion, a reliable determination does not yet exist.

3.3. Albedo

3.3.1. Ecliptic Comets (ECs)

2P/Encke: Using radiometry, *Fernández et al.* (2000) report 0.046 ± 0.023 for the V band.

9P/Tempel 1: Using radiometry, *Fernández et al.* (2003) report 0.072 ± 0.016 for the R band. However, as discussed in section 3.2.1, this large value probably results from coma contaminated visible magnitudes. The most likely value is $p_r = 0.048 \pm 0.007$.

10P/Tempel 2: From radiometry of the nucleus, *A'Hearn et al.* (1989) report an albedo of $0.022^{+0.004}_{-0.006}$ for a wavelength of 4845 Å. *Tokunaga et al.* (1992) report a near-infrared (1.25 to 2.20 μm) albedo of 0.04 to 0.07, which is consistent with the reddening of the nucleus in this wavelength regime compared to the visible.

19P/Borrelly: Buratti et al. (2003) used disk-resolved imaging of the nucleus obtained by Miniature Integrated Camera and Spectrometer (MICAS) instrument on the *Deep Space 1 (DS1)* mission, and a scattering model based on the *Hapke* (1986) formalism, to calculate a disk-integrated geometric albedo of 0.029 ± 0.006. Table 3 of *Buratti et al.* (2003) indicates that this is the p_V value, but we think that it corresponds, in fact, to the R band for two reasons. First, the *DS1* images have an effective wavelength of $0.66\,\mu$m, and second, the albedo was derived from the absolute R magnitudes, $R(1, 1, \alpha)$. Variations are, however, observed on the surface of the nucleus, and the two main types of terrains, smooth and mottled, exhibit mean normal reflectances of 0.03 and 0.022. The above albedo is lower than that assumed by *La+* (0.04) but, as discussed by *Buratti et al.* (2003), the

respective uncertainties in the *HST* and *DS1* measurements make the two results fully consistent. This justifies the superposition of the prolate spheroid model derived from the *HST* observations and a *DS1* image displayed in Fig. 2.

22P/Kopff: Using radiometry, *Lamy et al.* (2002) report 0.042 ± 0.006 for the V band.

28P/Neujmin 1: As discussed in §3.2.1, the maximum value of the infrared flux measured by *Campins et al.* (1987) leads to $p_V = 0.026$. This value and the color $(V - R) = 0.45$ leads to $p_R = 0.04$ in good agreement with the value $p_R = 0.03 \pm 0.01$ determined by *Jewitt and Meech* (1988). *Campins et al.* (1995) have revised their value to 0.06 ± 0.5 with probably on error in their uncertainty (0.05 likely), compatible with the above values.

29P/Schwassmann–Wachmann 1: Using radiometry, *Cruikshank and Brown* (1983) report $p_V = 0.13 \pm 0.04$. As emphasized in section 3.2, this value is controlled by the visible magnitude, which was *estimated*.

49P/Arend-Rigaux: The albedo has been constrained by many groups, all using ground-based radiometry. The results of *Millis et al.* (1988), revised by *Campins et al.* (1994), give $p_V = 0.04 \pm 0.01$. In the near-infrared (specifically J band), measurements by *Tokunaga and Hanner* (1985), 0.054 ± 0.010, and by *Brooke and Knacke* (1986), 0.03 ± 0.01, are consistent with the value at visible wavelengths.

107P/Wilson-Harrington: Using radiometry, *Campins et al.* (1995) report $p_J = 0.10 \pm 0.02$ using the STM and $p_J = 0.05 \pm 0.01$ using the ILM, the latter value being favored.

3.3.2. Nearly–Isotropic Comets (NICs)

1P/Halley: Resolved imaging of the nucleus led to a value of $0.04^{+0.02}_{-0.01}$, irrespective of the spectral bands "VIS", "RED" or "NIR" of the *VEGA* cameras (*Sagdeev et al.* 1986).

55P/Tempel-Tuttle: Using radiometry, *Fernández* (1999) and *Jorda et al.* (2000) both arrived at similar values for the R band: 0.06 ± 0.025 for the former, 0.045 for the latter.

109P/Swift-Tuttle: Fomenkova et al. (1995) used radiometry to estimate a nuclear size, from which the large-heliocentric distance observations by *O'Ceallaigh et al.* (1995) may be used to derive an approximate albedo of about 0.02 to 0.04 in the R band.

C/1983 H1 (IRAS-Araki-Alcock): Extensive datasets at many wavelengths allowed *Sekanina* (1988) to create a unified model of the properties of the nucleus. The implied albedo in the V band is 0.02 ± 0.01. *Groussin et al.* (2004) have re–analyzed these data and obtained a slightly larger value of 0.03 ± 0.01.

C/1995 O1 (Hale–Bopp): While more data were obtained on this comet than any other, the albedo derivation is problematic owing to the comet's strong coma swamping the nucleus during the whole apparition to date. *Campins and Fernández* (2003) combine the results of *Jorda et al.* (2000) and *Fernández* (1999), who both used radiometry, and find a compromise, but very unconstrained, value of 0.04 ± 0.03.

C/2001 OG108 (LONEOS): Using radiometry, *Abell et al.* (2003) report 0.03 ± 0.005 for the V band.

Table 4 summarizes these results on the albedo measurements of cometary nuclei.

3.4. Colors

Colors by themselves do not provide much information on the physical properties of cometary nuclei, but the distribution of colors compared to other solar system objects, or the correlation of colors with other parameters (e.g., size, orbital parameters, ...) has the potential of offering independent clues on the origin and evolution of these objects and their interrelationships. Near–infrared spectroscopic observations of cometary nuclei have been attempted in an effort to detect the spectral signals of water ice and silicates, as successfully performed on several KBOs and Centaurs (e.g., *Jewitt and Luu* 2001). Finally, we discuss the few thermal spectra obtained so far and their implications for the surface temperature of cometary nuclei.

3.4.1. Broadband Colors and Reflectivity:

The most common color characterization comes from color indices, for example $(B-V)$, $(V-R)$, $(V-I)$, etc. . As discussed in §3.1.2, magnitudes of nuclei observed at large heliocentric distances are very faint, and this often leading to large uncertainties in the indices. Continuum spectra of a few nuclei have been obtained, and they can be parametrized using the normalized reflectivity gradient $S' = dS/d\lambda/ < S >$, where S is the reflectivity (object flux density divided by the flux density of the Sun at the same wavelength, λ) and $< S >$ is the mean value of the reflectivity in the wavelength range over which $dS/d\lambda$ is computed (*Luu and Jewitt* 1990b). The gradient, S', is used to express the percentage change in the strength of the continuum per 1000 Å (%/1000 Å). Broadband color indices can also be converted to a normalized reflectivity gradient using the following relation (*Luu and Jewitt* 1990):

$$(V-R)_n = (V-R)_\odot + 2.5 \log \frac{2 + S'\Delta\lambda}{2 - S'\Delta\lambda} \qquad (12)$$

where $(V-R)_n$ and $(V-R)_\odot$ are the color indices of the nucleus and the Sun, respectively and $\Delta\lambda$ is the difference between the effective wavelengths of the two filters.

The quantity S' remains of interest as long as it is constant over a sufficiently large spectral interval. This is rarely the case and different values in different spectral intervals must be introduced. Then the S' values become strictly equivalent to the color indices via the above equation.

Table 5 is an updated version of the Table 3 in *Jewitt* (2002), summarizing all presently available data on the colors of cometary nuclei. It incorporates recent results from *Meech et al.* (2004), except for the nuclei of 22P/Kopff, 46P/Wirtanen, 87P/Bus and P/1993 K2 (Helin–Lawrence), which were active at the time of observations, from the compilation of *Hainaut and Delsanti* (2002), and from *Lowry and Weissman* (2003). We comment below on some of the results, starting with the ECs.

2P/Encke: Note the accurate $(V-R)$ from spectrophotometry. A value $(V-R) = 0.46 \pm 0.02$ is consistent with all the data and their respective error bars.

6P/d'Arrest: $(V-R) = 0.56 \pm 0.02$ is consistent with the results of *Jewitt* (2002) and *Meech et al.* (2004), while the value reported by *Lowry and Weissman* (2003), $(V-R) = 0.33 \pm 0.09$, is well outside the above uncertainty. $(R-I) = 0.45 \pm 0.04$ from *Jewitt* (2002) is, however, consistent with the results reported by *Lowry and Weissman* (2003), 0.33 ± 0.12. At the 2σ level, the two values of $(B-V)$ agree, and we adopt $(B-V) = 0.85^{+0.2}_{-0.07}$.

10P/Tempel 2: $(V-R) = 0.56 \pm 0.01$ is consistent with the three measurements.

14P/Wolf, 19P/Borrelly: Note the large uncertainties, making these measurements of limited value.

28P/Neujmin 1: There is an excellent agreement on the $(V-R)$ color of this large and

inactive nucleus. Taking the average of all measurements leads to $(V - R) = 0.47 \pm 0.20$, making it similar to D-type asteroids (*Campins et al.* 1987; *Fitzsimmons et al.* 1994) and most Trojans (*Jewitt and Luu* 1990).

45P/Honda–Mrkos–Pajdusakova: In addition to the results included in Table 5, *Lamy et al.* (1999) reported the first $(U - B)$ index ever measured on a comet nucleus, $(U - B) = 0.68 \pm 0.04$.

48P/Johnson: Note the large uncertainty of 0.3 on $(V - R)$.

49P/Arend–Rigaux: The result that $(V - R) = 0.47 \pm 0.01$, obtained by both filter photometry and spectrophotometry on this inactive nucleus, appears to be extremely accurate and reliable. Note the large uncertainty on the $(R - I)$ reported by *Lowry et al.* (2002), 0.54 ± 0.14 which makes it compatible with the result of *Millis et al.* (1988), $(R - I) = 0.43 \pm 0.02$.

86P/Wild 3: The surprising result that $(V - R) = 0.12 \pm 0.14$ makes this nucleus a very blue object, although the error bar is quite large.

107P/Wilson–Harrington: We favor the spectrophotometric result $(V-R) = 0.31 \pm 0.03$ of *Chamberlin et al.* (1996), which is intermediate between the two available photometric results.

There are only two NIC nuclei for which color information is available: 1P/Halley and 96P/Machholz 1.

1P/Halley: From in-situ imaging by the *Giotto* HMC, *Thomas and Keller* (1989) determined a constant reflectivity gradient $S' = 6 \pm 3$ per 1000 Å in the range 440–810 nm leading to $(B - V) = 0.72 \pm 0.04$, $(V - R) = 0.41 \pm 0.03$, $(V - I) = 0.80 \pm 0.09$, and $(R - I) = 0.39 \pm 0.06$.

96P/Machholz 1: The two available measurements are not consistent at the 1σ level.

3.4.2. Visible and Near-Infrared Spectra:

In principle, spectral analysis in the most effective way to characterize the surface properties of the cometary nuclei. First, it yields high accuracy color information as presented above and, second, it offers the possibility of detecting solid state absorption bands, namely those of water ice and minerals. With one exception, and contrary to the case for several Centaurs and KBOs, this expectation has failed to materialize, reinforcing for the time being the value of color information. In addition to the general difficulties of detecting cometary nuclei, spectral observations face the additional problem of very low signals per spectral element. This explains the paucity of ground–based nuclear spectra, mostly restricted to (nearly) inactive nuclei, and the clear superiority of in-situ spectral observations.

2P/Encke, 10P/Tempel 2, 21P/Giacobini–Zinner, 49P/Arend–Rigaux: Their visible spectra obtained at large r_h with a spectral resolution of 10–20 Å are presented by *Luu* (1993). No absorption features were detected, except for a downturn feature in the blue part of the spectrum of 21P, reminiscent of chondritic spectra.

19P/Borrelly: The short-wavelength infrared imaging spectrometer (SWIR) aboard DS1 secured 45 scans spectra of the nucleus in the 1.3–2.6 μm range (*Soderblom et al.* 2002). They reveal a strong positive slope toward the red and a single absorption feature at $\sim$2.39 μm, whose origin is unknown (fits of various hydrocarbons were attempted, but none were satisfactory).

28P/Neujmin 1: Observations at large r_h in the spectral range 0.9-2.4 μm by *Campins et al.* (2001) do not show a water ice signature, a result consistent with earlier observations

by *Campins et al.* (1987) and recent observations by *Licandro et al.* (2002).

82P/Gehrels 3: A featureless red spectrum in the range 0.4–0.98 μm, with a resolution of 30 Å, has been obtained by *De Sanctis et al.* (2000). This spectrum is very similar to those of D-type asteroids.

90P/Gehrels 1: Observations at large r_h in the spectral range 0.9–2.4 μm by *Delahodde et al.* (2002) show the absence of spectral signatures.

107P/Wilson–Harrington: A featureless spectrum in the range 0.38–0.62 μm with a resolution of 5 Å has been obtained by *Chamberlin et al.* (1996).

124P/Mrkos: Observed by *Licandro et al.* (2002) while inactive at $r_h = 1.85$ AU, its near-infrared (0.9–2.3 μm), low resolution spectrum is featureless and slightly redder than the Sun, resembling that of a D–type asteroid.

C/2001 OG108 (LONEOS): Observed by *Abell et al.* (2003) while inactive, its near-infrared (0.7–2.5 μm) is featureless, slightly redder than the Sun, resembling that of a D-type asteroid.

3.4.3. Thermal Spectrum – Surface Temperatures:

The surface temperature of the nucleus has been measured for only two comets, 1P/Halley and 19P/Borrelly, thanks to in-situ observations.

1P/Halley: The infrared radiation of its nucleus was measured at $r_h = 0.8$ AU by the IKS spectrometer aboard the VEGA 1 spacecraft in two wavelengths bands, 7–10 and 9–14 μm (*Combes et al.* 1986). The temperature was obtained with two independent and different methods, and the most probable maximum value lies in the range 360 – 400 K. The hottest region was not at the subsolar point, and the angular thermal lag was about

20° (*Emerich et al.* 1987). These results suggest that a large fraction of the nucleus surface of 1P/Halley is inactive and not cooled by sublimating ices or evolving gases. The surface may be a lag deposit crust, or perhaps a radiation processed mantle.

19P/Borrelly: The spectra recorded by SWIR aboard *DS1* at $r_h = 1.36\,\mathrm{AU}$ (*Soderblom et al.* 2002) permitted a determination of the temperature at the two tips of the elongated nucleus: 300 K and 345 K. These high temperatures are consistent with the absence of water ice bands (cf., the previous subsection) and, as for 1P/Halley, suggest that a large fraction of the nuclear surface is inactive (only ∼10% of its surface is active according to *Lamy et al.* 1998b).

3.5. Phase Function

In the above sections, we have highlighted the importance of the phase function $\Phi(\alpha)$ in the determination of the size of cometary nuclei and emphasized that it remains a non-negligible source of uncertainty. Aside from this technical aspect of the data reduction, the phase function of an atmosphereless body offers a powerful means for investigating the properties of its surface (e.g., roughness and single-particle albedo). Typically, the phase angle data are fit to a parametric model, for instance that of *Hapke* (1993). Of particular interest is the opposition effect, which is neglected when using simple phase laws, such as the one introduced in §3.2. In addition to the intrinsic difficulties of observing cometary nuclei, the determination of the phase function further requires observations at different phase angles, each one having to be corrected for the effect of the rotation of the nucleus. Ideally, this requires determining the light curve at each phase angle, so that the measurements may be phased to the same rotational position, say the maxima of the light curves (*Delahodde et al.* 2001).

2P/Encke: A detailed analysis of recent, original measurements and a large collection of historical data led *Fernández et al.* (2000) to derive $\beta = 0.06\,\mathrm{mag\,deg^{-1}}$. This very steep phase function makes 2P/Encke one of the most phase-darkened objects in the solar system and implies a very rough surface.

9P/Tempel 1: Fernández et al. (2003) estimated a phase coefficient $\beta = 0.07\,\mathrm{mag\,deg^{-1}}$ that is poorly constrained. It is indeed unlikely that such a steep phase function is correct.

19P/Borrelly: Combining the disk–integrated magnitudes calculated from the *DS1* images with the *HST* (*Lamy et al.* 1998b) and ground-based measurements (*Rauer et al.* 1999), *Soderblom et al.* (2002) and *Buratti et al.* (2003) determined $\Phi(\alpha)$ over a large range of phase angle, from 3° to 88°. The phase curve is very similar to that of the dark C–type asteroid 253 Mathilde (*Clark et al.* 1999). Except for a minor opposition effect restricted to $\alpha \lesssim 3°$, this phase curve is well approximated by a constant linear phase coefficient $\beta = 0.04\,\mathrm{mag\,deg^{-1}}$ over the interval 3–90°.

28P/Neujmin 1: Jewitt and Meech (1987) determined a phase coefficient $\beta = 0.034 \pm 0.012\,\mathrm{mag\,deg^{-1}}$. *Delahodde et al.* (2001) obtained phase coverage extending from 0.8 to 19° and have been able to correct several data points for the effects of rotation. A linear phase coefficient $\beta = 0.025 \pm 0.006\,\mathrm{mag\,deg^{-1}}$ applies down to $\alpha \sim 5°$. At smaller phase angles, the function steepens and a strong opposition effect appears at $\alpha \lesssim 1.5°$. This effect, comparable to those found on medium albedo $p_V \sim 0.15$ M–type asteroids, and icy satellites, is quite surprising for a cometary nuclei. As surface ice is excluded on such a low activity nucleus, a high surface porosity could perhaps be invoked, but this possible interpretation has not been investigated.

45P/Honda–Mrkos–Pajdusakova: As discussed in §3.2, there is a distinct possibility that the *HST* and ground–based observations can be reconciled by a steep phase function with $\beta = 0.06\,\mathrm{mag\,deg^{-1}}$, similar to that of 2P/Encke and 48P/Johnson.

48P/Johnson: Observations of a star-like nucleus at phase angles between 6° and 16° led *Jewitt and Sheppard* (2003) to derive $\beta = 0.0592\,\mathrm{mag\,deg^{-1}}$.

55P/Tempel–Tuttle: The combination of *HST* and ground–based observations allowed *Lamy et al.* (2003) to obtain the phase function in the interval $3° - 55°$ and to derive a linear phase coefficient $\beta = 0.041\,\mathrm{mag\,deg^{-1}}$, similar to those of 19P/Borrelly and asteroid Mathilde.

143P/Kowal–Mrkos: Observations of a star-like nucleus at phase angles between 5° and 12.7° led *Jewitt et al.* (2003) to derive a linear phase coefficient $\beta = 0.043 \pm 0.0014\,\mathrm{mag\,deg^{-1}}$.

3.6. Satellites of Cometary Nuclei

The detection of a satellite companion to a cometary nucleus, and the determination of its orbit, would be of unique value as it would provide access to the mass of the primary. If the mass of the nucleus is known, and if the size is independently derived, then the mean bulk density and porosity can be calculated, providing insight into the internal properties of the nucleus.

There are various processes leading to the formation of binary systems among small bodies. In the case of cometary nuclei, a companion could be primordial or could result from the capture of a large fragment ejected by the nucleus; the capture of an external object appears unlikely. To be of value in the sense described above, a satellite must be sufficiently large to allow its detection and should travel on a stable orbit for some time. The motion of such a possibly active object around a rotating, non-spherical and active primary is, however, extremely complex and is, in fact, a major concern for the *Rosetta* orbiter. We review below the few cases where a companion may have been directly or indirectly detected.

17P/1892 V1 (Holmes): In late 1892, this comet underwent a major outburst (leading to its discovery), then faded by 7–8 magnitudes, and flared up again by 6 magnitudes a couple of months later. *Whipple* (1983, 1984) proposed that a satellite could produce this double burst: first a grazing encounter on 4.6 November 1892 and a final impact on 16.3 January 1893. Several details of this scenario explain the observations rather well. *Whipple* (1999) estimated the crushing strength (compressive strength, force/area) from the momentum transfer during the collision of the secondary with the primary nucleus, and it ranges from 4.2×10^3 to 5.9×10^5 dynes cm^{-2}, corresponding to mean bulk densities of 0.2 and 1.5 g cm^{-3}, respectively. The idea of an hypothetical satellite remains however highly speculative.

26P/Grigg–Skjellerup: During the *Giotto* flyby of this comet in 1992, the in-situ optical probe experiment (OPE) recorded several "spikes". One of them was interpreted by *McBride* (1997) as an object 10–100 meters in radius sporting a weak dust coma. However, it is not clear whether this object was in a bound orbit, or slowly traveling away after possibly separating from the nucleus.

C/1995 O1 (Hale–Bopp): From his analysis of *HST* WFPC2 images taken in May–October 1996, *Sekanina* (1998a) reported the detection of a companion which could be bound. He estimated a mass ratio of $\simeq$0.1, a semi-major axis of $\simeq$180 km, and a period of 2–3 days for a primary nucleus of radius $\simeq$35 km. Our analysis of the same set of images using a fully anisotropic coma model (*Weaver and Lamy* 1997; *Toth et al.* 1999) does not support this detection. These latter authors conclude that the "satellite" is probably due to the residual signal when fitting an over-simplified elliptical coma model to the real, highly structured coma of Hale–Bopp. Such artifacts have been found in another analysis performed by *Sekanina* (1995), namely that of comet D/Shoemaker–Levy 9: clumps of positive residuals were identified as fragments, while clumps of identical but negative

residuals were also present.

Adaptive optics observations with the ESO 3.6 m telescope in the near-infrared performed on 1997 November 6 possibly revealed the presence of a satellite: *Marchis et al.* (1999) discussed the pros and cons of this interpretation, but did not reach a clear and firm conclusion. *HST* images taken on the same day, and on other days, with the Space Telescope Imaging Spectrograph (STIS), do not reveal any obvious companion (*Weaver et al.* 1999) at the location and magnitude expected if the ground-based detection were real. If there is a satellite, then either it remained within 1 STIS pixel (0.05 arcsec) of the primary for more than 3 months, or the *HST* observers were unlucky and observed near the time of an orbital transit event (i.e., when the two objects appear to move across each other).

Possible additional evidence for a companion of comet Hale–Bopp comes from the analysis of the complex morphology of its coma (jets and halos). *Vasundhara and Chakraborty* (1999) and *Sekanina* (1998b) have noted difficulties in explaining several coma features with a single rotating nucleus, thereby suggesting that two nuclei are involved, but the analysis of *Samarasinha* (2000) demonstrates that the coma morphology is consistent with a single nucleus.

C/2001 A2 (LINEAR): The splitting of this comet was accompanied by outbursts, and *Sekanina* (2002c) quoted the rare, but possible, scenario of the flaring of the primary nucleus due to collision with a companion that had been created by the fragmentation events (*Whipple* 1984; *Sekanina* 1982a). *Sekanina* (1997) had previously suggested that a part of the mantle of the nucleus (icy-dust mantle) could be lifted off the surface and then travel away from the primary during a non-tidal splitting. However, this is only speculation, and there is no direct evidence of a satellite around this comet.

Concluding remarks: While the occurrence of satellites for both main belt and near-Earth asteroids, Kuiper belt objects, and Trojans is steadily growing (*Merline et al.*

2002), there is still no definite, observational evidence that binary cometary nuclei exist. Since detecting and characterizing cometary nuclei remains a huge challenge, the detection of a smaller companion is probably beyond our present and near–future capabilities. Do double craters and crater chains (catenae) observed on planetary satellites (*Melosh and Schenk* 1993; *Melosh and Whitaker* 1994; *Schenk et al.* 1996) provide independent evidence of binary and multiple objects? Known double craters are plausibly created by the impact of two orbiting bodies and can likely be explained with the currently known asteroidal sources, and do not require a cometary component, but that does not mean that a cometary component is ruled out. Catenae are thought to be formed from tidally disrupted cometary nuclei, (an asteroidal origin is, however, not ruled out) but, in that case, the fragments are not orbiting one another; rather, the multiple objects are laid out in a line along their common orbit. In the case of a cometary impactor, fragmentation may have first taken place, leading to the creation of a trail of small bodies, very much like the case of D/Shoemaker–Levy 9.

4. ANALYSIS AND INTERPRETATION

4.1. Size Distribution of Cometary Nuclei

Figures 3a and b present the distribution functions of the effective radius $r_{n,v}$ of, respectively ECs and NICs, as summarized in Tables 1 and 2 (the range of radius has been truncated at 12 km for better legibility of the histograms at small sizes). These represent the largest data sets ever assembled. The histograms show several structures, which most likely result from the limited statistics in the data set. We note that there are not very many large cometary nuclei; only 2 EC and 2 NIC nuclei have radii larger than 10 km. The apparent roll-off in the number of small cometary nuclei is very likely an observational selection effect (i.e., smaller nuclei are simply harder to detect). A similar effect is often

encountered with flux-limited surveys, e.g., for the NEOs at magnitudes fainter than ∼17, but additional mechanisms cannot be excluded (see below). *Brandt et al.* (1996) advocated the idea of a large population of undetected ECs having very small nuclei, but they presented no observational evidence to support this hypothesis. For NICs, the above shortcomings are exacerbated by the small number of comets in the sample. However, if the sungrazing comets, which are probably the fragments of one or several large nuclei, are considered as full members of this family, then there is clear evidence of a large population of very small, sub–100 m, cometary nuclei (*Biesecker et al.* 2002). This clearly shows that under the right circumstances, e.g., coronagraphic observations of sun-grazers, small objects can be detected.

A more robust and physically enlightening way to view size distributions is to introduce cumulative distribution functions, which are less prone to artifacts. One can consider the cumulative luminosity function (CLF) $N_L(< H)$, where N_L is the number of nuclei with absolute magnitude brighter than H, and the cumulative size distribution (CSD) $N_S(> r_n)$, where N_S is the number of nuclei larger than radius r_n. If these two distributions are represented by power laws:

$$N_L(< H) \propto 10^{q_L H} \tag{13}$$

$$N_S(> r_n) \propto r_n^{-q_S} \tag{14}$$

and if all objects have the same albedo, then $q_S = 5q_L$ (*Weissman and Lowry* 2003). Quite recently, several groups have collected various data sets and studied the CLF and/or the CSD of ecliptic comets; their results are summarized in Table 6.

At stake here is the question of the origin of ECs. If they are collisional fragments of TNOs (*Stern* 1995; *Farinella and Davis*, 1996), then the theoretical value $q_S = 2.5$ for a collisionally relaxed population (*Dohnanyi* 1969) is expected. In reality, the question is probably more complex.

On the one hand, the model of *Dohnanyi* applies to a population of self-similar bodies having the same strength per unit mass. Several groups have attempted to relax this assumption, with *O'Brien and Greenberg* (2003) presenting the most comprehensive results on steady-state size distributions for collisional populations. In the range of sizes of interest for cometary nuclei, the size distribution of fragments is wavy, and oscillates about the distribution of a population evolved under pure gravity scaling. The differential size distribution of such a population is characterized by a power law with an exponent of -3.04. This translates into $q_S = 2.04$ using our notation for the cumulative distribution.

On the other hand, non–collisional fragmentation (i.e., splitting) is frequent among comets (see *Boehnhardt* 2004), and nuclei are progressively eroded by their repeated passages through the inner part of the solar system, so that we are certainly not observing a primordial, collisionally relaxed population of TNO fragments. A crude calculation by *Weissman and Lowry* (2003) indicates that a typical EC loses $\sim$400 m in radius at half of its lifetime as an active object. *Samarasinha* (2003) undertook a more comprehensive study of this problem in which mass loss includes outgassing and splitting events (rotational and tidal splitting). His only example for a population of nuclei with an initial differential size distribution having an exponent of -3 indeed shows considerable leveling off after 1000 years. Mass loss may therefore significantly distort the size distribution of nuclei, particularly at the low end. While it is tempting to introduce this kind of statistical correction to account for mass shedding, this approach certainly does not reflect the reality for any given comet, which could be at any stage of its orbital evolution. But a case-by-case correction faces the difficulty of the chaotic nature of the orbital evolution of ecliptic comets.

Figure 4a presents the CSD of 65 ecliptic comets for which we have reliable values of the effective radius $r_{n,v}$ (Table 1). Above some critical radius ($r_c \sim 1.6$ km), the CSD appears to follow a single power law. Below r_c, the distribution levels off, a likely result

of observational bias and mass loss, as discussed above. The determination of the power exponent q_S, and of the value of r_c, was performed using three different techniques. We first used the least-squares fit because it has been widely used for similar studies by various groups; we however stress that this method is NOT applicable to CSDs because the data points are not independent, which renders the standard χ^2 statistic meaningless. Next, we used a fit based on a maximum likelihood parameter estimation, namely the *M-estimate* technique based on the MEDFIT algorithm described by *Press et al.* (1986) and implemented as the routine LADFIT in IDL. This procedure returns the mean absolute deviation of the data from the power law but does not return an uncertainty on the power exponent. Finally, we calculated the probability P_{KS} that the observed distribution for $r_n > r_c$ and the model distribution $N(> r_n) \propto r_n^{-q_S}$ are drawn from the same parent distribution using the Kolmogorov–Smirnov (K-S) test. We found that the optimum cut-off value is $r_c = 1.6\,\mathrm{km}$ and then explored the variation of P_{KS} in the neighborhood of the value of q_S determined by the M-estimate technique (Figure 5). The high value of P_{KS} (0.953) for the nominal value of q_S returned by the M-estimate fit is encouraging, as is the result that the distribution of P_{KS} values is symmetric about the nominal M-estimate value. In order to define an uncertainty on q_S, we adopted the criterion that $P_{KS} \geq 0.5$, which implies that $q_S = 1.9 \pm 0.3$ for a cut-off $r_c = 1.6\,\mathrm{km}$ (Table 6).

As the largest comets are removed from the CSD, the M-estimate technique tends to consider the remaining largest nuclei as outliers, yielding steeper slopes. As a first test, we removed the largest nucleus in our data base, namely 29P/Schwassmann–Wachmann 1 (the deletion of this comet may also be justified on the basis that it is more properly classified as a Centaur, rather than an EC), and obtained a nominal value of $q_S = 2.1$ from the M-estimate fit, with a P_{KS} value of 0.86. Although this result is consistent with the previous one, given the uncertainties, we note that the distribution of P_{KS} values is not centered on the nominal value of q_S returned by the M-estimate fit.

In a second step, we also removed the next largest nucleus, namely 28P/Neujmin 1, and obtained a nominal value of $q_S = 2.4$, with P_{KS} only reaching 0.62. Note also that the distribution of P_{KS} values is even more skewed away from the nominal M-estimate value, which suggests that q_S is not very well-determined.

In summary, we conclude that q_S could be as small as $\sim$1.6 and as large as $\sim$2.5, with a preferred value of $\sim$2.0. However, we will quote $q_S = 1.9 \pm 0.3$ because that is our result for the CSD that includes all the ECs for which reliable data have been obtained.

Table 6 shows that our result is intermediate between those of *Lowry et al.* (2002; $q_S = 1.6 \pm 0.1$) and *Weissman and Lowry* (2003; $q_S = 1.59 \pm 0.03$, recently revised to $q_S = 1.79 \pm 0.05$; *Weissman, private communication*), on the one hand, and *Fernandez et al,* (1999; $q_S = 2.65 \pm 0.25$), on the other hand. Regarding the first group of authors, we note that they incorrectly included 8P/Tuttle, a quite large nucleus, in their data set and that their power exponent has been revised upward to be nearly compatible with our range (note also that their quoted uncertainty is underestimated owing to their use of least-squares fitting). Regarding the second group, i.e., *Fernandez et al.* (1999), we concur with *Weissman and Lowry* (2002) in noting that their fitted slope covers only 12 comets over a very small range of radius, namely a factor of only 1.6. *Fernandez et al.* (1999) have further limited their sample to those nuclei having perihelion distances $q < 2\,\mathrm{AU}$, fearing a possible bias, with nuclei with $q > 2\,\mathrm{AU}$ being systematically larger than those with $q < 2\,\mathrm{AU}$. We have examined this question in detail, and figure 6 shows that there is no evidence for a systematic trend of size of the nucleus with perihelion distance. While there is indeed a larger number of small nuclei ($r_n < r_c$) with $q < 2\,\mathrm{AU}$ than with $q > 2\,\mathrm{AU}$, the two populations of larger nuclei ($r_n > r_c$) have similar statistical properties (at least at the present level of accuracy), as already noted by *Weissman and Lowry* (2003). This is thus irrelevant when fitting the size distribution of nuclei with $r_n > r_c$ to a power law, and, in

fact, has not been considered by the other groups listed in Table 6.

The comparison with the result of *Meech et al.* (2003; $q_S = 2.5$) is not straightforward because it was obtained from a Monte Carlo reconstruction of the CSD that attempts to remove various selection effects, i.e., to *unbias* the observed CSDs. From their table 11, we estimate $q_S \sim 1.5$ but we wonder whether this observed CSD includes both the short–period and long–period comets, as it is the case for their histogram displayed in their figure 6. We note that these authors truncated their original distribution ($q_S = 2.5$) and that, in fact, their best fit model is truncated below $r_n = 5.0\,\mathrm{km}$. It will be interesting to see how their result evolves when their Monte Carlo simulation is applied to a larger data set, such as ours.

It is tempting to compare our result for the distribution of ECs, $q_S \sim 1.9 \pm 0.3$, with the general trend of the power law of a collisionally population evolved with pure gravity scaling, $q_S = 2.04$ (*O'Brian and Greenberg* 2003). On the one hand, it must be kept in mind that the simulated distribution is in fact wavy in the size interval of cometary nuclei, so that different values of q_S may hold in different size intervals. On the other hand, our data set has not yet been corrected for bias effects and the statistics still remain limited, at essentially all sizes. We need far more measurements before we can conclusively determine the size distribution of ECs. As a way of testing how the distribution could evolve, we decided to incorporate additional objects. Our sample already includes highly evolved nuclei such as 28P/Neujmin 1. We now go one step further and include the population of asteroidal objects thought to be dormant or extinct comets, on the basis of their Tisserand parameters, or their association with meteor streams. The cometary origin of these NEOs is still highly speculative, and many of them may be bona fide asteroids coming from the outer regions of the asteroidal belt, including the Hilda group and Jupiter Trojans (*Fernandez et al.* 2002). Selection effects are also different from those of the ECs, and any

future unbiasing should reflect these differences. For the purpose of the present exercise, we considered 21 "cometary" NEOs that can be associated with ECs, and whose sizes have been determined (Table 7), thus bringing the data base to 86 objects. The "cometary" NEOs tend to be larger on average than the ECs, thus significantly filling the 2-10 km radius range, but flattening the CSD simply because they are more of them at larger sizes; indeed, we found $q_S = 1.6 \pm 0.2$, P_{KS} reaching 0.85 when including these NEOs. The experiment of removing 29P and 28P has also been performed, and the results are illustrated in Figure 5b. Because the new CSD is better constrained, the impact of removing these objects is much reduced compared to the case of ECs alone. We further note that the new CSD better fits a power law function, thus reducing the differences between the M-estimate and K–S determinations of q_S.

Table 8, adapted from *Weissman and Lowry* (2003), displays the power exponents q_S and q_L for various minor body populations in the solar system. The power exponent of the CSD of KBOs is quite large, $q_S = 3.15 - 3.45$, but strictly applies to objects with $r_n > 20$ km. It is not clear whether this value extends down to smaller sizes to allow a meaningful comparison with ECs. In fact, it has been suggested that KBOs follow a broken power law with the larger objects ($r_n \gtrsim 50$ km) retaining their primordial size distribution with the above value of q_S, while the smaller objects represent collisional fragments having a shallower distribution (e.g., *Davis and Farinella* 1997), which could then be rather similar to that of the ECs. The power exponent of the CSD of Centaurs, $q_S = 2.7 - 3.0$, is also larger than that of the ECs. However, the statistics are rather poor, and we found that, from the data of 9 Centaurs reported by *Barucci et al.* (2004), it is very difficult to fit a power law to the observed CSD: the exponent can take any value, from 3.1 down to 1.2, depending on the imposed cut–off at small sizes.

The CSD of ecliptic comets is beginning to look remarkably similar to that of

Near-Earth objects: note the result of *Stuart* (2001), $q_S = 1.96$ which is essentially identical to our value. For the main-belt asteroids, size distributions are so well-defined that changes in the power exponent can be recognized in different size regimes (see the details in *Jedicke and Metcalfe*, 1998), and we have simply indicated the ranges. NEOs and main-belt asteroids are thought to be collisionally dominated populations, yet they have power exponents significantly different from the canonical value of $q_S = 2.5$ obtained by *Dohnanyi* (1969).

A final comparison is that with the CSD of the fragments of comet D/1999 S4 (LINEAR): from water production rates measured following its breakup, *Makinen et al.* (2001) found that the measurements could best be explained by a fragment size distribution having $q_S = 1.74$, which is within the range we estimate for the ECs.

The question of the size distribution of ECs at the lower end, $r_c < 1.6\,\mathrm{km}$, remains totally open. The possible influence of both observational and evolutionary biases has been mentioned already, but a real depletion cannot be excluded. Indeed, the depletion of small nuclei is supported by the measurements of crater distributions on several airless bodies of the solar system, where cratering from comets is believed to dominate, e.g., Europa (*Chapman et al.* 1997) and Ganymede and Callisto (*Zahnle et al.* 2001).

Figure 4b displays the CSD of the 13 nearly-isotropic cometary nuclei whose effective radii, $r_{n,v}$, have been determined (Table 2). Also plotted is the CSD of this population augmented by the 12 asteroidal objects thought to be dormant or extinct NICs on the basis of their Tisserand parameters (Table 7). Owing to the poor statistics, we did not attempt to fit power laws to the observed CSDs. We note, however, based on the present data set, the rather shallow CSD of the NICs and the lack of small nuclei that NICs apparently share with ECs.

4.2. Shape and Rotation Period of Cometary Nuclei

Figure 7 displays the distribution of the axial ratio a/b of cometary nuclei. One should bear in mind that the bulk of the values are, strictly speaking, lower limits. There is not enough data for NICs to draw any conclusion. For ECs, the histogram is highly skewed with a median value of $\sim$1.5, and there is *a priori* no reason to suspect that this property is biased by the aspect angle. There are a few cases of highly-elongated nuclei with $a/b > 2$, the maximum value being 2.6 at present.

Figure 8 displays the distribution of rotational periods. One should bear in mind that most of them are not accurately determined because of the scarcity of data points to define the light curves. The range of 5 to 70 hrs is remarkably similar to that of the periods of main–belt asteroids and NEOs, excluding the monolithic fast rotators (e.g., *Whiteley et al.* 2002). We further note that the bulk of the nuclei measured so far have periods in a more restricted range, 5 to 18 hrs, but this may result from observational bias.

The results on rotational periods and axial ratios can be used to estimate lower limits on the density of the nuclei, assuming that they are strengthless (i.e., that cometesimals are not physically bound) and that they are not rotating faster than the centrifugal limit for breakup (*Luu and Jewitt* 1992; *Meech* 1996). Figure 8 displays the relevant diagram, where periods are plotted versus axial ratios. Lines corresponding to the critical rotational period for different bulk densities of the nucleus are also plotted. The figure suggests that the fastest rotating nuclei are stable against centrifugal disruption, if their bulk densities exceed $\sim$0.6 g cm^{-3} (see also *Weissman et al.* 2004).

4.3. Albedos of Cometary Nuclei

One of the features evident in Table 4 is the very narrow range of albedos of cometary nuclei, namely 0.02 to 0.06. 29P/Schwassmann–Wachmann 1 stands as an exception with possibly $p = 0.13$ according to *Cruikshank and Brown* (1983), suggesting that this object may indeed be better classified as a Centaur. We further note that the lowest values have been measured at 4845 Å. As most nuclei have a red color, converting these values to the V band slightly increases them. As an example, we find $p_V = 0.025$ for 10P/Tempel 2 and $p_V = 0.030$ for 49P/Arend–Rigaux. The average value for the 13 nuclei listed in Table 4, excluding 29P, is $p_V = 0.038 \pm 0.009$ and $p_R = 0.042 \pm 0.017$, assuming a typical normalized reflectivity gradient of $S' = 10\%/1000$ Å. These values nicely bracket the canonical albedo of 0.04, which is, therefore, fully justified. The range of albedos is so narrow that looking for trends is almost hopeless. This question has been recently investigated by *Campins and Fernández* (2003), who concluded that there is no trend with perihelion distance and a slight trend of decreasing albedo with increasing nuclear radius, the correlation being significant only at the 2σ level.

4.4. Colors of Cometary Nuclei

Figure 9 displays the distributions of the $(B - V)$, $(V - R)$, and $(R - I)$ color indices, excluding 19P/Borrelly for which the uncertainty is too large, which can be compared to the solar indices $(B - V)_\odot = 0.65$, $(V - R)_\odot = 0.35$ and $(R - I)_\odot = 0.28$. The mean values of the indices $< (B - V) >= 0.82$, $< (V - R) >= 0.41$ and $< (R - I) >= 0.38$ confirm the well known result that cometary nuclei are statistically redder than the Sun. Their colors are, however, very diverse, as already discussed for a smaller sample (*Luu* 1993), from slightly blue to very red. Even if we exclude 14P/Wolf and 86P/Wild 3, for which the uncertainty in $(V - R)$ is very large, there are two comets, 43P/Wolf–Harrington

and 107P/Wilson–Harrington, which have a well determined $(V - R) = 0.31 \pm 0.03$, significantly less that of the Sun. The reddest nucleus in the present sample is that of 143P/Kowal–Mrkos, with $(V - R) = 0.58$, still less red than the average $(V - R) = 0.61$ of KBOs (*Jewitt* 2002).

As pointed out in §4.4, colors by themselves do not reveal much about the physical properties, but the distribution of colors compared to other solar system objects may provide information on their interrelationships. This topic is discussed in *Jewitt* (2004).

5. SUMMARY, OPEN ISSUES, AND FUTURE DIRECTIONS

5.1. Current status

Remarkable progress has been made during the past decade in measuring the sizes of cometary nuclei, but it is also clear that this field is still in its infancy. Reliable data exist for only 65 comets, so any conclusions regarding the distribution of sizes is necessarily tentative and subject to future revision. Measurements are needed for substantially more comets, at least doubling or tripling the current number, before confidence can be gained in the conclusions regarding the size distribution. Our current best estimate, $q_S = 1.9 \pm 0.3$, is conspicuously different from that of the KBO and Centaur populations, but is similar to that of the NEOs. This value also corresponds to that of a collisionally evolved population with pure gravity scaling, but we re–emphasize that *O'Brian and Greenberg* (2003) showed that this distribution is, in fact, wavy in the size range relevant to ECs.

The situation for cometary albedos is even worse, in the sense that reliable values are available for only about a dozen objects. Nevertheless, we are struck by the relatively small range in the albedo (0.04 ± 0.02), which suggests that the surfaces of cometary nuclei are exceptionally dark, contrary to the early expectations for these "icy" bodies.

Measuring accurate shapes of cometary nuclei is sometimes possible but requires intensive observing campaigns, generally extending over several days. Furthermore, the aspect angle of the rotational axis usually varies with time, so that observations at widely-separated places in the comet's orbit are desirable to obtain a clear picture of the comet's rotational properties and true shape. Although there are some examples of highly-elongated cometary nuclei, with the major axis being up to 2.6 times larger than the minor axis, most cometary nuclei seem to differ from spherical bodies by $\sim$50%. However we must keep in mind that the axial ratio values are often lower limits. Fortunately, conclusions regarding the size distribution of cometary nuclei are not strongly affected by uncertainties in the shapes.

It is also difficult to obtain reliable color data on cometary nuclei. While the color of the nucleus itself does not provide unique information on the physical properties, color data are useful for comet-to-comet comparisons, which may suggest differences in surface properties, and, especially, in making comparisons with other minor bodies in the solar system (e.g., Centaurs, TNOs, and asteroids). The colors of cometary nuclei are diverse, with some being highly reddened compared to solar color, some being neutral, and a few having a slightly blue color.

5.2. Outstanding issues and future investigations

An important, unresolved issue concerns the interpretation of disk-integrated thermal measurements, which, in principle, provide robust determinations of sizes and albedos. The so-called *Standard Thermal Model* for asteroids is often used to interpret cometary thermal data, although its applicability to objects having a mixture of dust and ice is questionable.

A totally open issue is the nature of the size distribution of cometary nuclei at the small

end of the spectrum. Does the relatively steep power law derived from the intermediate-sized objects extend indefinitely to smaller sizes? Or is the size distribution truncated at some value that depends on the physical formation mechanism (e.g., gravitational instability within the solar nebula) or destruction mechanism (e.g., , total disruption)?

What is the bias in ecliptic comet discoveries and how does that affect the current distribution of sizes? Why do we observe so few large ($r_n \gtrsim 5$ km) cometary nuclei?

How does evolution affect the physical properties of cometary nuclei? Is there really a continuum of surface properties that is dependent on the activity level and physical evolution (e.g., with a youthful Chiron at one end and an aged 2P/Encke on the other) ? Continual loss of the surface layers through repeated passages through the inner solar system obviously affects the size, and probably the shape and color, of cometary nuclei, and how do we account for this in estimating the primordial distribution of physical properties? Some combination of improved modeling and observations of nuclei will help, but it is not yet clear that these issues can ever be resolved satisfactorily.

Splitting events obviously affect the size and shape of cometary nuclei, and how do we estimate their effect on the distribution functions? Perhaps better data on the splitting rates of nuclei, coupled with a better understanding of the physical mechanism(s) for splitting events, will help to resolve these issues, but that remains to be seen.

Of course, one of the most interesting avenues for future exploration is the relationship between cometary nuclei and the other minor bodies in the solar system. Can we use the size distribution of cometary nuclei to conclude that they are a collisionally-evolved population? In particular, can the size distribution and the shapes of cometary nuclei be used to conclude that they are collisional fragments of the TNOs? If the Centaurs are TNOs on the road to becoming ecliptic comets, then perhaps Centaurs and these comets share common physical properties. If not, can the differences be explained by

evolutionary effects? Although cometary nuclei generally contain much more ice than asteroids do, perhaps "evolved" comets share many common characteristics with asteroids. In addition, at least some asteroids, and many cometary nuclei, are thought to have porous, "rubble-pile" physical structures (*Davis et al.* 1985; *Weissman* 1986); does this point to commonalities in their formation mechanism?

It seems clear that remote observations with 2-3 m telescopes will continue to play a critical role in measuring the physical properties of cometary nuclei as a population. We can certainly hope to make as much progress during the next decade as we have witnessed in the previous one, and we can look forward to many new advances in our understanding of the physical properties of cometary nuclei in the future. During its remaining lifetime, and subject to approval of the relevant programs, *HST* can essentially complete a survey of the bulk of the known population of ECs and provide unique, accurate color data. Large ground–based telescopes (e.g., *Keck, Very Large Telescope*) will also contribute by detecting nuclei at large heliocentric distances, where they are presumed inactive. With its unsurpassed sensitivity, *SIRTF* will be capable of detecting the nuclei of a large fraction of the ECs in the mid–infrared, thus providing albedo–independent determinations of their size. *Herschel* will also be able to provide albedo–independent size determinations, but for larger, more distant nuclei in the submillimeter wavelength range. Finally, the *Atacama Large Millimetre Array (ALMA)* will be able to detect a significant number of nuclei at 1.3 mm. Combining *ALMA* and *SIRTF* data should provide robust information on the long–wavelength emissivity and internal thermal properties of cometary nuclei.

Future spacecraft encounters will undoubtedly shed further light on the nature of cometary nuclei, and will even start to address the diversity issue in a serious way as more and more objects come under intense scrutiny. While we very much regret the loss of the *CONTOUR* mission, which would have flown by 1P/Encke and 73P/Schwassmann-

Wachmann 3, we now look forward to the flybys of 81P/Wild 2 (*Stardust* mission) and 9P/Tempel 1 (*Deep Impact* mission), the latter also probing the interior of the nucleus. Space investigations of cometary nuclei will culminate with the *Rosetta* mission, whose orbiter will accompany the nucleus of 67P/Churyumov–Gerasimenko from a heliocentric distance of 3.6 AU to perihelion at 1.3 AU and observe it at all spatial scales down to a few millimeters, thus allowing an unprecedented view of how the activity starts and evolves. The *Rosetta* lander will perform a broad range of in-situ observations and analysis of the surface and subsurface regions of the nucleus.

6. CONCLUSION

When David Jewitt presented the first "modern" review of the physical properties of cometary nuclei, at the 30th Liège conference in 1992 (*Jewitt* 1992) just 10 years ago, his sample was limited to 4 ECs, 1 HTC, and Chiron. His review incorporated rotation and precession, internal and surface properties, and a comparison with asteroids. At the 1996 Asteroids, Comets, and Meteor (ACM) conference, Karen Meech's review discussed 17 ECs, 7 HTCs, and 2 Centaurs (Chiron and 29P). For the Comets II book, the study of cometary nuclei is divided among 10 chapters, with questions such as the physical properties, rotation, surface properties, internal properties, and the relationship with other minor bodies deserving their own, separate chapters. Our review of the physical properties of cometary nuclei discusses 65 ECs and 13 NICs, with the Centaurs being treated in a different chapter. This illustrates the tremendous advancement of research on the cometary nucleus during the past decade. And since there has been only one cometary space mission during the past 10 years, namely *Deep Space 1*, the bulk of the progress has been achieved by ground and space observatories, demonstrating that the use of better techniques and better detectors, coupled with new telescopes (but some old ones as well), is capable of

achieving what was long considered hopeless. On the one hand, we are far from fully understanding cometary nuclei, as illustrated above by the list of outstanding issues. On the other hand, the future is bright as new facilities will soon allow us to push the present limits of our observational capabilities even further, while forthcoming cometary space missions will allow us to study a few nuclei in unprecedented detail.

7. ACKNOWLEDGEMENTS

We thank O. Hainaut, S. Lowry, G. Tancredi, and P. Weissman for kindly making their latest results available to us in advance of publication. We are very much grateful to P. Weissman for his thorough review of an earlier version of this chapter, which led to substantial improvements. We further thank G. Bernstein, H. Boehnhardt, J. Fernández, J. Licandro, and N. Samarasinha for their constructive remarks. PLL and IT acknowledge the support of the French Programme National de Planétologie, jointly funded by CNRS and CNES and of the bilateral French- Hungarian cooperation program. IT further acknowledges the support of the Université de Provence and of the Hungarian State Research Foundation for Sciences (OTKA) through grant No. T025049. HAW acknowledges financial support by NASA through grants HST–GO–8699.01–A and HST–GO–8876.01–A from the Space Telescope Science Institute (STScI), which is operated by the Association of Universities for Research in Astronomy, Inc., under NASA contract NAS5-26555. This work is partly based on observations made with the NASA/ESA *Hubble Space Telescope* and obtained at the STScI.

REFERENCES

Abell P.A., Fernández Y.R., Pravec P., French L.M., Farnham T.L., Gaffey M.J., Hardersen P.S., Kusnirak P., Sarounova L., and Sheppard S.S. (2003) Physical characteristics of asteroid-like comet nucleus C/2001 OG108 (LONEOS). *LPSC, 34*, 1253.

Abergel A., and Bertaux J.-L. (1990) Rotation states of the nucleus of Comet Halley compatible with spacecraft images. *Icarus, 86*, 21-29.

A'Hearn M.F., Campins H., Schleicher D.G., Millis R.L. (1989) The nucleus of comet P/Tempel 2. *Astrophys. J., 347*, 1155-1166.

A'Hearn M.F. and the Deep Impact Science Team (2002) The Deep Impact Mission. In *Cometary Science after Hale–Bopp*. Session 6a: What can we learn from space missions ? (Puerto de La Cruz, Tenerife, Spain, 21–25 January, 2002) (Poster).

Allen D.A. (1971) The method of determining infrared diameters. In *Physical Studies of Minor Planets*. Proceedings of IAU Colloq. 12, held in Tucson, AZ, March, 1971. T. Gehrels, Ed., NASA SP 267, p. 41.

Altenhoff W.J., Batrla W.K., Huchtmeier W.K., Schmidt J., Stumpff P., and Walmsley M. (1983) Radio observations of comet 1983 d. *Astron. Astrophys., 125*, L19-L22.

Altenhoff W.J., and Stumpff P. (1995) Size estimate of "asteroid" 2060 Chiron from 250 GHz measurements. *Astron. Astrophys., 293*, L41-L42.

Altenhoff W.J., Bieging J.H., Butler B., Butner H.M., Chini R., Haslam C.G.T., Kreysa E., Martin R.N., Mauersberger R., McMullin J., Muders D., Peters W.L., Schmidt J., Schraml J.B., Sievers A., Stumpff P., Thum C., von Kap-Herr A., Wiesemeyer H., Wink J.E., and Zylka R. (1999) Coordinated radio continuum observations of comets Hyakutake and Hale–Bopp from 22 to 860 GHz. *Astron. Astrophys., 348*, 1020-1034.

Barucci A.M. et al. (2004) Physical characteristics of TNOs and Centaurs. In *Comets II.* (M. Festou, H.U. Keller, and H.A. Weaver, Eds.), University of Arizona Press, Tucson.

Belton M.J.S. (1990) Rationalization of comet Halley's periods. *Icarus, 86*, 30-51.

Belton M.J., Mueller B.E.A., Julian W.H., and Anderson A.J. (1991) The spin state and homogenity of comet Halley's nucleus. *Icarus, 93*, 183-193.

Belton M.J.S. (2000) The excited rotational state of 2P/Encke. *Bull. Amer. Astron. Soc., 32*, Abstr. [36.12].

Benner L.A.M., Ostro S.J., Giorgini J.D., Jurgens R.E., Mitchell D.L., Rose R., Rosema K.D., Slade M.A., Winkler R., Yeomans D.K., Campbell D.B., Chandler J.F., and Shapiro I.I. (1997) Radar detection of Near-Earth Asteroids 2062 Aten, 2101 Adonis, 3103 Eger, 4544 Xanthus, and 1992 QN. *Icarus, 130*, 296-312.

Biesecker D.A., Lamy P., St. Cyr O.C., Llebaria A., and Howard R.A. (2002) Sungrazing comets discovered with the SOHO/LASCO coronographs 1996–1998. *Icarus, 157*, 323-348.

Bobrovnikoff N.T. (1931) On the spectra of comets 1910 I, 1911 IV, 1929 d. *Publ. Astron. Soc. Pacific, 43*, 61-65.

Bockeleé-Morvan D., Biver N., Moreno R., Colom P., Crovisier J., Gérard E., Henry F., Lis D.C., Matthews H., Weaver H.A., Womack M., and Festou M.C. (2001) Outgassing behavior and composition of comet C/1999 S4 (LINEAR) during its disruption. *Science, 292*, 1339-1343.

Boehnhardt H., and Birkle K. (1994) Time variable coma structures in comet P/Swift–Tuttle. *Astron. Astrophys. Suppl. Ser. 107*, 101-120.

Boehnhardt H., Birkle K., and Osterloh M. (1996) Nucleus and tail studies of comet P/Swift–Tuttle. *Earth, Moon, and Planets, 73*, 51-70.

Boehnhardt H., Babion J., and West R.M. (1997) An optimized detection technique for faint moving objects on a star-rich background. *Astron. Astrophys., 320*, 642-651.

Boehnhardt H., Rainer N., Birkle K., Schwehm G. (1999) The nuclei of comets 26P/Grigg-Skjellerup and 73P/Schwassmann–Wachmann 3. *Astron. Astrophys., 341*, 912-917.

Boehnhardt H., Delahodde C., Sekiguchi T., Tozzi G.P., Amestica R., Hainaut O.R., Spyromilio J. Tarenghi M., West R.M., Schulz R., and Schwehm G. (2002). VLT observations of comet 46P/Wirtanen. *Astron. Astrophys., 387*, 1107-1113.

Boehnhardt H. (2004) Split comets and comet outburst. In *Comets II.* (M. Festou, H.U. Keller, and H.A. Weaver, Eds.), University of Arizona Press, Tucson.

Bottke W.F., Morbidelli A., Jedicke R., Petit J.-M., Levison H.F., Michel P., and Metcalfe T.S. (2002) Debiased orbital and absolute magnitude distribution of the Near-Earth Objects. *Icarus 156*, 399-433.

Bowell E., Hapke B., Domingue D., Lumme K., Peltoniemi J., and Harris A.W. (1989) Application of photometric models to asteroids. In *Asteroids II* (R.P. Binzel, T. Gehrels, and M.S. Matthews, Eds.) University of Arizona, Tucson, pp. 524-556.

Brandt J.C., A'Hearn M.F., Randall C.E., Schleicher D.G., Shoemaker E.M., and Stewart A.I.F. (1996) Small comets (SCs): an unstudied population in the Solar System inventory. In *Completing the Inventory of the Solar System.* Astron. Soc. Pacific Conferences Proceedings, Vol. 107, (T.W. Rettig and J.M. Hahn, Eds.), pp. 289-297.

Brooke T.Y., and Knacke R.F. (1986) The nucleus of comet P/Arend–Rigaux. *Icarus, 67*, 80-87.

Brown R.H., Cruikshank D.P., and Griep D. (1985) Temperature of comet IRAS–Araki–Alcock (1983 d). *Icarus, 62*, 273-281.

Brown R.H. (1985) Ellipsoidal geometry in asteroid thermal models – The standard radiometric model. *Icarus, 64*, 53-63.

Buratti B.J., Hicks M.D., Soderblom L.A., Britt D., Oberst J., and Hillier J.K. (2003) Deep Space 1 photometry of the nucleus of comet 19P/Borrelly. *Icarus*, in press.

Bus S.J., Buie M.W., Schleicher D.G., Hubbard W.B., Marcialis R.L., Hill R., Wasserman L.H., Spencer J.R., Millis R.L., Franz O.G., Bosh A.S., Dunham E.W., Ford C.H., Young J.W., Elliott J.L., Meserole R., Olkin C.B., McDonald S.W., Foust J.A., Sopata L.S., and Bandyopadhyay R.M. (1996) Stellar occultation by 2060 Chiron. *Icarus, 123*, 478-490.

Campbell D.B., Harmon J.K., and Shapiro I.I. (1989) Radar observations of comet Halley. *Astrophys. J., 338*, 1094-1105.

Campins H., A'Hearn M.F., and McFadden L-A. (1987) The bare nucleus of comet Neujmin 1. *Astrophys. J., 316*, 847-857.

Campins H. (1988) The anomalous dust production in periodic comet Encke. *Icarus, 73*, 508-515.

Campins H., Telesco C.M., Osip D.J., Rieke G.H., Rieke M.J., and Schulz B. (1994) The color temperature of (2060) Chiron: A warm and small nucleus. *Astron. J., 108*, 2318-2322.

Campins H., and Schleicher D.G. (1995) Comet d'Arrest: A small and rapidly rotating nucleus ? *Bull. Amer. Astron. Soc., 27*, 1113.

Campins H., Osip D.J., Rieke G.H., and Rieke M.J. (1995) The radius and albedo of comet-asteroid transition object 4015 Wilson–Harrington. *Planet. Space Sci., 43*, 733-736.

Campins H., Licandro J., Chamberlain M., and Brown R.H. (2001) Constraints on the surface composition of comet 28P/Neujmin 1. *Bull. Amer. Astron. Soc., 33*, Abstr. [31.08].

Campins H., and Fernández Y.R. (2003) Observational constraints on surface characteristics of comet nuclei. *Earth, Moon, and Planets*, in press.

Carlson N. (1990) 52P/Harrington–Abell. *MPC 17685*.

Chamberlin A.B., McFadden L-A., Schulz R., Schleicher D.G., and Bus S.J. (1996) 4015 Wilson–Harrington, 2201 Oljato, and 3200 Phaethon: Search for CN emission. *Icarus, 119*, 173-181.

Chapman C.R., Merline W.J., Bierhaus B., Keller J., and Brooks S. (1997) Impactor populations on the Galilean satellites. *Bull. Amer. Astron. Soc., 29*, Abstr. [12.10].

Clark B.E., Veverka J., Helfenstein P., Thomas P.C., Bell J., Harch A., Robinson M.S., Murchie S.L., McFadden L.A., and Chapman C.R. (1999) NEAR photometry of asteroid 253 Mathilde. *Icarus, 140*, 53-65.

Clark B.E., Helfenstein P., Bell J.F., Peterson C., Veverka J., Izenberg N.I., Domingue D., Wellnitz D., and McFadden L. (2002) NEAR infrared spectrometer photometry of asteroids 433 Eros. *Icarus, 155*, 189-204.

Combes M., Moroz V.I., Crifo J.F., Lamarre J.M. Charra J., Sanko N.F., Soufflot A., Bibring J.P., Cazes S. Coron N., Crovisier J., Emerich C., Encrenaz T., Gispert R., Grigoryev A.V., Guyot G., Krasnopolsky V.A., Nikolsky Yu.V., and Rocard F. (1986) Infrared sounding of comet Halley from VEGA 1. *Nature, 321*, 266-268.

Cruikshank D.P., and Brown R.H. (1983) The nucleus of comet P/Schwassmann–Wachmann 1. *Icarus, 56*, 377-380.

Cruikshank D.P., Roush T.L., Bartholomew M.J., Geballe T.R., Pendleton Y.J., White S.M., Bell J.F., Davies J.K., Owen T.C., de Bergh C., Tholen D.J., Bernstein M.P., Brown R.H., Tryla K.A., Dalle Ore C.M. (1998) The composition of Centaur 5145 Pholus. *Icarus, 135*, 389-407.

Davis D.R., Chapman C.R., Weidenschilling S.J., and Greenberg R. (1985) Collisional history of asteroids – Evidence from Vesta and Hirayama families. *Icarus, 62*, 30-53.

Davis D.R., and Farinella P. (1997) Collisional evolution of Edgeworth–Kuiper belt objects. *Icarus, 125*, 50-60.

Delahodde C.E., Meech K.J., Hainaut O., and Dotto E. (2001) Detailed phase function of comet 28P/Neujmin 1. *Astron. Astrophys., 376*, 672-685.

Delahodde C.E., Hainaut O.R., Romon-Martin J., and Lamy P.L. (2002) VLT near-infrared spectra of distant comets: First results with 90P/Gehrels 1. In *Proceedings of the Asteroids, Comets, Meteors 2002 Conference*, 29 July – 2 August, 2002, Berlin. Abstr. [20-08p].

Delahodde C.E. et al. (2003) Comet 111P/Helin–Roman–Crockett. In preparation.

Delbo M., Harris A.W., Binzel R.P., Pravec P. and Davies J.K. (2003) Keck observations of near-Earth asteroids in the thermal infrared. *Icarus, 166*, in press.

Delsemme A.H., and Rud D.A. (1973) Albedos and cross-sections for the nuclei of comets 1969 IX, 1970 II and 1971 I. *Astron. Astrophys., 28*, 1-6.

De Sanctis M.C., Lazzarin M., Barucci M.A., Capria M.T., and Coradini A. (2000) Comet P/Gehrels 3: spectroscopic observations and nucleus models. *Astron. Astrophys., 354*, 1086-1090.

Dohnanyi J.S. (1969) Collisional model of asteroids and their debris. *J. Geophys. Res., 74*, 2431-2554.

Donn B. (1976) In *The Study of Comets*. (Eds.: B. Donn et al.), NASA SP-393, pp. 611-621. NASA, Washington, DC.

Duncan M., et al. (2004) Origin and dynamical evolution of ecliptic comets. In *Comets II*. (M. Festou, H.U. Keller, and H.A. Weaver, Eds.), University of Arizona Press, Tucson.

Dones L., Weissman P., Levison H., and Duncan M. (2004) Oort cloud formation and dynamics. In *Comets II*. (M. Festou, H.U. Keller, and H.A. Weaver, Eds.), University of Arizona Press, Tucson.

Emerich C., Lamarre J.M., Gispert R., Coron N., Combes M., Encrenaz T., Crovisier J., Rocard E. Bibring J.P., and Moroz V.I. (1987b) Temperature of the nucleus of Comet Halley. In *Proceedings of the International Symposium on the Diversity and Similarity of Comets*, (E, Rolfe, and B. Battrick, Eds.) ESA Publication Division, ESTEC, Noordwiijk, The Netherlands. *ESA SP-278*, pp. 703-706.

Farinella P., and Davis D.R. (1996) Short–period comets: Primordial bodies or collisional fragments? *Science, 273*, 938-941.

Farnham T., Schleicher D.G., Williams W.R., and Smith B.R. (1999) The rotation state and active regions of comet Hale–Bopp (1995 O1). *Bull. Amer. Astron. Soc., 31*, Abstr. [30.01].

Farnham T., Schleicher D.G., Woodney L.M., Eberhardy C.A., Birch P.V., and Levy L. (2001) Imaging and photometry of comet C/1999 S4 (LINEAR) before perihelion and after breakup. *Science, 292*, 1348-1353.

Fay T.D., and Wisniewski W. (1978) The light curve of the nucleus of comet d'Arrest. *Icarus, 34*, 1-9

Feierberg M.A., Witteborn F.C., Johnson J.R., and Campins H. (1984) 8– to 13–micron spectrophotometry of comet IRAS–Araki–Alcock. *Icarus, 60*, 449-454.

Fernandez J.A., Tancredi G., Rickman H., and Licandro J. (1999) The population, magnitudes, and sizes of Jupiter Family Comets. *Astron. Astrophys., 352*, 327-340.

Fernandez J.A., Gallardo T., Brunini A. (2002) Are there many Jupiter-family comets among the Near-Earth Asteroid population? it Icarus, 159, 358-368.

Fernández Y.R. (1999) Physical properties of cometary nuclei. PhD Thesis. University of Maryland. College Park.

Fernández Y.R., Wellnitz D.D., Buie M.W., Dunham E.W., Millis R.L., Nye R.A., Stansberry J.A., Wasserman L.H., A'Hearn M.F., Lisse C.M., Golden M.E., Person M.J., Howell R.R., Marcialis R.L., and Spitale J.N. (1999) The inner coma and nucleus of Hale–Bopp: Results from a stellar occultation. *Icarus, 140*, 205-220.

Fernández Y.R., Lisse C.M., Ulrich Käufl H., Peschke S.B., Weaver H.A., A'Hearn M.F., Lamy P., Livengood T.A., and Kostiuk T. (2000) Physical properties of the nucleus of comet 2P/Encke. *Icarus, 147*, 145-160.

Fernández Y.R., Jewitt D.C., and Sheppard S.S. (2001) Low albedos among extinct comet candidates. *Astrophys. J., 553*, L197-L200.

Fernández Y.R., Jewitt D.C., and Sheppard S.S. (2002a) Thermal properties of Centaurs Asbolus and Chiron. *Astron. J., 123*, 1050-1055.

Fernández Y.R., Jewitt D.C., and Sheppard S.S. (2002b) Comet 57P/du Toit–Neujmin–Delporte. *IAU Circular, 7935*, 2002 July 20 (Ed.: D.W.E. Green, CBAT).

Fernández Y.R., Lowry S.C., Weissman P.R., and Meech K.J. (2002c) New dominant periodicity in photometry of comet Encke. *Bull. Amer. Astr. Soc., 34*, Abstr. [27.06]

Fernández Y.R. (2003) The nucleus of comet Hale–Bopp (C/1995 O1): Size and activity. *Earth, Moon, and Planets, 89*, 3-25.

Fernández Y.R., Meech K.J., Lisse C.M., A'Hearn M.F., Pittichová J., and Belton M.J.S. (2003) The nucleus of Deep Impact target comet 9P/Tempel 1. *Icarus, 164*, 481-491.

Fitzsimmons A., and Williams I.P. (1994) The nucleus of comet P/Levy (1991 XI) *Astron. Astrophys.. 289*, 304-310.

Fomenkova M.N., Jones B., Pina R., Puetter R., Sarmecanic J., Gehrz R., and Jones T. (1995) Mid-infrared observations of the nucleus and dust of comet P/Swift–Tuttle. *Astron. J., 110*, 1866-1874 + Plate 103.

Garradd G.J. (1997) Comet 2P/Encke. *IAU Circular, 6717*, 1997 August 13 (Ed.: B.G. Marsden, CBAT).

Gladman B., Kavelaars J.J., Petit J.-M., Morbidelli A., Holman M.J., and Loredo T. (2001) The structure of the Kuiper Belt: Size distribution and radial extent. *Astron. J. 122*, 1051-1066.

Goldstein R.M., Jurgens R.F., and Sekanina Z. (1984) A radar study of comet IRAS–Araki–Alcock 1983 d. *Astron. J., 89*, 1745-1754.

Green S.F., Meadows A.J., and Davies J.K. (1985) Infrared observations of the extinct cometary candidate minor planet (3200) 1983 TB. *Mon. Not. Roy. Astr. Soc., 214*, 29P-36P.

Groussin O., and Lamy P.L. (2003) Activity on the surface of the nucleus of comet 46P/Wirtanen *Astron. Astrophys.*, in press.

Groussin O., Lamy P.L., Jorda L., and Toth I. (2003a) The nucleus of comets 126P/IRAS and P/Hartley 2. *Astron. Astrophys.*, in press.

Groussin O., Lamy P.L. (2003b) Properties of the nucleus of Centaurs Chiron and Chariklo *Astron. Astrophys.*, in press.

Groussin O., Lamy P., Gutiérrez P.J., and Jorda L. (2004) The nucleus of comet IRAS–Araki–Alcock (C/1983 H1). *Astron. Astrophys.*, submitted.

Gutiérrez P.J., Ortiz J.L., Rodrigo R., Lôpez-Moreno J.J. (2001) Effects of irregular shape and topography in thermophysical models of heterogeneous cometary nuclei. *Astron. Astrophys., 374*, 326-336.

Gutiérrez P.J., de León J., Jorda L., Licandro J., Lara L.M., and Lamy P. (2003) New spin period determination for comet 6P/d'Arrest. *Astron. Astrophys., 407*, L37-L40.

Hainaut O.R. et al. (1996) Comet 43P/Wolf–Harrington. *Minor Planet Circular* 27955.

Hainaut O.R., Meech K.J., Boehnhardt H., and West R.M. (1998) Early recovery of comet 55P/Tempel–Tuttle. *Astron. Astrophys., 333*, 746-752.

Hainaut O.R. and Delsanti A.C. (2002) Colors of Minor Bodies in the Outer Solar System. A statistical analysis. *Astron. Astrophys., 389*, 641-664.

Hanner M.S., Giese R.H., Weiss K., and Zerull R. (1981) On the definition of albedo and application to irregular particles. *Astron. Astrophys., 104*, 42-46.

Hanner M.S., Aitken D.K., Knacke R., McCorkle S., Roche P.F., and Tokunaga A.T. (1985) Infrared spectrophotometry of comet IRAS–Araki–Alcock (1983 d) – A bare nucleus revealed? *Icarus, 62*, 97-109.

Hanner M.S., Newburn R.L., Spinrad H., and Veeder G.J. (1987) Comet Sugano–Saigusa–Fujikawa (183 V) – A small, puzzling comet. *Astron. J., 94*, 1081-1087.

Hapke B. (1986) Bidirectional reflectance spectroscopy. IV – The extinction coefficient and opposition effect. *Icarus, 67*, 264-280.

Hapke B. (1993) *Theory of Reflectance and Emittance Spectroscopy.* Cambridge University Press, New York.

Harmon J.K., Campbell D.B., Hine A.A., Shapiro I.I., and Marsden B.G. (1989) Radar observations of comet IRAS–Araki–Alcock 1983 d. *Astrophys. J., 338*, 1071-1093.

Harmon J.K., Nolan M.C., Ostro S.J., and Campbell D.B. (2004) Radar studies of comet nuclei and grain comae. In *Comets II.* (M. Festou, H.U. Keller, and H.A. Weaver, Eds.), University of Arizona Press, Tucson.

Harris A.W. (1998) A thermal model for Near-Earth Asteroids. *Icarus, 131*, 291-301.

Harris A.W., and Lagerros J.S.V. (2002) Asteroids in the thermal infrared. In *Asteroids III*, (Eds.: W.F. Bottke, A. Cellino, P. Paolicchi, and R.P. Binzel), Univ. of Arizona, Tucson. pp. 205-218.

Irvine, W. M. and 40 colleagues (1984) Radioastronomical observations of comets IRAS-Araki-Alcock (1983d) and Sugano-Saigusa-Fujikawa (1983e). *Icarus, 60* 215-220.

Jedicke R., and Metcalfe T.S. (1998) The orbital and absolute magnitude distribution of main belt asteroids. *Icarus, 131*, 245-260.

Jewitt D.C., and Meech K.J. (1985) Rotation of the nucleus of P/Arend–Rigaux. *Icarus, 64*, 329-335.

Jewitt D.C., and Meech K.J. (1987) CCD photometry of comet P/Encke. *Astron. J., 93*, 1542-1548.

Jewitt D.C., and Meech K.J. (1988) Optical properties of cometary nuclei and a preliminary comparison with asteroids. *Astrophys. J., 328*, 974-986.

Jewitt D., and Luu J. (1989) A CCD portrait of comet P/Tempel 2. *Astron. J., 97*, 1766-1790, Plates Nos. 105-106, pp. 1984-1842.

Jewitt D. (1991) Cometary photometry. In *Comets in the post-Halley Era.* Vol. 1, pp. 19-65. (R.L.Jr. Newburn, M. Neugebauer, and J. Rahe, Eds.), Kluwer Academic Publishers (*Astrophys. and Space Sci. Libr., 167*, Vol. 1.

Jewitt D.C. (1992) Physical properties of cometary nuclei. Invited review, in *Proceedings of the 30th Liége International Astrophysical Colloquium*, (Eds.: A. Brahic, J.-C. Gerard, and J. Surdej), pp. 85-112, Univ. Liége Press, Liége.

Jewitt D., and Kalas P. (1998) Thermal observations of centaur 1997 CU26. *Astrophys. J., 499*, L103-L106.

Jewitt D.C., and Luu J.X. (2001) Colors and spectra of Kuiper Belt objects. *Astron. J., 122*, 2099-2114.

Jewitt D. (2001) From Kuiper Belt Objects to cometary nucleus: The missing ultra-red matter. *Astron. J., 123*, 1039-1049.

Jewitt D. (2002) From Kuiper Belt to cometary nucleus. *ESA SP-500*, 11-19.

Jewitt D , Sheppard S. and Fernández Y. (2003) 143P/Kowal–Mrkos and the shapes of cometary nuclei *Astron. J., 125*, 3366–3377.

Jewitt D., and Sheppard S. (2003) The nucleus of comet 48P/Johnson. Submitted to the *Astron. J.*

Jewitt D. (2004) Comets: Interrelations and Origins. In *Comets II.* (M. Festou, H.U. Keller, and H.A. Weaver, Eds.), University of Arizona Press, Tucson.

Johnson R.E. (1991). Irradiation effects in a comet's outer layers. *J. Geophys. Res., 96*, 17553-17557.

Jorda L., and Lecacheux J. (1992) Periodic Comet Swift–Tuttle. *IAU Circular, 5664*, 1992 November 27 (Ed.: B.G. Marsden, CBAT).

Jorda L., Rembor K., Lecacheux J., Colom P., Colas F., Frappa E., and Lara L.M. (1999) The rotational parameters of Hale–Bopp (C/1995 O1) from observations of the dust jets at Pic du Midi Observatory. *Earth, Moon, and Planets, 77*, 167-180.

Jorda L., Lamy P., Groussin O., Toth I., A'Hearn M.F., and Peschke S. (2000) ISOCAM observations of cometary nuclei. In *Proc. ISO beyond Point Sources: Studies of Extended Infrared Emission.* (September 4–9, 1999, ISO Data Centre, Villafranca del Castillo, Madrid, Spain. Eds. R.J. Laureijs, K. Leech and M.F. Kessler.). *ESA-SP 455*, p. 61.

Kamél L. (1990) The Comet Light Curve Catalog/Atlas – A presentation. In *Proceedings of a Meeting Asteroids, Comets, Meteors 1989.* (June 12–16, 1989, Uppsala, Eds.: C.-I. Lagerkvist, H. Rickman, and B.A. Lindblad). p. 363.

Kamél L. (1992) The comet Light Curve Atlas. The comet Light Curve Catalogue/Atlas. III – The Atlas. *Astron. Astrophys. Suppl. Ser., 92*, 85-149.

Kamoun P.G., Pettengill G.H., and Shapiro I.I. (1982) Radar observations of cometary nuclei. In *Comets.* (Eds.: L.L. Wilkening), University of Arizona Press, Tucson, AZ, pp. 288-296.

Kamoun P.G., Campbell D., Pettengill G., and Shapiro I. (1999) Radar observations of three comets and detection of echoes from one: P/Grigg–Skjellerup. *Planet. Space Sci., 47*, 23-28.

Keller H.U., Arpigny C., Barbieri C., Bonnet R.M., Cazes S., Coradini M., Cosmovici C.B., Delamere W.A., Huebner W.F., Hughes D.W., Jamar C., Malaise D., Reitsema H.J., Schmidt H.U., Schmidt W.K.H., Seige P., Whipple F.L., and Wilhelm K. (1986) First Halley Multicolour Camera imaging results from GIOTTO. *Nature, 321*, 320-326.

Keller H.U., Delamere W.A., Reitsema H.J., Huebner W.F., and Schmidt H.U. (1987) Comet P/Halley's nucleus and its activity. *Astron. Astrophys., 187*, 807-823.

Keller H.U. (1990) The nucleus. In *Physics and Chemistry of Comets.* (W.F. Huebner, Ed.), pp. 13-68, Springer-Verlag, Berlin.

Keller H.U., Crudt W., Kramm J.-R., and Thomas N. (1994) Images of the Nucleus of Comet Halley obtained by the Halley Multicolour Camera (HMC) on board the Giotto spacecraft. *ESA SP-1127* Vol 1, p. 69.

Keller H.U., Thomas N., and Britt D. (2004) In situ observations of comet nuclei In *Comets II.* (M. Festou, H.U. Keller, and H.A. Weaver, Eds.), University of Arizona Press, Tucson.

Krešák L., Carusi A., Perozzi E., and Valsecchi G.B. (1984) Periodic comets Neujmin 3 and Van Biesbroeck. *IAU Circular, 3940*, 1984 April 25 (Ed.: B.G. Marsden, CBAT).

Lamy P.L., and Toth I. (1995) Direct detection of a cometary nucleus with the Hubble Space Telescope. *Astron. Astrophys., 293*, L43-L45.

Lamy P.L., Toth I., Grün E., Keller H.U., Sekanina Z., and West R.M. (1996) Observations of comet P/Faye 1991 XXI with the Planetary Camera of the Hubble Space Telescope. *Icarus, 119*, 370-384.

Lamy P.L., Toth I., Jorda L., and Weaver H.A. (1998a) The nucleus and the inner coma of comet 46P/Wirtanen. *Astron. Astrophys., 335*, L25-L29.

Lamy P.L., Toth I., and Weaver H.A. (1998b) Hubble Space Telescope Observations of the nucleus and inner coma of comet 19P/Borrelly 1994l. *Astron. Astrophys., 337*, 945-954.

Lamy P.L. and the HST WFPC2 comet team (1998c) Comet 55P/Tempel–Tuttle. *IAU Circular, 6851*, 1998 March 27 (Ed.: D.W.E. Green, CBAT).

Lamy P.L., Toth I., A'Hearn M.F., and Weaver H.A. (1999a) Hubble Space Telescope observations of the nucleus of comet 45P/Honda–Mrkos–Pajdusakova and its inner coma. *Icarus, 140*, 424-438.

Lamy P.L., Jorda L., Toth I., Groussin O., A'Hearn M.F., and Weaver H.A. (1999b) Characterization of the nucleus of comet Hale–Bopp from HST and ISO observations. *Bull. Amer. Astron. Soc., 31*, p. 1116, Abstr. [27.03].

Lamy P.L., Toth I., Weaver H.A., Delahodde C., Jorda L., and A'Hearn M.F. (2000) The nucleus of 13 short–period comets. *Bull. Amer. Astr. Soc., 32*(3), 1061, Abstr. [36.04].

Lamy P.L., Toth I., Weaver H.A., Delahodde C., Jorda L., and A'Hearn M.F. (2001) The nucleus of 10 short–period comets. *Bull. Amer, Astr. Soc., 33*(3), 1093, Abstr. [31.01].

Lamy P.L., Toth, I., A'Hearn M.F., Weaver H.A., and Weissman P.R. (2001) Hubble Space Telescope observations of the nucleus of comet 9P/Tempel 1. *Icarus, 154*, 337-344.

Lamy P.L., Toth I., Jorda L., Groussin O., A'Hearn M.F., and Weaver H.A. (2002) The nucleus of comet 22P/Kopff and its inner coma. *Icarus, 156*, 442-455.

Lamy P.L., Toth I., Jorda L., Groussin O., A'Hearn M.F., and H.A. Weaver (2003a) The nucleus of comet 55P/Tempel–Tuttle and its inner coma. *Icarus*, submitted.

Lamy P.L., Toth I., Weaver H.A., Jorda L., and Kaasalainen M. (2003b) The nucleus of comet 67P/Churyumov–Gerasimenko, the new target of the ROSETTA mission. *Bull. Amer. Astron. Soc., 35*, [30.04].

Larsen J.A., Gleason A.E., Danzl N.M. Descour A.S., McMillan R.S., Gehrels T., Jedicke R., Montani J.L., and Scotti J.V. (2001) The Spacewatch Wide-Field Area Survey for bright Centaurs and Trans-Neptunian Objects. *Astron. J. 121*, 562-579.

Lecacheux J., Jorda L., Enzian A., Klinger J., Colas F., Frappa E., and Laques P. (1996) Comet C/1996 B2 (Hyakutake). *IAU Circular, 6354*, 1996 March 26 (Ed.: D.W.E. Green, CBAT).

Leibowitz E.M., and Brosch N. (1986) Periodic photometric variations in the near nucleus zone of P/Giacobini–Zinner. *Icarus, 68*, 430-441.

Levison H.F. (1996) Comet taxonomy. In *Completing the Inventory of the Solar System.* Astron. Soc. Pacific Conferences Proceedings, Vol. 107, (T.W. Rettig and J.M. Hahn, Eds.), pp. 173-192.

Levison H.F., Morbidelli A., Dones L., Jedicke R., Wiegert P.A., Bottke W.F. Jr. (2002) The mass disruption of Oort cloud comets. *Science, 296*, 2212-2215.

Licandro J., Bellot R., Luis R., Boehnhardt H., Casas R., Goetz B., Gomez A., Jorda L., Kidger M., Osip D., Sabalisk N., Santos P., Serr-Ricart M., Tozzi G.P., and West R. (1998) The rotation period of C/1995 O1 (Hale–Bopp). *Astrophys. J., 501*, L221-L225.

Licandro J., Tancredi G., Lindgren M., Rickman H., and Gil Hutton R. (2000) CCD photometry of cometary nuclei, I: Observations from 1990-1995. *Icarus, 147*, 161-179.

Licandro J., Guerra J.C., Campins H., Di Martino M., Lara L.M., Gil-Hutton R., and Tozzi G.P. (2002) The surface of cometary nuclei related minor icy bodies. *Earth, Moon, and Planets, 90*, 495-496.

Licandro J., Campins H., Hergenrother C., and Lara L.M. (2003) Near-infrared spectroscopy of the nucleus of comet 124P/Mrkos. *Astron. Astrophys., 398*, L45-L48.

Lisse C.M., Fernández Y.R., Kundu A., A'Hearn M.F., Dayal A., Deutsch L.K., Fazio G.G., Hora J.L., and Hoffmann W.F. (1999) The nucleus of comet Hyakutake (C/1996 B2). *Icarus, 140*, 189-204.

Lowry S.C., Fitzsimmons A., Cartwright I.M., and Williams I.P. (1999) CCD photometry of distant comets. *Astron. Astrophys., 349*, 649-659.

Lowry S.C., and Fitzsimmons A. (2001) CCD photometry of distant comets II. *Astron. Astrophys., 365*, 204-213.

Lowry S.C., Fitzsimmons A., and Collander-Brown S. (2003) CCD photometry of distant comets. III. Ensemble properties of Jupiter-family comets. *Astron. Astrophys., 397*, 329-343.

Lowry S.C., and Weissman P.R. (2003) CCD observations of distant comets from Palomar and Steward observatories. *Icarus, 164*, 492-503.

Lowry S.C., Weissman P., Sykes M.V., and Reach W.T. (2003) Observations of periodic comet 2P/Encke: physical properties of the nucleus and first visual-wavelength detection of its dust trail. *LPSC 34*, 2056.

Lunine J., et al. (2004) Physico and chemical phenomena in the solar nebula. In *Comets II.* (M. Festou, H.U. Keller, and H.A. Weaver, Eds.), University of Arizona Press, Tucson.

Luu J., and Jewitt D. (1990a) The nucleus of comet P/Encke. *Icarus, 86*, 69-81.

Luu J., and Jewitt D. (1990b) Cometary activity of 2060 Chiron. *Astron. J., 100*, 913-932.

Luu J., and Jewitt D. (1991) Periodic comet Chernykh (1991 o). *IAU Circular, 5347*, 1991 September 16 (Ed.: B.G. Marsden, CBAT).

Luu J.X., and Jewitt D.C. (1992) Near-aphelion CCD photometry of comet P/Schwassmann–Wachmann 2. *Astron. J., 104*, 2243-2249.

Luu J.X. (1993) Spectral diversity among the nuclei of comets. *Icarus, 104*, 138-148.

Luu, J.X., Jewitt D.C., and Trujillo Ch. (2000) Water ice in 2060 Chiron and its implications for Centaurs and Kuiper Belt Objects. *Astrophys. J., 531*, L151-L154.

Lyttleton R.A. (1953) *The Comets and their Origin.* Cambridge University Press.

Lyttleton R.A. (1963) Book Review (Buchbesprechungen über): *The Nature of Comets* by N.B. Richter, with an Introduction by R.A. Lyttleton, London, Methen 1963. In *Ztschr. f. Astrophysik, 58*, 295-296.

Mäkinen J.T.T., Bertaux J.-L., Pulkkinen T.I., Schmidt W., Kyrölä E., Summanen T., Quémerais E., and Lallement R. (2001) Comets in full sky L-alpha maps of the SWAN instrument. I. Survey from 1996 to 1998. *Astron. Astrophys. 368*, 292-297.

Marchis F., Boehnhardt H., Hainaut O.R., and Le Mignant D. (1999) Adaptive optics observations of the innermost comet of C/1995 O1. Are there a "Hale" and a "Bopp" in comet Hale–Bopp ? *Astron. Astrophys., 349*, 985-995.

Manteca P. (2001) Comet 51P/Harrington. *IAU Circular, 7769*, 2001 December 8 (Ed.: D.W.E. Green, CBAT).

Marsden B.G. (1974) Comets in 1973. *Quart. J. Roy. Astron. Soc., 15*, 433-460.

Marsden B.G., and Roemer E. (1978) Comet in 1974. *Quart. J. Roy. Astron. Soc., 19*, 38-58.

Marsden B.G. (2002) Comet 57P/du Toit–Neujmin–Delporte. *IAU Circular, 7934*, 2002 July 13, (Ed.: B.G. Marsden, CBAT).

McBride N., Green S.F., Levasseur-Regourd A.C., Goidet-Devel B., and Renard J.-B. (1997) The inner dust coma of comet 26P/Grigg–Skjellerup: multiple jets and nucleus fragments ? *Mon. Not. R. Astr. Soc., 289*, 535-553.

Meech K.J., and Jewitt D.C. (1987) Observations of Comet P/Halley at minimum phase angle. *Astron. Astrophys., 187*, 585-593.

Meech K.J. (1992) Observations comet Černis (1983 XII) at 19.4 and 20.9 AU. *Bull. Amer. Astron. Soc., 24*, p. 993, Abstr. [29.06].

Meech K.J., Belton M.J.S., Mueller B.E.A., Dicksion M.W., and Li, H.R. (1993) Nucleus properties of P/Schwassmann–Wachmann 1. *Astron. J., 106*, 1222-1236.

Meech K.J., Bauer J.M., and Hainaut O.R. (1997) Rotation of comet 46P/Wirtanen. *Astron. Astrophys., 326*, 1268-1276.

Meech K.J. (1996) Physical properties of cometary nuclei. Invited paper in *Proceedings of the conference on Asteroids, Comets, Meteors 1996*, Paris–Versaille, 1996. *Adv. Space Res.*, in press.

Meech K.J. and Newburn R. (1998) Observations and modelling of 81P/Wild 2. *Bull. Amer. Astron. Soc., 30*, 1094. Abstr. [42.03].

Meech et al. (2000) unpublished, cf. Meech et al. (2002).

Meech K.J., and Hainaut O.R. (2002). Distant comet observations. In *Tidal and Collisional Interactions of Small Bodies in the Solar System*, Astrophysics and Space Science Library, in press.

Meech K.J., Hainaut O.R., and Marsden B.G. (2004) Comet nucleus size distribution from HST and Keck Telescopes. *Icarus*, in press.

Melosh H.J., and Schenk P. (1993) Split comets and the origin of crater chains on Ganymede and Callisto. *Nature, 365*, 731.

Melosh H.J., and Whitaker E.A. (1994) Lunar crater chains. *Nature, 369*, 713.

Merényi E., Foldy L., Szego K, Toth I., Kondor A. (1990) The landscape of comet Halley. *Icarus, 86*, 9-20.

Merline W.J., Weidenschilling S.J., Durda D.D., Margot J.L., Pravec P., and Storss A.D. (2002) Asteroids do have satellites. In *Asteroids III*, (Eds.: W.F. Bottke, A. Cellino, P. Paolicchi, and R.P. Binzel), Univ. of Arizona, Tucson. In press.

Millis R.L., A'Hearn M.F., and Campins H. (1988) An investigation of the nucleus and coma of comet P/Arend–Rigaux. *Astrophys. J., 324*, 1194-1209.

Mueller B.E.A. (1992) CCD–photometry of comets at large heliocentric distances. In Proc. Asteroids, Comets, Meteors III, (1991). (Eds.: A. Harris and E.L.G. Bowell), LPI Houston, TX. pp. 425-428.

Mueller B.E.A., and Ferrin I. (1996) Change in the rotational period of comet P/Tempel 2 between 1988 and 1994 apparitions. *Icarus, 123*, 463-477.

Mueller B.E.A., and Samarasinha N.H. (2001) Lightcurve observations of 19P/Borrelly. *Bull. Amer. Astron. Soc., 33*, Abstr. [28.02].

Nelson R.M., Soderblom L.A., and Hapke B.W. (2004) Are the circular dark features on comet Borrelly's surface albedo variations or pits ? *Icarus*, in press.

O'Brian D.P, and Greenberg R. (2003) Steady-state size distributions for collisional populations: Analytical solution with size-dependent strength. *Icarus*, in press.

O'Ceallaigh D.P., Fitzsimmons A., and Williams I.P. (1995) CCD photometry of comet 109P/Swift–Tuttle. *Astron. Astrophys., 297*, L17-L20.

Ostro S.J. (1996) NASA/JPL radar telescope observes nucleus of comet Hyakutake. *JPL News Release 9620*, 1996 March 29. http://www.jpl.nasa.gov/release/96/hyakurad.html.

Peale S.J., and Lissauer, J.J. (1989) Rotation of Halley's comet. *Icarus, 79*, 396-430.

Pittichová J. (1997) On the rotation of the IRAS–Araki–Alcock nucleus. *Planet. Space Sci., 45*, 791-794.

Press W.H., Flannery B.P., Teukolsky S.A., and Vetterling W.T. (1986) Numerical Recipes, Cambridge University Press, Cambridge.

Prialnik D., Benkhoff J., and Podolak M. (2004) Modeling comet nuclei. In *Comets II.* (M. Festou, H.U. Keller, and H.A. Weaver, Eds.), University of Arizona Press, Tucson.

Qi C., Blake G.A., Muhleman D.O., and Gurwell M.A. (1998) Interferometric of comet Hale–Bopp with the Owens Valley Millimeter Array. *Bull. Amer. Astron. Soc., 30*, p. 1451, Abstr. [55.20p].

Rauer H., Hahn G., Harris A., Helbert J., Mottola S., and Oberst J. (1999) Nuclear parameters of comet P/Borrelly. *Bull. Amer. Astron. Soc., 31*, Abstr. [37.03].

Roemer E. (1965) Observations of comets and minor planets. *Astron. J., 70*, 387-402.

Roemer E. (1966) The dimensions of cometary nuclei. In *Nature et Origine des comètes.* Proc. Coll. Inst. Univ. Liège, pp. 23-28.

Roemer E. (1968) Dimensions of the nucleus of periodic and near-parabolic comets. *Astron. J., 73*, 33.

Russell H.N. (1916) On the albedo of the planets and their satellites. *Astrophys. J., 43*, 173-195.

Sagdeev R.Z., Szabo F., Avenasov G.A., Cruvellier P., Szabo L., Szego K., Abergel A., Balazs A., Barinov I.V., Bertaux J.-L., Blamount J., Detaille M., Demarelis E., Dul'nev G.N., Endroczy G., Gardos M., Kanyo M., Kostenko V.I., Krasikov V.A., Nguyen-Trong T., Nyitrai Z., Renyi I., Rusznyak P., Shamis V.A., Smith B., Sukhanov K.G., Szabo F., Szalai S., Tarnopolsky V.I., Toth I., Tsukanova G., Valnicek B.I., Varhalmi L., Zaiko Yu.K., Zatsepin S.I., Ziman Ya.L., Zsenei M., and Zhukov B.S. (1986a) Television observations of comet Halley from VEGA spacecraft. *Nature, 321*, 262-266.

Sagdeev R.Z., Avenasov G.A., Ziman Ya.L., Moroz V.I., Tarnopolsky V.I., Zhukov B.S., Shamis V.A., Smith B.A., and Toth I. (1986b) TV experiment of the VEGA mission: Photometry of the nucleus and the inner coma. *ESA SP-250 Vol. II*, 317-326.

Sagdeev R.Z., Szego K., Smith B.A., Larson S., Merenyi E., Kondor A., and Toth I. (1989) The rotation of P/Halley. *Astron, J., 97*, 546-551.

Samarasinha N.H., and A'Hearn M.F. (1991) Observational and dynamical constraints on the rotation of comet P/Halley. *Icarus, 93*, 194-225.

Samarasinha N.H. (2000) The coma morphology due to an extended active region and the implications the spin state of comet Hale–Bopp. Proc. Coll. Inst. Univ. Liège. *Astrophys. J., 529*, L107-L110.

Samarasinha N.H. (2001) A model for the breakup of comet C/1999 S4 (LINEAR). *Icarus, 154*, 540-544.

Samarasinha N.H. (2003) Rotation and activity of comets *Adv. Space Res.*, in press.

Samarasinha N.H., and Jorda L. (2004) Rotation states of comet nuclei. In *Comets II.* (M. Festou, H.U. Keller, and H.A. Weaver, Eds.), University of Arizona Press, Tucson.

Scotti J.V. (1994) Periodic comet Harrington (1994 g). *IAU Circular, 6089*, 1994 October 5 (Ed.: B.G. Marsden, CBAT).

Schenk P.M., Asphaug E., McKinnon W.B., Melosh H.J., and Weissman P.R. (1996) Cometary nuclei and tidal disruption: The geologic record of crater chains on Callisto and Ganymede. *Icarus, 121*, 249-274.

Schuller F. (1930) Comet Schwassmann–Wachmann (1930 d). *IAU Circular, 288*, 1930 June 16 (Ed.: E. Stromgren, BCTA, IAU, Copenhagen).

Sekanina Z. (1976) A continuing controversy: Has the cometary nucleus been resolved ? In *The Study of Comets.* (Eds.: B. Donn et al.), NASA SP-393, pp. 537-587. NASA, Washington, DC.

Sekanina Z. (1981) Distribution and activity of discrete emission areas on the nucleus of periodic comet Swift–Tuttle. *Astron. J., 86*, 1741-1773.

Sekanina Z. (1982a) The problem of split comets in review. In *Comets.* (Eds.: L.L. Wilkening). University of Arizona Press, Tucson, AZ, pp. 251-287.

Sekanina Z. (1982b) Comets Hartley (1982 b, 1982 c). (Comet 79P/du Toit–Hartley). *IAU Circular, 3665*, 1982 February 11 (Ed.: B.G. Marsden, CBAT).

Sekanina Z. (1984) Precession model for the nucleus of periodic comet Kopff. *Astron. J., 89*, 1573-1586.

Sekanina Z. (1987) Anisotropic emission from comets: Fans versus jets. 1. Concept and modeling. In *Proceedings of the International Symposium on the Diversity and Similarity of Comets.* (Eds.: B. Battrick, E. Rolfe, and R. Reinhard. ESA Publ. Division, ESTEC, Noordwiijk, The Netherlands). *ESA SP-278*, 315-322.

Sekanina Z. (1988) Nucleus of comet IRAS–Araki–Alcock (1983 VII). *Astron. J., 95*, 1876-1894.

Sekanina Z. (1989) Comprehensive model for the nucleus of comet P/Tempel 2 and its activity. *Astron. J., 102*, 350-388.

Sekanina Z. (1995) Evidence on size and fragmentation of the nuclei of comet Shoemaker–Levy 9 from Hubble Space Telescope images. *Astron. Astrophys., 304*, 296-316.

Sekanina Z. (1997) The problem of split comets revisited. *Astron. Astrophys., 318*, L5-L8.

Sekanina Z. (1998a) Detection of a satellite orbiting the nucleus of comet Hale–Bopp (C/1995 O1). *Earth, Moon, Planets, 77*, 155-163.

Sekanina Z. (1998b) Modeling dust halos in comet Hale–Bopp (1995 O1): Existence of two active nuclei. *Astrophys. J., 509*, L133-L136.

Sekanina Z. (2001) Comet 51P/Harrington. it IAU Circular, 7773, 2001 December 13 (Ed.: D.W.E. Green, CBAT).

Sekanina Z. (2002a) Comet 57P/du Toit–Neujmin–Delporte. *IAU Circular, 7946*, 2002 August 3 (Ed.: C.W. Hergenrother, CBAT).

Sekanina Z. (2002b) Comet 57P/du Toit–Neujmin–Delporte. *IAU Circular, 7957*, 2002 August 19 (Ed.: D.W.E. Green, CBAT).

Sekanina Z. (2002c) Recurring outbursts and nuclear fragmentation of comet C/2001 A2 (LINEAR). *Astrophys. J., 572*, 679-684.

Schleicher D.G., and Osip D.J. (2002) Long- and short-term photometric behavior of comet Hyakutake (1996 B2). *Icarus, 159*, 210-233.

Sheppard S.S., Jewitt D.C., Trujillo Ch.A., Brown M.J.I., and Ashley M.C.B. (2000) A Wide-Field CCD survey for Centaurs and Kuiper Belt Objects. *Astron. J. 120*, 2687-2694.

Slipher V.M. (1927) The spectrum of the Pons-Winnecke comet and the size of the cometary nucleus. *Lowell Obs. Bull., 3, No. 86*, 135-137.

Soderblom L.A., Becker T.L., Bennett G., Boice D.C. Britt D.T. Brown R.H. Buratti B.J. Isbell C., Giese B., Hare T., Hicks M.D., Howington-Kraus E., Kirk R.L., Lee M., Nelson R.M., Oberst J., Owen T.C., Rayman M.D., Sandel B.R., Stern S.A., Thomas N., and Yelle R.V. (2002) Observations of comet 19P/Borrelly by the Miniature Integrated Camera and Spectrometer aboard Deep Space 1. *Science, 296*, 1087-1091.

Spencer, J.R., Lebofsky L.A., and Sykes M.V. (1989) Systematic biases in radiometric diameter determination. *Icarus, 78*, 337-354.

Stern S.A. (1995) Collisional time scales in the Kuiper Disk and their implications. *Astron. J., 110*, 856-868.

Stuart J.S. (2001) A Near-Earth Asteroid population estimate from the LINEAR survey. *Science, 294*, 1691-1693.

Szabó Gy.M., Csák B., Sárneczky K., and Kiss L.L. (2001) Photometric observations of distant active comets. *Astron. Astrophys., 374*, 712-718.

Szegő K. (1988) Modelling a cometary nucleus. *Astrophys. Space Sci., 144*, 439-449.

Szegő K. (1991) P/Halley, the model comet, in view of the imaging experiment a board the VEGA spacecraft. In *Comets in the Post-Halley Era.* (R.L. Newburn, M. Neugebauer, and J. Rahe, Eds.), pp. 723-731. Kluwer Academic, Dordrecht.

Tancredi G., Fernández J.A., Rickman H., and Licandro J. (2000) A catalog of observed nuclear magnitudes of Jupiter family comets. *Astron. Astrophys. Suppl. Ser., 146*, 73-90.

Thomas N., and Keller H.U. (1989) The colour of Comet P/Halley's nucleus and dust. *Astron. Astrophys., 213*, 487-494.

Tokunaga, and Hanner M.S. (1985) Does comet P/Arend–Rigaux have a large dark nucleus? *Astrophys. J., 296*, L13-L16.

Toth I., Lamy P.L., Jorda L., and Weaver H.A. (1999) The properties of the nucleus of comet Hale–Bopp from Hubble Space Telescope observations. In Asteroids, Comets, Meteors 1999, Cornell University, Ithaca, NY, 26–30 July 1999, Contributed No. [05.12].

Toth I. and Lamy P.L. (2000) Spectral properties of the nucleus of short-period comets. *Bull. Amer. Astr. Soc., 32*, 1063, Abstr. [37.05].

Toth I., Lamy P.L., and Weaver H.A. (2003). Hubble Space Telescope observations of the nucleus fragment 73P/Schwassmann–Wachmann 3-B. *Bull. Amer. Astr. Soc., 35*, Abstr. [38.05].

Trujillo Ch.A., Jewitt D.C., and Luu J.X. (2001) Properties of the Trans-Neptunian Belt: Statistics from the Canada-France-Hawaii Telescope Survey. *Astron. J. 122*, 457-473.

Van Biesbroeck G. (1962) Comet observations. *Astron. J., 67*, 422-428.

Vasundhara R., and Chakraborty P. (1999) Modeling of jets from comet Hale–Bopp (C/1995 O1): Observations from the Vainu Bappu observatory. *Icarus, 140*, 221-230.

Veeder G.J., Hanner M.S., and Tholen D.J. (1987) The nucleus of comet P/Arend–Rigaux. *Astron. J., 94*, 169-173.

Vorontsov-Velyaminov B. (1946) Structure and mass of cometary nuclei. *Astrophys. J., 104*, 226-233.

Weaver H.A., and Lamy P.L. (1997) Estimating the size of Hale–Bopp's nucleus. *Earth, Moon, Planets, 79*, 17-33.

Watanabe J.-I. (1987) The rotation of comet 1983 VII IRAS–Araki-Alcock. *Publ. Astron. Soc. Jap., 39*, 485-503.

Weidenschilling S.J. (2004) Formation of planetesimals/cometesimals in the solar nebula. In *Comets II.* (M. Festou, H.U. Keller, and H.A. Weaver, Eds.), University of Arizona Press, Tucson.

Weissman P.R. (1980) Physical loss of long-period comets. *Astron. Astrophys.* **85**, 191-196.

Weissman P.R. (1986) Are cometary nuclei primordial rubble piles ? *Nature, 320*, 242.

Weissman P.R., Doressoundiram A., Hicks M., Chamberlin A., Larson S., Hergenrother C. (1999) CCD photometry of comet and asteroid targets o space missions. *Bull. Amer. Astr. Soc., 31*, Abstr. [33.03].

Weissman P.R., Asphaug E., and Lowry S. (2004) Structure and density of cometary nuclei. In *Comets II.* (M. Festou, H.U. Keller, and H.A. Weaver, Eds.), University of Arizona Press, Tucson.

Weissman P.R., and Lowry S.C. (2003) The size distribution of Jupiter-family cometary nuclei. *LPSC*, Abstract No. 2003, and to be submitted to *Science.*

Weissman P.R., and Bottke W.F. Jr., and Levison H.F. (2003) Evolution of Comets into Asteroids. In *Asteroids III.* Eds.: W.F. Bottke, A. Cellino, P. Paolicchi, and R.P. Binzel. University of Arizona Press, Tucson, AZ. In press.

West R.M., Hainaut O., and Smette A. (1991) Post-perihelion observations of P/Halley. III – an outburst at R = 14.3 AU. *Astron. Astrophys., 246*, L77-L80.

Whipple F.L. (1950) A comet model. I. Acceleration of Comet Encke. *Astrophys. J., 111*, 374-474.

Whipple F.L. (1983) Comets: Nature evolution and decay. In *Highlights of Astronomy* (Ed.: R.M. West), Vol. 6, pp. 323-331, cf.*Bull. Amer. Astr. Soc., 15*, p. 805, Abstr. [4.7].

Whipple F.L. (1984) Comet P/Holmes, 1892 III: A case of duplicity ? *Icarus, 60*, 522-531.

Whipple F.L. (1999) Note on the structure of comet nuclei. *Planet. Space Sci., 47*, 301-304.

Whiteley R.J., Tholen D.J., and Hergenrother C.W. (2002) Lightcurve analysis of four new monolithic fast-rotating asteroids. *Icarus, 157*, 139-154.

Yoshida S., Aoki T., Soyano T., Tarusawa K.-i., van Driel W., Hamabe M., Ichikawa T., Watanabe J.-i., and Wakamatsu K.-i. (1993) Spiral dust-jet structures of comet P/Swift–Tuttle 1992 t. *Publ. Astron. Soc. Jap., 45*, L33-L37.

Zahnle K., Schenk P., Sobieszczyk S., Dones L., and Levison H.F. (2001) Differential cratering of synchronously rotating satellites by ecliptic comets. *Icarus, 153*, 111-129.

FIGURE CAPTIONS

Fig. 1. The minimum to maximum projected area (S_{min}/S_{max}) of rotating prolate ellipsoids with different axial ratios (values are marked near the curves) plotted versus the aspect angle. The corresponding light curve amplitudes are also indicated (Δm).

Fig. 2. The prolate spheroid model of the nucleus of comet 19P/Borrelly derived from the *HST* observations made in 1994 is verified by the best in-situ image taken by the *Deep Space 1* spacecraft in 2001 (cf. *Lamy et al.* 1998b; *Soderblom et al.* 2002).

Fig. 3. Distributions of the effective radius $r_{n,v}$ for ecliptic comets (a), for nearly–isotropic comets (b), and for ecliptic "cometary" NEOs (c). Note that the largest nuclei are excluded to allow legibility of the histograms at small sizes.

Fig. 4. Cumulative size distributions of the nuclei of ecliptic comets (a) and of nearly–isotropic comets (b) are represented by the solid circles while the open circles apply to the populations augmented by the "cometary" NEOs. The two solid lines in panel (a) correspond to optimum power law fits according to the Kolmogorov-Smirnov test, from the cut-off radius $r_c = 1.6\,\mathrm{km}$ up to the largest bodies.

Fig. 5. The Kolmogorov-Smirnov probability as a function of the exponent of the power law fitting the observed CSDs down to a cut-off radius $r_c = 1.6\,\mathrm{km}$. The top panel (a) corresponds to the distribution of ECs as listed in Table 1 while the bottom panel (b) to the distribution of ECs + "cometary" NEOs as listed in Table 7. The circles apply to the nominal case while the other symbols apply to two experiments where 29P/Schwassmann-Wachmann 1 is removed (triangles) and where 28P/Neujmin 1 is further removed (squares). The open symbols correspond to the M-estimate (i.e., maximum likelihood) solution while the solid symbols correspond to the least–squares fit solution.

Fig. 6. The effective radius $r_{n,v}$ of the cometary nuclei versus heliocentric distance for ecliptic comets (solid circles), for nearly–isotropic comets (open circles), and for "cometary" NEOs (open squares).

Fig. 7. Distribution of the lower limits of the axial ratio for cometary nuclei. The comet nucleus is assumed to be a prolate spheroid rotating around its axis of maximum moment of inertia for both ecliptic comets and nearly–isotropic comets.

Fig. 8. Distribution of the rotational periods for cometary nuclei.

Fig. 9. Rotational periods versus axial ratio for the cometary nuclei assumed to be prolate spheroids. The solid lines show curves of critical rotation for densities of 0.02, 0.06, 0.20, 0.60, $2.0\,\mathrm{g\,cm^{-3}}$ (from top to bottom).

Fig. 10. The distributions of the $(B-V)$, $(V-R)$ and $(R-I)$ color indices of the ecliptic comets, excluding 19P/Borrelly. The average values of the color indices are displayed and the color indices of the Sun are indicated.

TABLE 1. Nuclei of the Ecliptic Comets (ECs)

Comet	Effective radius (km)								a/b	P_{rot}
	La+	Lo+	Li+	Me+	Sc	Others	Ta+	$r_{n,v}$	(min)	(hr)
2P/Encke	–	4.4	–	–	3.2	2.4 3.1 4.5	2.4(1.3)	2.4	2.6	11.
4P/Faye	1.77	–	–	–	2.3	–	2.2(1.7)	1.77	1.25	–
6P/d'Arrest	–	1.6	–	1.71	–	3.5	1.5	1.6	1.2	7.0
7P/Pons–Winnecke	–	2.6	–	–	–	–	1.5	2.6	–	–
9P/Tempel 1	3.13	2.4	–	3.07	3.2	3.32	2.3(1.9)	3.1	1.40	41.0
10P/Tempel 2	4.63	–	–	4.93	4.1	3.1 5.9	2.9	5.3	1.7	9.0
14P/Wolf	–	2.33	–	–	2.0	–	1.3	2.33	–	–
15P/Finlay	–	–	–	–	–	–	0.9	–	–	–
16P/Brooks 2	–	–	–	–	–	–	1.7	–	–	–
17P/Holmes	1.71	–	–	–	–	–	2.0(1.6)	1.71	–	–
19P/Borrelly	2.4	1.9	–	–	–	2.4 2.50	3.0(2.2)	2.2	2.5	25.0
21P/Giacobini–Zinner	–	–	–	–	–	1.9	1.0	1.0	1.5	9.5
22P/Kopff	1.67	1.8	–	$<$2.9	–	2.46	1.8	1.67	1.7	12.30
24P/Schaumasse	–	–	–	–	1.1	–	0.8	–	–	–
26P/Grigg–Skjellerup	–	$\leq$1.5	1.5	–	1.9	1.44	1.3(1.2)	1.3	1.10	–
28P/Neujmin 1	–	–	–	11.44	–	10.22 10.6	9.1	10.7	1.50	12.75
29P/Schwassmann–Wachmann 1	–	–	–	15.4	–	20.0	–	15.4	2.6	14(32.3)
30P/Reinmuth 1	–	$\leq$3.8	–	–	3.4	–	1.3(1.0)	–	–	–
31P/Schwassmann–Wachmann 2	–	–	–	–	3.2	3.1	3.2	3.1	1.6	5.58
32P/Comas Solá	–	–	–	–	3.6	–	– (2.1)	–	–	–
33P/Daniel	–	–	–	–	1.1	–	0.9	–	–	–
36P/Whipple	–	2.32	–	–	2.8	–	2.3(1.9)	2.32	–	–
37P/Forbes	0.81	–	1.1	–	2.0	–	1.0	0.96	–	–
39P/Oterma	–	–	–	–	–	–	9.1(3.2)	–	–	–
40P/Väisälä 1	–	$\leq$3.6	–	–	1.8	–	1.5	–	–	–
41P/Tuttle–Giacobini–Kresák	–	–	–	–	–	–	0.7	0.70	–	–
42P/Neujmin 3	–	–	–	–	1.0	–	0.6	–	–	–
43P/Wolf–Harrington	–	3.4	$\ll$3.1	–	–	–	1.8	1.8	–	–
44P/Reinmuth 2	1.61	$\leq$3.0	–	–	1.8	–	1.5	1.61	–	–
45P/Honda–Mrkos–Pajdušáková	0.34	1.34	–	–	1.1	–	0.5(0.3)	0.8	1.30	–
46P/Wirtanen	0.62	$\leq$2.6	–	$<$1.66		0.56 0.7	0.7(0.6)	0.60	1.20	6.0
47P/Ashbrook–Jackson	2.8	$\leq$6.1	3.1	–	4.8	–	2.9(2.5)	2.8	1.4	$>$44
48P/Johnson	–	$\leq$3.5	3.7	–	–	2.87	2.2	2.87	1.35	29.0
49P/Arend–Rigaux	–	4.6	–	–	3.9	4.8 5.1	3.2	4.24	1.63	13.47
50P/Arend	0.95	–	–	–	–	–	3.0(1.0)	0.95	–	–
51P/Harrington	–	$\leq$1.9	–	–	2.1	–	1.4(0.2)	–	–	–
52P/Harrington–Abell	–	–	1.4	–	1.3	1.0	1.1	1.3	–	–
53P/Van Biesbroeck	–	–	$\ll$6.7	3.33	3.9	–	3.8(3.3)	3.33	–	–
54P/de Vico–Swift	–	$\leq$2.1	–	–	–	–	–	–	–	–
56P/Slaughter–Burnham	–	–	–	1.56	–	–	1.5	1.56	–	–

(continued)

Comet	Effective radius (km)								a/b	P_{rot}
	La+	Lo+	Li+	Me+	Sc	Others	Ta+	$r_{n,v}$	(min)	(hr)
57P/duToit–Neujmin–Delporte	–	≤1.1	–	–	–	–	1.6	–	–	–
58P/Jackson–Neujmin	–	–	–	–	–	–	0.6	–	–	–
59P/Kearns–Kwee	0.79	–	–	–	2.0	–	1.1	0.79	–	–
60P/Tsuchinshan 2	–	–	–	–	–	–	0.8	–	–	–
61P/Shajn–Schaldach	0.64	0.92	–	–	1.0	–	1.1(1.0)	0.64	1.27	>18
62P/Tsuchinshan 1	–	–	–	–	–	–	0.8	–	–	–
63P/Wild 1	1.45	≤0.6	–	–	–	–	1.5	1.45	–	–
64P/Swift–Gehrels	–	≤1.9	1.6	–	–	–	1.7(2.2)	1.6	–	–
65P/Gunn	–	≤8.8	≪11.7	–	–	–	4.8	–	–	–
67P/Churyumov–Gerasimenko	1.98	≤2.9	–	–	–	2.8	2.5(2.0)	2.0	1.3	12.3
68P/Klemola	–	–	–	–	–	–	2.2	2.2	–	–
69P/Taylor	–	≤3.4	–	–	–	–	2.9	–	–	–
70P/Kojima	1.86	–	–	–	1.3	–	1.2	1.86	1.10	>22
71P/Clark	0.68	≤0.9	–	1.31	–	–	1.3(0.8)	0.68	–	–
72P/Denning–Fujikawa	–	–	–	–	–	–	– (0.8)	–	–	–
73P/Schwassmann–Wachmann 3	0.68*	≤0.9	–	–	– (1.3)	<1.3	1.0	–	1.16*	–
74P/Smirnova–Chernykh	2.23	≤12.7	≪11.2	–	–	–	6.0	2.23	1.14	>20
75P/Kohoutek	–	≤1.5	–	–	2.0	–	1.8	–	–	–
76P/West–Kohoutek–Ikemura	0.33	–	–	–	1.6	–	1.3	0.33	1.47	>13
77P/Longmore	–	–	–	–	–	–	2.4	–	–	–
78P/Gehrels 2	–	1.42	–	–	–	–	2.1	1.42	–	–
79P/duToit–Hartley	–	1.4	–	–	1.9	–	1.2	1.4	–	–
81P/Wild 2	–	2.0	≪5.7	–	–	2.0	2.2(2.0)	2.0	–	–
82P/Gehrels 3	0.73	–	<3.0	–	2.1	–	2.0	0.73	1.6	>50
83P/Russell 1	–	≤0.5	–	–	–	–	–	–	–	–
84P/Giclas	0.90	–	–	–	1.3	–	1.4(1.2)	0.90	–	–
86P/Wild 3	0.43	≤0.9	–	0.65	1.3	3.1	0.9	0.43	1.35	>11
87P/Bus	0.28	≤0.6	–	<3.42	2.0	–	1.3	0.28	2.20	>25
88P/Howell	–	–	–	–	1.9	–	1.1(1.0)	–	–	–
89P/Russell 2	–	≤2.2	–	–	1.2	–	1.1	–	–	–
90P/Gehrels 1	–	–	–	–	3.4	–	2.8	–	–	–
91P/Russell 3	–	–	–	–	–	–	1.3	–	–	–
92P/Sanguin	–	1.73	–	1.19	–	–	–	1.19	–	–
94P/Russell 4	–	–	–	–	–	–	1.9	–	–	–
97P/Metcalf–Brewington	–	2.2	1.5	–	–	–	1.3	1.7	–	–
98P/Takamizawa	–	–	3.7	–	2.3	–	2.4(3.0)	–	–	–
99P/Kowal 1	–	–	–	–	4.4	–	4.8	–	–	–
100P/Hartley 1	–	<1.2	–	–	–	–	1.3	–	–	–
101P/Chernykh	–	–	–	–	2.4	–	2.2	–	–	–
103P/Hartley 2	0.8	≤5.8	≪5.3	–	2.4	–	3.8	0.8	–	–

(continued)

Comet	Effective radius (km)								a/b	P_{rot}
	La+	Lo+	Li+	Me+	Sc	Others	Ta+	$r_{n,v}$	(min)	(hr)
104P/Kowal 2	–	1.0	–	–	–	–	–	1.0	–	–
105P/Singer–Brewster	–	–	–	–	1.0	–	1.0(0.8)	–	–	–
106P/Schuster	0.94	–	–	–	–	–	0.8	0.94	–	–
107P/Wilson–Harrington	–	1.77	–	1.96	–	2.0	–	1.7	1.2	6.10
108P/Ciffreo	–	–	–	–	1.4	–	– (1.1)	–	–	–
110P/Hartley 3	2.15	–	–	–	2.4	–	1.9	2.15	1.30	10
111P/Helin–Roman–Crockett	–	$\leq$1.5	–	–	2.4	0.6	1.5	0.6	–	–
112P/Urata–Niijima	0.90	–	–	–	0.9	–	0.7	0.90	–	–
113P/Spitaler	–	$\leq$2.0	–	–	1.0	–	1.1	1.10	–	–
114P/Wiseman–Skiff	0.78	–	–	–	–	–	– (0.8)	0.78	–	–
115P/Maury	–	–	–	1.11	–	0.8	1.11	–	–	
116P/Wild 4	–	–	–	–	–	–	3.5(3.0)	–	–	–
117P/Helin–Roman–Alu 1	–	–	–	–	3.9	–	3.5)	–	–	–
118P/Shoemaker–Levy 4	–	2.4	–	–	–	–	1.7	2.4	–	–
119P/Parker–Hartley	–	$\leq$4.0	–	–	–	–	2.5(2.1)	–	–	–
120P/Mueller 1	–	1.5	–	–	1.9	–	0.8	1.5	–	–
121P/Shoemaker–Holt 2	–	1.62	–	–	–	–	2.6	1.62	–	–
123P/West–Hartley	–	–	–	–	–	–	2.2(1.7)	–	–	–
124P/Mrkos	–	–	–	–	–	–	1.6	–	–	–
125P/Spacewatch	–	–	–	–	1.0	–	0.8	0.80	–	–
128P/Shoemaker–Holt 1	–	2.12 2.48	–	–	–	–	2.0	2.3	–	–
129P/Shoemaker–Levy 3	–	–	–	–	–	–	– (2.4)	–	–	–
130P/McNaught–Hughes	–	–	–	–	1.8	–	1.7(1.5)	–	–	–
131P/Mueller 2	–	–	–	–	–	–	0.8	–	–	–
132P/Helin–Roman–Alu 2	–	–	–	–	–	–	0.9	–	–	–
134P/Koval–Vávrová	–	–	–	–	–	–	1.4	–	–	–
135P/Shoemaker–Levy 8	–	–	–	–	1.6	–	1.5(1.3)	–	–	–
136P/Mueller 3	–	–	–	–	–	–	1.9(1.5)	–	–	–
137P/Shoemaker–Levy 2	–	$\leq$3.4	4.5	–	–	–	2.9	2.90	–	–
138P/Shoemaker–Levy 7	–	–	–	–	–	–	0.8(1.0)	–	–	–
139P/Väisälä-Oterma	–	$\leq$4.6	–	–	–	–	2.6	–	–	–
140P/Bowell–Skiff	–	–	–	–	–	–	– (2.3)	–	–	–
141P/Machholz 2	–	–	–	–	–	–	– (1.0)	–	–	–
143P/Kowal–Mrkos	–	–	–	–	–	5.7	– (2.6)	5.4	1.5	17.2
144P/Kushida	–	–	–	–	–	–	– (1.2)	–	–	–
147P/Kushida–Muramatsu	0.21	$\leq$2.0	–	–	–	–	2.3(1.9)	0.21	1.53	9.5
148P/Anderson–LINEAR	–	–	–	–	–	–	– (2.1)	–	–	–
152P/Helin–Lawrence	–	$\leq$6.0	–	$<$1.74	–	–	4.6	–	–	–
154P/Brewington	–	–	–	–	–	–	1.5	–	–	–

(continued)

Comet	Effective radius (km)								a/b	P_{rot}
	La+	Lo+	Li+	Me+	Sc	Others	Ta+	$r_{n,v}$	(min)	(hr)
P/1993 W1 (Mueller 5)	–	–	–	–	–	–	2.1	–	–	–
P/1994 A1 (Kushida)	–	–	–	–	–	–	1.2	–	–	–
P/1994 J3 (Shoemaker 4)	–	–	–	–	–	–	3.3	–	–	–
P/1995 A1 (Jedicke)	–	–	–	–	–	–	3.0	–	–	–
P/1996 A1 (Jedicke)	–	–	–	–	–	–	5.0	–	–	–
P/1997 C1 (Gehrels)	–	–	–	–	–	–	2.3	–	–	–
P/1997 G1 (Montani)	–	–	–	–	–	–	2.5	–	–	–
P/1997 V1 (Larsen)	–	–	–	–	–	–	3.6	–	–	–
P/1998 S1 (LINEAR–Mueller)	–	–	–	–	–	–	– (4.2)	–	–	–
P/1999 D1 (Hermann)	–	–	–	–	–	–	– (0.7)	–	–	–
P/1999 RO28 (LONEOS)	–	–	–	–	–	–	– (0.1)	–	–	–

Notes:
See text for the references.
New radii given by *Ta+* are in brackets.

* Fragment B.

TABLE 2. Nuclei of the Nearly–Isotropic Comets (NICs)

Comet	Effective radius (km)						$r_{n,v}$	a/b	P_{rot}
	La+	Lo+	Li+	Me+	Sc	Others		(min)	(hr)
1P/Halley*	–	–	–	–	–	–	5.5	2.0	52.8; 177.6
8P/Tuttle	–	–	7.8	–	–	–	7.8	–	–
55P/Tempel–Tuttle	1.80	–	–	–	–	1.8	1.80	1.50	–
96P/Machholz 1	–	–	3.5	–	–	2.8	3.2	1.4	6.38
109P/Swift–Tuttle	–	–	–	13.7	–	11.8–12.5	13.0	–	69.4
126P/IRAS	1.57	–	–	–	–	–	1.57	–	–
P/1991 L3 (Levy)	–	–	–	–	–	5.8	5.8	1.3	8.34
C/1983 H1 (IRAS–Araki–Alcock)	–	–	–	–	–	3.5	3.5	–	51.0
C/1983 J1 (Sugano–Saigusa–Fujikawa)	–	–	–	–	–	0.37	0.37	–	–
C/1983 O1 (Černis)	–	–	–	<10.5	–	–	–	–	–
C/1984 K1 (Shoemaker)	–	–	–	<6.4	30.6	–	–	–	–
C/1984 U1 (Shoemaker)	–	–	–	<6.4	29.3	–	–	–	–
C/1986 P1 (Wilson)	–	–	–	–	16.1	<6.0	–	–	–
C/1987 A1 (Levy)	–	–	–	<4.0	2.1	–	–	–	–
C/1987 H1 (Shoemaker)	–	–	–	<4.0	26.7	–	–	–	–
C/1987 F1 (Torres)	–	–	–	<5.9	–	–	–	–	–
C/1988 B1 (Shoemaker)	–	–	–	<6.1	16.1	–	–	–	–
C/1988 C1 (Maury–Phinney)	–	–	–	<6.1	1.1	–	–	–	–
C/1995 O1 (Hale–Bopp)	37	–	–	–	–	30	37	2.6	11.34
C/1996 B2 (Hyakutake)	–	–	–	–	–	2.4	2.4	–	6.27
C/1997 T1 (Utsonomiya)	–	–	–	–	–	<5.8	–	–	–
C/1999 S4 (LINEAR)**	–	–	–	–	–	0.4	0.4	–	–
C/2001 OG108 (LONEOS)	–	–	–	–	–	8.9	8.9	1.3	57.19

Notes:
See text for the references.
(*): See Table 3. The two periods correspond to the SAM and LAM rotations.
(**): Pre-breakup nucleus size.

TABLE 3. Cometary nuclei with known shape and size

Comet	$a \times b \times c$ (km×km×km)	$1 : a/b : a/c$	Notes
1P/Halley	$7.65 \pm 0.25 \times 3.61 \pm 0.25 \times 3.61 \pm 0.25$	$1 : 2.13 : 2.13$	(1)
	$7.21 \pm 0.15 \times 3.7 \pm 0.1 \times 3.7 \pm 0.1$	$1 : 1.95 : 1.95$	(2)
10P/Tempel 2	$8 \times 4 \times 4$	$1 : 2.0, c = b$	(3)
	$8.2 \times 4.9 \times 3.5$	$1 : 1.67 : 2.34$	(4)
19P/Borrelly	$4.0 \pm 0.1 \times 1.60 \pm 0.02 \times 1.60 \pm 0.02$	$1 : 2.5, c = b$	(5)
	$4.4 \pm 0.15 \times 1.80 \pm 0.08 \times 1.80 \pm 0.08$	$1 : 2.4, c = b$	(6)

Notes:
(1) *VEGA* 1, 2 *TVS* in-situ imaging (*Merényi et al.* 1989)
(2) *GIOTTO HMC* in-situ imaging (*Keller et al.* 1994)
(3) Ground-based CCD photometry (*Jewitt and Luu* 1989)
(4) Ground-based observations and modeling (*Sekanina* 1989)
(5) *DEEP SPACE 1 MICAS* in-situ imaging (*Buratti et al.* 2003)
(6) *HST WFPC2* high precision photometry (*Lamy et al.* 1998b)

TABLE 4. Albedos of Cometary Nuclei

Comet	Geom. Albedo	λ
Ecliptic Comets:		
2P/Encke	0.046 ± 0.023	V
9P/Tempel 1	0.05 ± 0.02	R
10P/Tempel 2	$0.022^{+0.004}_{-0.006}$	4845
"	$0.04 - 0.07$	JHK
19P/Borrelly	0.03	
22P/Kopff	0.042 ± 0.006	V
28P/Neujmin 1	0.026	V
"	0.03 ± 0.01	R
49P/Arend-Rigaux	0.04 ± 0.01	V
"	0.054 ± 0.010	J
"	0.03 ± 0.01	J
107P/Wilson-Harrington	0.05 ± 0.01	J
Nearly–Isotropic Comets:		
1P/Halley	$0.04^{+0.02}_{-0.01}$	V,R,I
55P/Tempel-Tuttle	0.06 ± 0.025	R
"	0.045	R
109P/Swift-Tuttle	$0.02 - 0.04$	R
C/1983 H1 IRAS-Araki-Alcock	0.03 ± 0.01	V
C/1995 O1 Hale-Bopp	0.04 ± 0.03	
C/2001 OG108 (LONEOS)	0.03 ± 0.005	V

λ = band or wavelength (in Å) to which albedo applies. References are given in the text.

TABLE 5. Colors of cometary nuclei

Comet	$(B-V)$	$(V-R)$	$(R-I)$	Phot.[a]	Ref.[b]
Solar colors	0.65	0.35	0.28		
Ecliptic Comets:					
2P/Encke	0.78±0.02	0.48±0.02	–	S	LJ90
	–	0.43±0.05	–	F	J02
	–	0.38±0.06	–	F	J02
	–	0.37±0.09	–	F	HD02
6P/d'Arrest	0.78±0.04	0.54±0.04	0.45±0.04	F	J02
	–	0.62±0.08	–	F	M+02
	1.08±0.12	0.33±0.09	0.33±0.12	F	LW03
10P/Tempel 2	–	0.53±0.03	–	F	JM88
	–	0.58±0.03	–	S	JL89
	–	0.56±0.02	–	F	M+02
14P/Wolf	–	0.02±0.22	0.25±0.35	F	Lo+03
19P/Borrelly	–	0.25±0.78	–	F	Lo+03
21P/Giacobini-Zinner	0.80±0.03	0.50±0.02	–	S	L93
22P/Kopff	0.77±0.05	0.50±0.08	0.42±0.03	F	La+02
26P/Grigg-Skjellerup	–	0.42±0.10	–	F	B+99
28P/Neujmin 1	–	0.46±0.04	–	F	Ca+87
	–	0.45±0.05	–	F	JM88
	–	0.50±0.04	–	F	JM88
	–	0.45±0.05	–	F	D+01
	–	0.48±0.06	–	F	M+02
45P/HMP*	1.12±0.03	0.44±0.03	0.20±0.03	F	La+99
46P/Wirtanen	–	0.45±0.10	–	F	La+98a
48P/Johnson	–	0.50±0.30	–	F	Li+00
49P/Arend-Rigaux	0.77±0.03	0.47±0.01	0.43±0.02	F	M+88
	–	0.47±0.01	–	S	L93
	–	0.40±0.30	–	F	Li+00
	–	0.49±0.11	0.54±0.14	F	Lo+03
53P/Van Biesbroeck	–	0.34±0.08	–	F	M+02
73P/SW3	–	0.48±0.17	–	F	B+99
86P/Wild 3	–	0.12±0.14	–	F	M+02
107P/W-H**	–	0.31±0.03	–	S	Ch+96
	–	0.41±0.02	–	F	M+02
	0.61±0.05	0.20±0.04	–	F	LW03
	0.75±0.06	–	–	F	LW03
143P/Kowal-Mrkos	0.84±0.02	0.58±0.02	0.55±0.02	F	J+03
	0.80±0.02	0.58±0.02	0.57±0.02	F	J+03
Nearly–Isotropic Comets:					
1P/Halley	0.72±0.04	0.41±0.03	0.39±0.06	F/HMC	TK89
96P/Machholz 1	–	0.43±0.03	–	F	M+02
	–	0.30±0.05	–	F	Li+00
C/2001 OG108 (LONEOS)	0.76±0.03	0.46±0.02	0.44±0.03	F	A+03

[a] F = filter photometry, S = spectrophotometry; HMC = in-situ measurements by the GIOTTO Halley Multicolour Camera

[b] References: A+03 (Abell *et al.* 2003); B+99 (Boehnhardt *et al.* 1999); Ca+87 (Campins *et al.* 1987); Ch+96 (Chamberlin *et al.* 1996); D+01 (Delsanti *et al.* 2001); HD02 (Hainaut and Delsanti 2002); JM88 (Jewitt and Meech 1988); JL89 (Jewitt and Luu 1989); J+03 (Jewitt *et al.* 2003); LJ90 (Luu and Jewitt 1990); L93 (Luu 1993); La+98a (Lamy *et al.* 1998a); La+02 (Lamy et al. 2002); Li+00 (Licandro *et al.* 2000); Lo+03 (Lowry *et al.* 2003); LW03 (Lowry and Weissman 2003); M+88 (Millis *et al.* 1988); M+02 (Meech *et al.* 2004); TK (Thomas and Keller 1989).

*45P/HMP: 45P/Honda–Mrkos–Pajdusakova, **107P/W-H: 107P/Wilson-Harrington.

TABLE 6. Power exponents of the Cumulative Luminosity Function (CLF) and of the Cumulative Size Distribution (CSD) of the nuclei of ecliptic comets

Reference	CLF	CSD
Fernández *et al.* (1999)	0.53 ± 0.05	2.65 ± 0.25
Lowry *et al.* (2002)	0.32 ± 0.02	1.6 ± 0.1
Meech *et al.* (2003)	–	2.5*
Weissman and Lowry (2003)	0.32 ± 0.01	1.59 ± 0.03
Weissman (private communication)	0.36 ± 0.01	1.79 ± 0.05
This work	0.38 ± 0.06	1.9 ± 0.3

*From Monte Carlo simulations after truncation at small radii.

TABLE 7. Physical properties of probable dormant or extinct comets

Name	T_J	r_n	p_V	Note	Association	Ref.
Selected NEOs and possible dead comets based on $T_J \lesssim 3$ and low albedo ($\lesssim 0.05$):						
1580 Betulia	3.07	3.75 ± 0.15	0.034 ± 0.004	–	EC	Fe99
3552 Don Quixote	2.31	9.2 ± 0.4	0.045 ± 0.003	1983 SA	EC	Fe99
1983 VA	2.97	1.35 ± 0.05	0.07 ± 0.01	–	EC	Fe99
2000 EJ37	2.44	5.8	–	–	EC	Fe+03
2000 OG44	2.74	$3.87^{+0.50}_{-0.40}$	$0.038^{+0.018}_{-0.017}$	–	EC	Fe+01
2000 PG3	2.55	$3.08^{+1.42}_{-0.95}$	$0.021^{+0.031}_{-0.017}$	–	EC	Fe+01
2000 SB1	2.81	$3.57^{+0.92}_{-0.62}$	$0.019^{+0.015}_{-0.010}$	–	EC	Fe+01
2000 VU2	2.62	6.0	–	–	EC	Fe+03
2000 YN30	2.64	1.4	–	–	EC	Fe+03
2001 KX67	2.85	1.6	–	–	EC	Fe+03
2001 NX17	2.79	9.3	–	–	EC	Fe+03
2001 OB74	2.98	1.0	–	–	EC	Fe+03
2001 QF6	2.28	2.6	–	–	EC	Fe+03
2001 QL169	2.97	0.4	–	–	EC	Fe+03
2001 QQ199	2.32	10.2	–	–	EC	Fe+03
2001 RC12	2.69	1.6	–	–	EC	Fe+03
2001 SJ262	2.98	0.16	–	–	EC	Fe+03
2001 TX16	2.77	3.7	–	–	EC	Fe+03
5335 Damocles	1.14	8.5	0.03	(a)	NIC(HTC)	Le+02
15504 1999 RG33	1.95	14.8	0.03	(a)	NIC(HTC)	Le+02
20461 1999 LD31	-1.54	6.8	0.03	(a)	NIC(HTC)	Le+02
1996 PW	1.72	6.5	0.03	(a)	NIC(ERC)	Le+02
1997 MD10	0.98	2.5	0.03	(a)	NIC(HTC)	Le+02
1998 WU24	1.40	3.9	0.03	(a)	NIC(HTC)	Le+02
1999 LE31	-1.31	$9.05^{+4.04}_{-2.71}$	$0.031^{+0.030}_{-0.020}$	–	NIC(HTC)	Fe+01
1999 XS35	1.42	1.4	0.03	(a)	NIC(HTC)	Le+02
2000 AB229	0.78	6.2	0.03	(a)	NIC(ERC)	Le+02
2000 DG8	-0.62	$8.64^{+2.26}_{-1.83}$	$0.027^{+0.022}_{-0.015}$	–	NIC(HTC)	Fe+01
2000 HE46	-1.51	$3.55^{+1.10}_{-0.78}$	$0.023^{+0.021}_{-0.013}$	–	NIC(HTC)	Fe+01
Selected NEOs associated with meteor stream:						
2101 Adonis	1.40	0.28(b)	?	meteor stream	EC	Fe99
2212 Hephaistos	3.1	2.85	?	meteor stream	EC	Fe99
3200 Phaeton	4.51	2.35 ± 0.25	0.11 ± 0.02	meteor stream	EC	Fe99

Notes:

T_J: Tisserand parameter with respect to Jupiter.
(a): Radius derived from absolute magnitude (*Le+02*) using an albedo of 0.03.
(b): Averaged radius derived from the radar measurements made by *Benner et al.* (1997).

References:

Fe99: from the list compiled by *Fernández* (1999); Fe+01: *Fernández et al.* (2001);
Fe+03: *Fernández et al.* (2003); Le+02: *Levison et al.* (2002).

TABLE 8. Power exponents of the CSD and CLF for various minor object populations

Population	CSD	CLF	Reference
KBOs ($r > 20$ km)	3.45	0.69	*Gladman et al.* (2001)
	3.20 ± 0.10	0.64 ± 0.02	*Larsen et al.* (2001)
	3.15 ± 0.10	0.63 ± 0.06	*Trujillo et al.* (2001)
Centaurs	2.70 ± 0.35	0.54 ± 0.07	*Larsen et al.* (2001)
	3.0	0.6	*Sheppard et al.* (2001)
ECs	1.9 ± 0.3	0.38 ± 0.06	This work
ECs + "cometary" NEOs	1.6 ± 0.2	0.32 ± 0.04	This work
Near-Earth objects	1.75 ± 0.10	0.35 ± 0.02	*Bottke et al.* (2002)
	1.96	0.39	*Stuart* (2001)
Main belt asteroids	1.25–2.80	0.25–0.56	*Jedicke & Metcalfe* (1998)

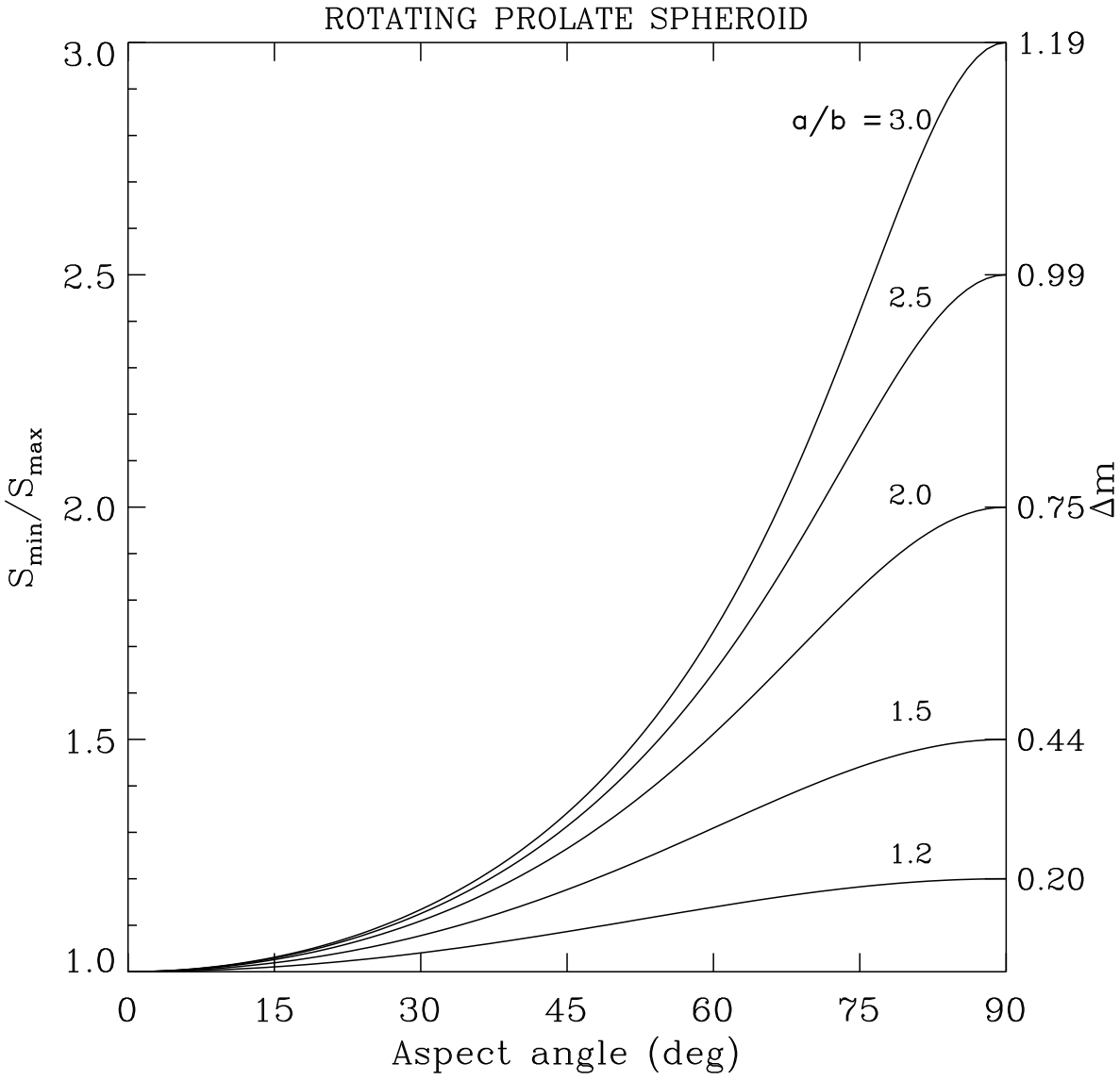
ROTATING PROLATE SPHEROID
3.0
2.5
2.0
1.5
1.0
S_{min}/S_{max}
1.19
0.99
0.75
0.44
0.20
Δm
a/b = 3.0
2.5
2.0
1.5
1.2
0
15
30
45
60
75
90
Aspect angle (deg)

Fig. 1.—

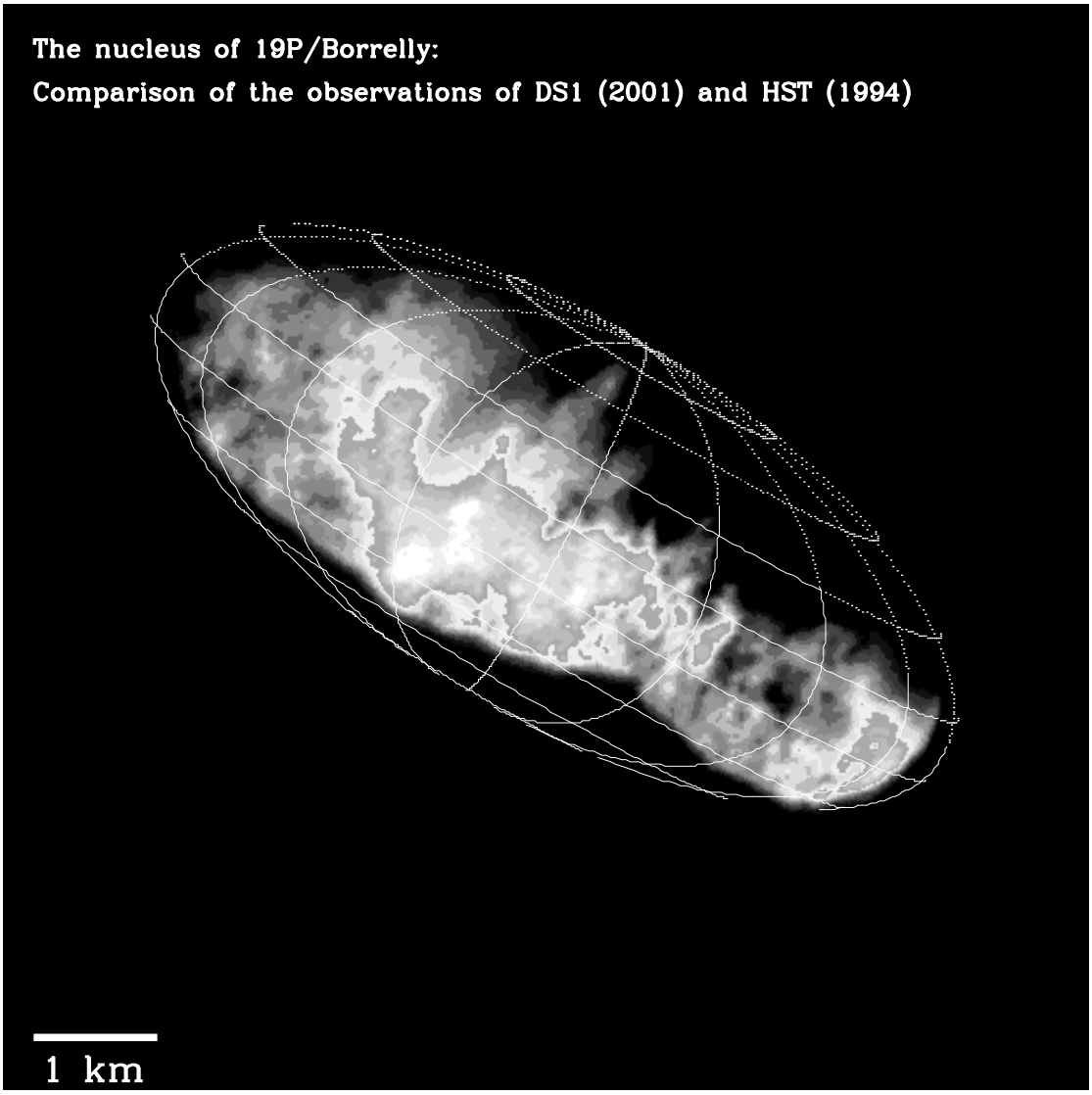
The nucleus of 19P/Borrelly:
Comparison of the observations of DS1 (2001) and HST (1994)
1 km

Fig. 2.—

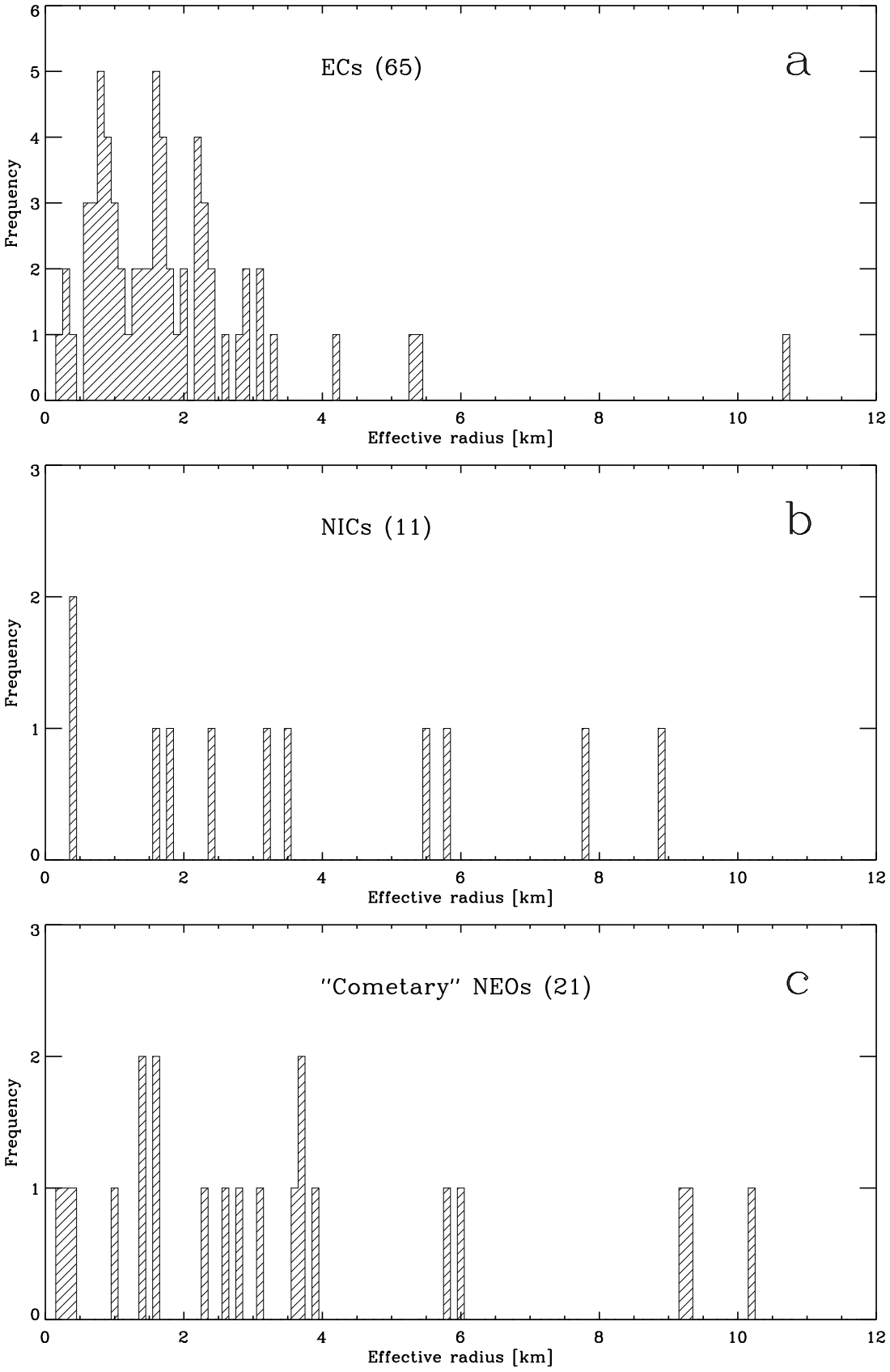
ECs (65)
a
Frequency
Effective radius [km]
NICs (11)
b
Frequency
Effective radius [km]
"Cometary" NEOs (21)
c
Frequency
Effective radius [km]

Fig. 3.—

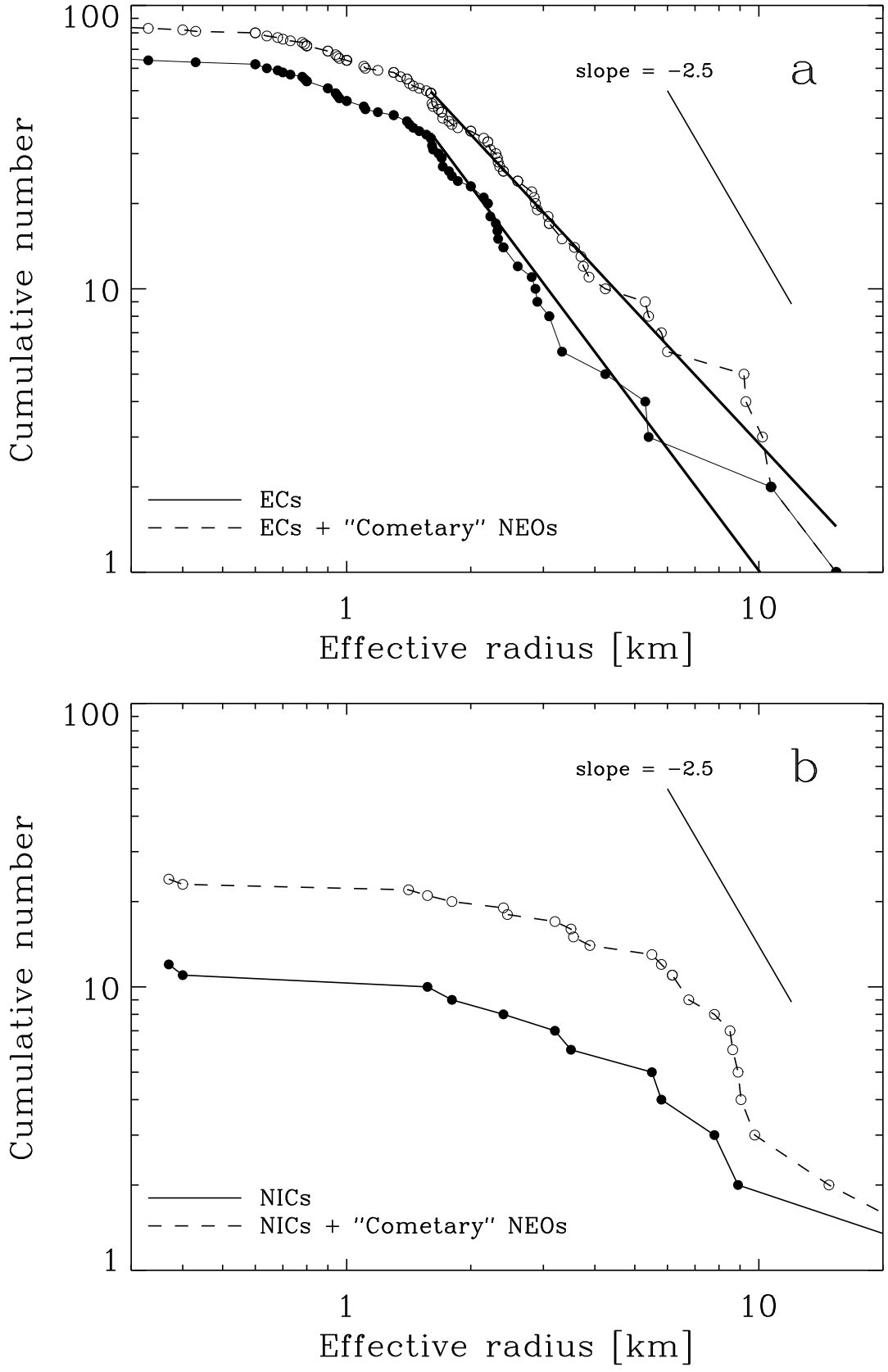
100
10
1
Cumulative number
slope = −2.5
a
ECs
ECs + "Cometary" NEOs
1
10
Effective radius [km]
100
10
1
Cumulative number
slope = −2.5
b
NICs
NICs + "Cometary" NEOs
1
10
Effective radius [km]

Fig. 4.—

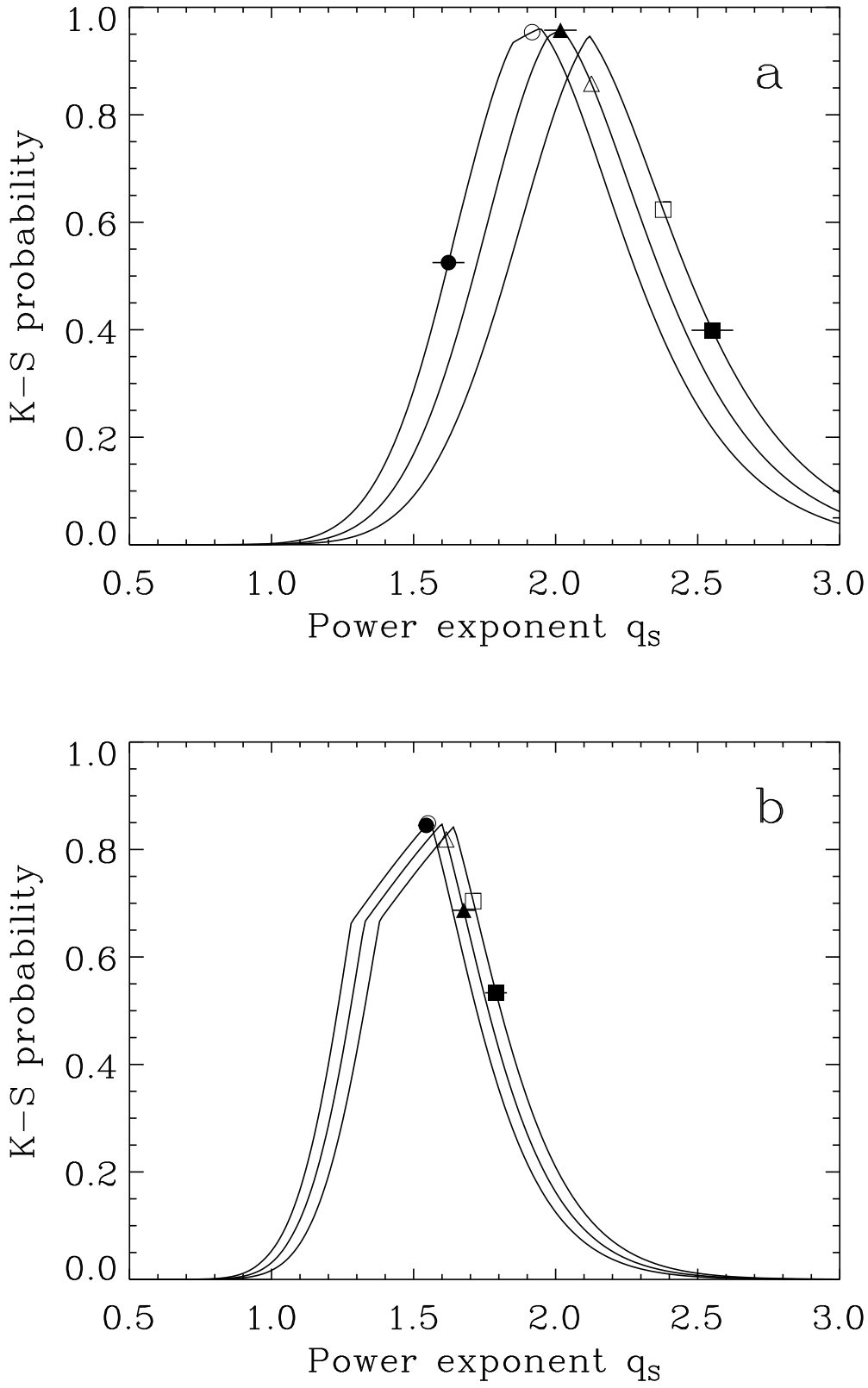
a
b
K–S probability
Power exponent q_s
0.0
0.2
0.4
0.6
0.8
1.0
0.5
1.0
1.5
2.0
2.5
3.0

Fig. 5.—

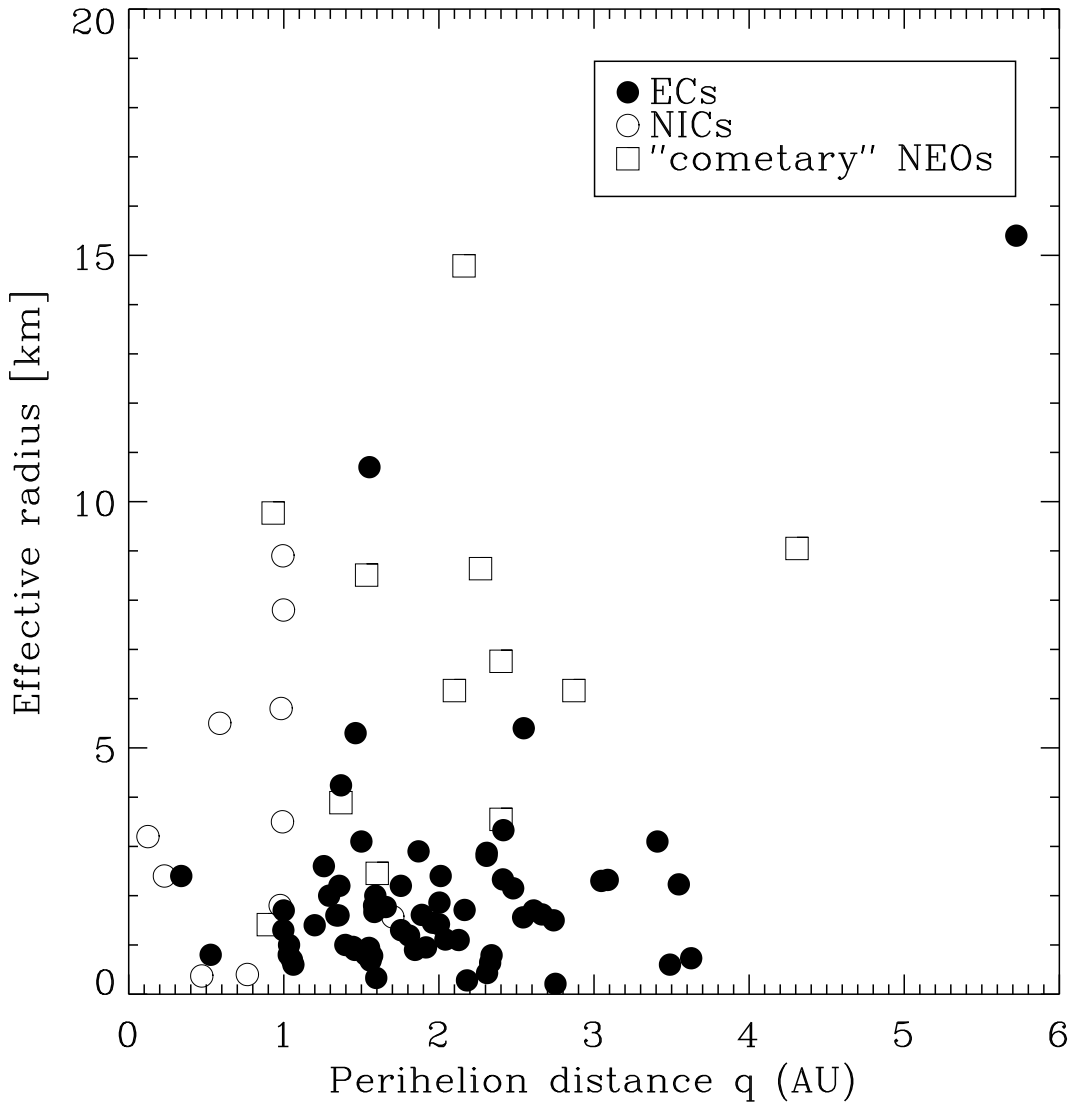
ECs
NICs
"cometary" NEOs
Effective radius [km]
Perihelion distance q (AU)
0
5
10
15
20
0
1
2
3
4
5
6

Fig. 6.—

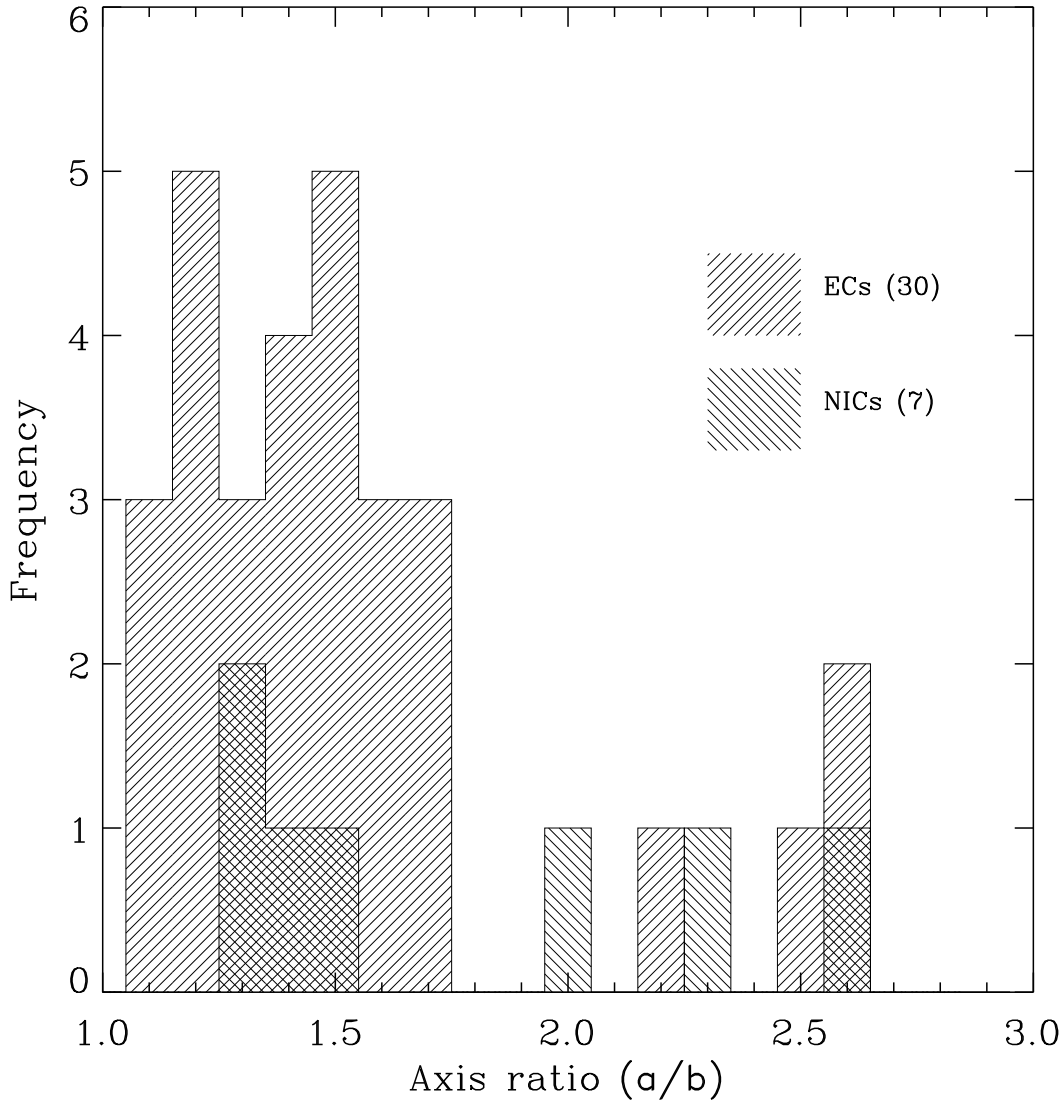

Fig. 7.—

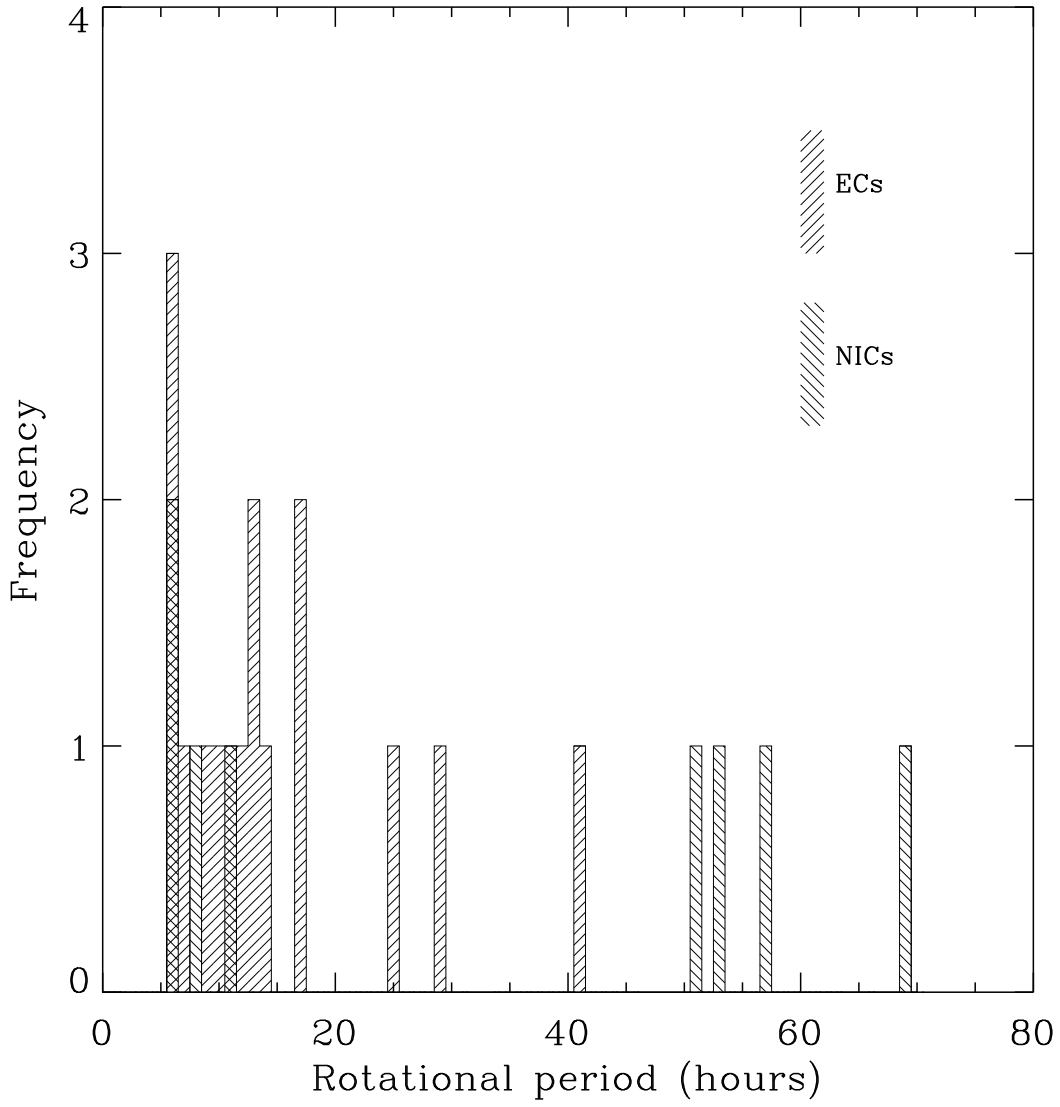
4
3
2
1
0
Frequency
ECs
NICs
0
20
40
60
80
Rotational period (hours)

Fig. 8.—

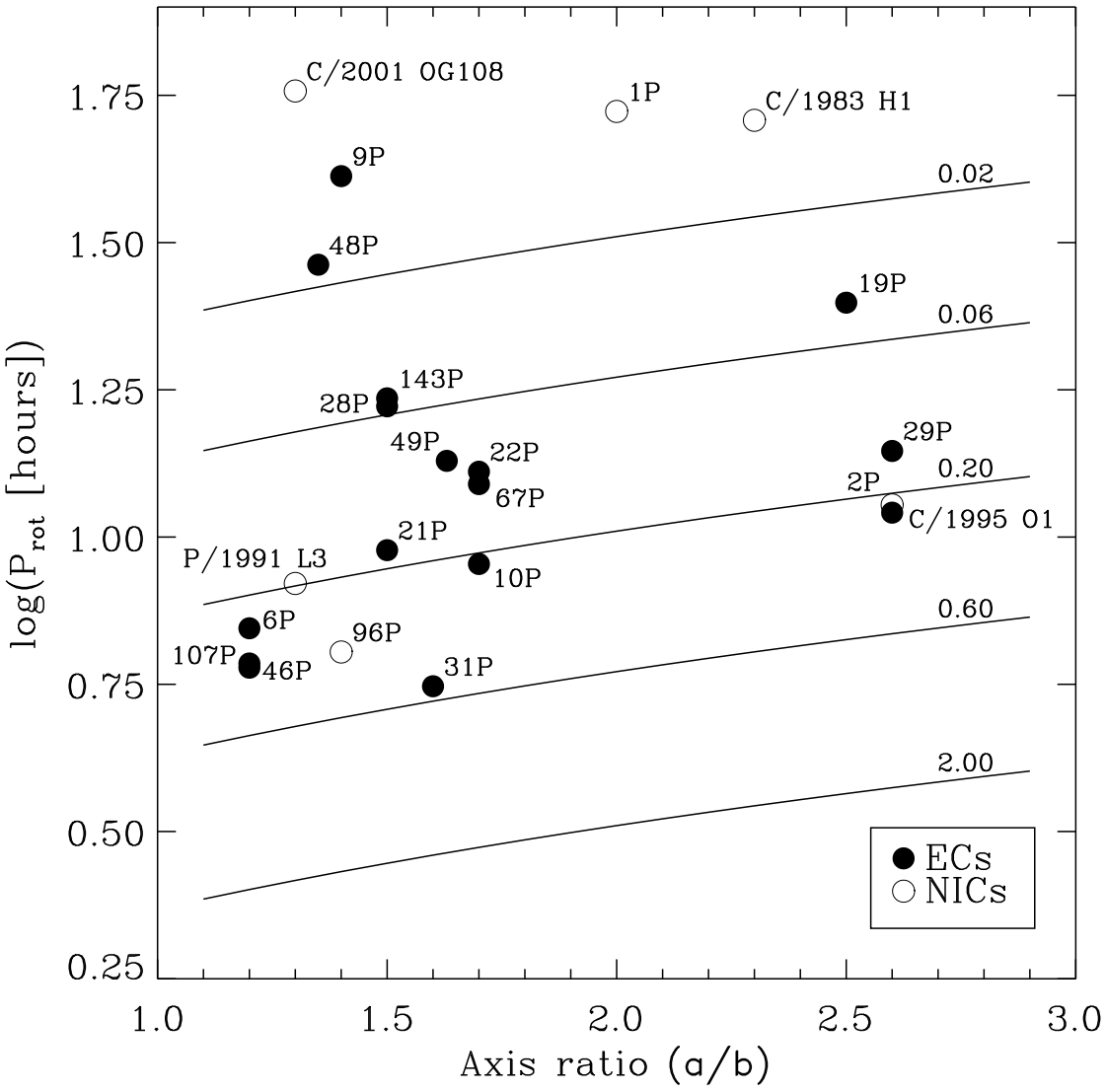
C/2001 OG108
1P
C/1983 H1
9P
0.02
48P
19P
0.06
143P
28P
29P
49P
22P
0.20
2P
67P
C/1995 O1
21P
P/1991 L3
10P
0.60
6P
96P
107P
46P
31P
2.00
ECs
NICs
log(P_rot [hours])
Axis ratio (a/b)
1.75
1.50
1.25
1.00
0.75
0.50
0.25
1.0
1.5
2.0
2.5
3.0

Fig. 9.—

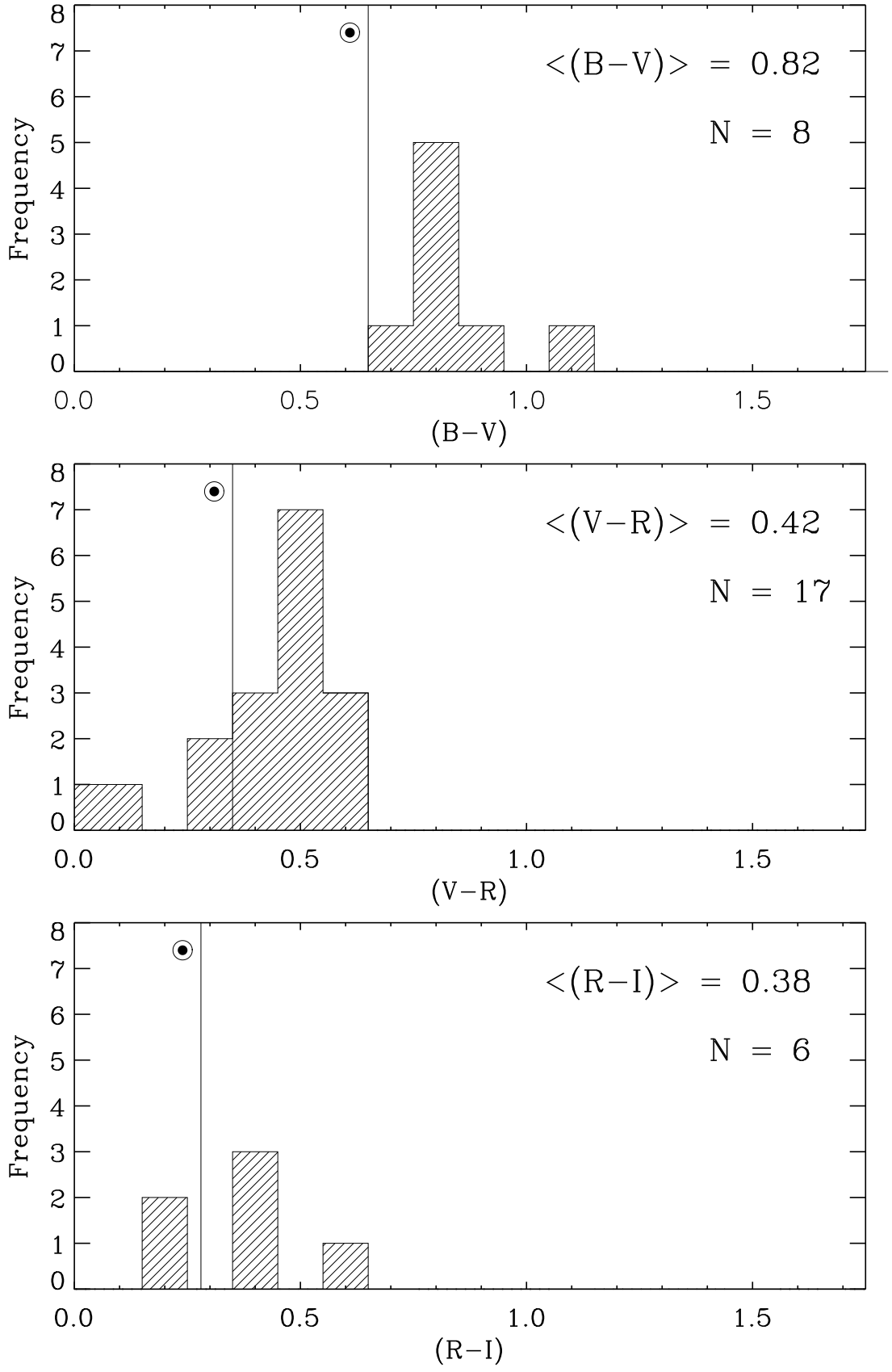
<(B−V)> = 0.82
N = 8
Frequency
(B−V)
<(V−R)> = 0.42
N = 17
Frequency
(V−R)
<(R−I)> = 0.38
N = 6
Frequency
(R−I)

Fig. 10.—